
INVESTIGATION OF SI/C-BASED ANODES FOR LI-ION BATTERIES

Janis Dölle



Berlin 2014

Investigation of Si/C-based anodes for Li-Ion batteries

vorgelegt von
M.Sc.
Janis Dölle
aus Peine, Deutschland

Von der Fakultät II - Mathematik und Naturwissenschaften
der Technischen Universität Berlin
zur Erlangung des akademischen Grades

Doktor der Naturwissenschaften
-Dr. rer. nat.-

genehmigte Dissertation

Promotionsausschuss:

Vorsitzender: Prof. Dr. Reinhard Schomäcker

Gutachter: Prof. Dr. Robert Schlögl

Gutachter: Prof. Dr. Martin Lerch

Gutachterin: Prof. Dr. Christina Roth

Tag der wissenschaftlichen Aussprache: 22.10.2014

Berlin 2014

Die vorliegende Arbeit wurde in der Zeit von November 2011 bis September 2014 im Technologiezentrum Isenbüttel der Volkswagen AG, dem Fritz-Haber-Institut der Max-Planck Gesellschaft in Berlin und an der Technischen Universität in Berlin unter der Leitung von Prof. Dr. Robert Schlögl und Prof. Dr. Martin Lerch angefertigt.

“The most beautiful experience we can have is the mysterious - the fundamental emotion which stands at the cradle of true art and true science.”

— Albert Einstein

Zusammenfassung

Die Energiedichte von Lithium-Ionen Batteriezellen (Li-Ionen) ist von entscheidender Bedeutung für die Leistungsfähigkeit und Reichweite von elektrischen und hybridischen Fahrzeugen sowie für Geräte der Unterhaltungselektronik und der stationären Energiespeicherung. Zur signifikanten Erhöhung der Energiedichte sind neue Aktivmaterialien für die positive (Kathode) und negative (Anode) Elektrode in Li-Ionen Batterien unabdingbar. Ein erfolgversprechender Kandidat als neues Aktivmaterial für die Anode ist Silicium (Si), da dieses eine deutlich höhere theoretische spezifische Kapazität besitzt als Graphit (C) (3578 mAh g^{-1} vs. 372 mAh g^{-1}), das derzeit in kommerziellen Li-Ionen Batteriezellen verwendet wird. Ein Hauptgrund für die Schwierigkeiten Si-basierte Anoden in kommerzielle Li-Ionen Batterien zu integrieren, liegt in der großen Volumenänderung, die das Si während der Lithiierung und Delithiierung vollzieht. Ein möglicher Weg zur gleichzeitigen Steigerung der Kapazität und der Minimierung des Einflusses der Volumenänderung ist die Verwendung von Si/C Materialien bzw. Kompositen.

Das Ziel dieser Arbeit besteht darin, neue Erkenntnisse und mögliche Lösungswege zur Verbesserung von Si/C-Anoden zu entwickeln und deren Effekte auf die Degradation zu untersuchen. Es werden zunächst die elektrochemischen Grundlagen des Themengebiets erläutert. Anschließend wird eine kurze Einordnung zu den Zielen der folgenden experimentellen Arbeiten und Resultate durchgeführt. Weiterhin werden die Ergebnisse einer neuen Elektrolytzusammensetzung und deren Auswirkung auf die Zyklenstabilität, den Kapazitätsverlauf und die Grenzflächeneigenschaften analysiert. Die erhaltenen Ergebnisse führen zu dem Schluss, dass der neu entwickelte Elektrolyt zu einer stabileren SEI (Solid Electrolyte Interphase) führt, welches wiederum die Performance der Anode positiv beeinflusst.

Darüber hinaus wird eine neue elektrochemische Vorbehandlungsmethode für Si/C-Anoden vorgestellt und deren Einfluss auf die Performance und Grenzflächeneigenschaften charakterisiert. Die Methode führt zu einer geringeren irreversiblen Kapazität in den ersten Batteriezyklen und wird elektrochemisch in einer Lösung bestehend aus Fluoroethylencarbonat (FEC), Lithium(bis)oxalatoborat (LiBOB) und Lithiumnitrat (LiNO_3) durchgeführt. Die Ergebnisse zeigen eine deutlich verbesserte Kapazität und Zyklenstabilität im Vergleich zu unbehandelten Anoden. Die analytischen Untersuchungen deuten weiterhin auf eine stabilere Grenzfläche Anode/Elektrolyt hin und unterstreichen deren entscheidenden Einfluss auf die Leistungsfähigkeit der Batteriezelle.

Abstract

Increasing the energy density of Li-Ion batteries is crucial to improve the performance of electric vehicles, hybrid electric vehicles as well as consumer electronics and energy storage devices. To achieve significantly higher energy densities new active materials for the positive and negative electrodes of Li-Ion batteries are needed. One promising candidate as an active material for anodes in future Li-Ion batteries is silicon (Si), due to its higher theoretical capacity compared to graphite (C), which is currently used as the anode material in commercial Li-Ion battery cells. However the performance of Si-based anode materials is still unsatisfactory for commercial applications. The low cycling stability is believed to be a consequence of the high volume expansion of Si and its detrimental effects on the electrode framework. One possible way to increase the capacity and limit the detrimental effects of the volume expansion is the incorporation of Si/C-based anodes in Li-Ion batteries.

The aim of this thesis is to provide new insights and possible solutions for Si/C-based anodes in Li-Ion batteries. Therefore, the theoretical background needed to follow this thesis is provided. At the beginning, important electrochemical relationships and battery specific parameters are discussed. Subsequently, the characteristics and differences of C and Si as anode active materials are described as well as different approaches to improve the cycling stability of Si-based anodes. A new electrolyte formulation and its effect on the cycling stability, capacity retention, and interface properties is described and the obtained results led to the conclusion of a more stable SEI (Solid Electrolyte Interphase) with the new electrolyte, which positively influences the performance of Si/C-anodes.

Moreover, a new pretreatment method to increase the cycling stability and capacity retention for Si/C-based anodes is introduced. This method leads to a decreased irreversible capacity during the first battery cycles. The pretreatment of Si/C-based anodes is conducted electrochemically in a solution containing fluoroethylene carbonate (FEC), lithium(bis)oxalate borate (LiBOB), and lithium nitrate (LiNO_3). The results display significantly increased performances for the pretreated anodes compared to non-pretreated anodes and the analytical results of the samples reveal that a more stable electrode/electrolyte interface is formed, which proved to be crucial for an improved battery performance. Moreover, this method could be a possible way to increase the stability of Si/C-based anodes in the future.

Acknowledgement

First and foremost, I would like to thank my advisor Prof. Dr. Robert Schlögl, Director of the Department of Inorganic Chemistry at the Fritz Haber Institute of the Max Planck Society, for his guidance and especially for giving me the chance to conduct my PhD research in his group. Thank you very much for the discussions and thank you for teaching me during the last years, which was essentially to accomplish my PhD thesis.

I would like to acknowledge Prof. Dr. Martin Lerch for supervising my PhD at the Technical University of Berlin and for taking his time to review my PhD thesis. I also want to thank Prof. Dr. Christina Roth for reviewing my PHD thesis as an external reviewer and Prof. Dr. Reinhard Schomäcker for taking the chair of the examination board.

My special thanks goes to Dr. Julian Tornow, former group leader of the Electrochemistry group at the Fritz Haber Institute, and Dr. Mirko Herrmann from the Volkswagen AG for the supervision and guidance during my PhD thesis.

Thank you for all the discussions, which were so valuable to complete this project and also for taking you the time to review my final dissertation. You both taught me a lot during the last years and I am very thankful that I had the chance to learn from you.

My special thanks go to Gisela Weinberg und Dr. Nicole Giliard from the Fritz Haber Institute for helping me with the SEM and EDX measurements and for the good discussions concerning this work.

I would also like to acknowledge Linda Brinkhaus and Christoph Franke from the Volkswagen AG for sharing the office with me. Thank you for your support, for the good discussions, and especially for taking care of a good and fun working atmosphere.

Moreover I would like to express my gratitude to all the co-workers at the Fritz Haber Institute for your effort, help, and the discussions especially during the PhD-days.

At the Volkswagen AG I would like to thank my colleagues from the Department of Battery and Fuels and the Volkswagen Varta Microbattery Joint Venture. I would like to thank especially: Dr. Jörg Huslage, Dr. Wolfgang Zipprich, Dr. Carla Cavalca de Araujo, Oliver Gröger, Dr. Marius Schrader, Stanislaw Ljahov, Enrica Jochler, and Dr. Chiara Poggi. I am very

thankful for your help and guidance during the last years.

Last but not least, I would like to thank my family who has always supported me. I am grateful for your trust and thankful for your help in all the good and bad times. This support made my whole work possible.

Finally to my wife and my son:

Thank you for your help, support, understanding, and most importantly your love. I am more than happy that you are a part of me. Thank you so much!

Table of Content

Zusammenfassung	I
Abstract	II
Acknowledgement	III
1 Introduction	1
2 Theoretical Concepts	4
2.1 Fundamental thermodynamics	4
2.1.1 Cell Voltage	4
2.1.2 Capacity	8
2.1.3 Energy density in Li-Ion batteries	9
2.1.4 Power density in Li-Ion batteries	10
2.1.5 Current rate.....	10
2.1.6 Efficiency in Li-Ion batteries	11
2.2 Graphite, the state of the art anode material	11
2.3 Silicon: the new anode material of choice?	15
2.3.1 Electrochemical formation of lithium-silicon alloys.....	16
2.3.2 Lithiation and delithiation process of silicon at room temperature.....	17
2.3.3 Volume changes of silicon	20
2.3.4 Approaches to improve silicon containing active materials.....	21
2.4 Electrolyte	25
2.5 The electrode/electrolyte interface	29
2.6 SEI in silicon-based anodes	32
2.7 Electrolyte additives	35
2.8 Binder	38
3 Aim of the current work	41
4 A new LiNO ₃ based electrolyte formulation for Si/C-anodes with enhanced performance in Li-Ion batteries	43
4.1 . Introduction	43
4.2 . Experimental	45
4.3 . Results.....	47
4.4 Discussion	58
4.5 Conclusion	60
5 Solid Electrolyte Interphase in a beaker– New pretreatment method for improved Si/C-anodes in Li-Ion batteries.....	61

5.1 . Introduction	61
5.2 . Experimental	63
5.3 . Results.....	65
5.4 . Discussion.....	75
5.5 . Conclusion	77
6 Conclusion and outlook.....	78
6.1 Conclusion	78
6.2 Outlook	82
Appendix.....	83
A References	83
B List of Abbreviations	96
C List of Figures	99
D List of Tables	102
E Curriculum Vitae	103
F List of Publications	105
G List of Patents	105
H Eidesstattliche Versicherung	106

1 Introduction

Reducing the dependency on fossil fuels to decrease the amount of greenhouse gases is a key aspect to create a healthier and environmentally friendly society and minimizes the accelerated global warming which is believed to be in part a direct consequence of the increased emission of greenhouse gases like carbon dioxide (CO_2). Moreover, reducing the consumption of fossil fuels or natural gases are urgently needed due to the finite availability of e.g. oil and gas which could be consumed till the end of the century [1]. One important pathway to tackle the above mentioned problems is to electrify a vehicle's powertrain. To achieve this goal, one has to develop proper energy storage devices which are capable to reversibly store enough energy to power the vehicle for a certain time and distance. Energy storage devices such as rechargeable batteries are a key device to replace the common combustion engine by a fully or partly electrified powertrain. In particular, the Li-Ion battery gained much attention in recent years since it exhibits higher gravimetric and volumetric energy densities as well as cycle life than conventional battery technologies such as Ni-MH (Nickel-Metal Hydride) or Ni-Cd (Nickel-Cadmium) [2]. The Li-Ion battery is currently the state of the art energy storage device for portable electronic technologies and more and more dominates the market of electric and hybrid vehicles. However, the achievable energy densities are significantly lower compared to the energy densities of e.g. gasoline. To reduce this gap, a lot of research is dedicated to the investigation and characterization of new low cost, safe, and high performing rechargeable battery technologies. One way to achieve higher energy densities of Li-Ion batteries is the development of new materials exhibiting a higher voltage and lithium storage capability.

Basically, a Li-Ion battery cell is an electrochemical galvanostatic cell consisting of four main parts: the negative electrode (anode), the positive electrode (cathode), the separator, and the electrolyte. The electrolyte should be Li (lithium) conductive, electronically insulating, and connects the positive and negative electrodes. The two electrodes are capable of reversibly store Li^+ during the charging and discharging process. The positive electrode in current Li-Ion batteries typically consists of Lithium-Metal-Oxides as active material. In most cases, the applied electrolyte is a Li-salt dissolved in nonaqueous, aprotic, carbonate-based solvents. On the anode side, most Li-Ion battery cells use carbonaceous or graphite-based active materials. In recent years, the interest in the research and development of new active materials for the anode and cathode in Li-Ion battery cells has been increased significantly. Interesting candidates as new active materials on the anode are typically metals or semimetals which are able to electrochemically and reversibly form alloys with Li (lithium). These materials exhibit very high theoretical rechargeable capacities due to the higher amount of Li which

can be reversibly stored in alloys compared to the carbonaceous or graphite-like carbons which exhibit an intercalation based storage mechanism (graphite is the active material in anodes of state of the art Li-Ion battery cells). For example, silicon (Si) is able to store 3.75 Li atoms per atom of Si (in the form of the following composition: $\text{Li}_{15}\text{Si}_4$). The higher amount of Li that can be reversibly stored leads to a significantly increased theoretical gravimetric capacity of Si with $\sim 3578 \text{ mAh g}^{-1}$ compared to $\sim 372 \text{ mAh g}^{-1}$ for graphite.

In the literature, it is assumed that the main drawback of Si-based anode materials is the high volume expansion taking place during the lithiation and delithiation process which can be up to $\sim 280 \%$ compared to the original volume [3]. These volumetric changes can lead to several degradation processes e.g. strong mechanical strains, pulverization, loss of electrical contact between the different anode components, and to the current collector [3]. However, the effects of the volume changes on the stability and structure of the anode/electrolyte interface as well as the cycling stability in Li-Ion batteries are not fully understood. To tackle the above mentioned difficulties several research strategies have been reported to reduce the effects of the volume changes during the charge and discharge operation. Possible ways are the application of nanosized Si particles, new polymeric binder systems, special cycling conditions, and the use of different electrolyte compositions and additives to alter the interface properties. Yet, the reported results are still unsatisfactory and do not fulfill the requirements of an anode material in commercial Li-Ion batteries. Recent findings suggest that the main degradation mechanisms take place at the anode/electrolyte interface. During the operation of a Li-Ion battery the formation of a so called Solid Electrolyte Interphase (SEI) can be observed. The SEI usually results from decomposition products of the unstable electrolyte at low potentials which precipitate at the surface of the anode and subsequently passivate the negative electrode from the electrolyte. The SEI is necessary to prevent the continuous electrolyte decomposition during the cycling process. Nevertheless, it has the disadvantage that Li is irreversibly consumed during the formation process. Until today, only little is known about the SEI's influence in Si-based anodes on the electrochemical performance of a Li-Ion battery.

The aim of the present thesis is to gain more knowledge on how certain changes in the battery cell system influence the overall performance of Si/C-anodes and to find new ways to improve the cycling stability and capacity retention of these electrodes. In the first chapter, the specific electrochemical characteristics needed to understand battery operations are described. Moreover, the properties of graphitic carbon (C) and Si as possible anode materials are discussed and approaches that are described in the literature in order to increase the performance of Si-based anodes are introduced. One way to influence the SEI properties in

Li-Ion batteries is to alter the electrolyte solution because the SEI mainly consists of the decomposition products of the electrolyte. Therefore, a new electrolyte formulation has been developed which leads to a significant increase in cycling stability and capacity. These results are presented in chapter 4. Another approach that has been analyzed is the effect of a new electrochemical pretreatment procedure in a solution which only contains substances leading to a more stable anode/electrolyte interface. The results and effects of this approach on the performance and understanding of Si/C-anodes and its interface characteristics are described in chapter 5.

The obtained results in this thesis underline the strong influence of the interface properties on the cycling performance in Si-based anodes for Li-Ion batteries and present two possible pathways how the cycling performance and capacity retention could be increased for future Si/C-based anodes in commercial Li-Ion batteries.

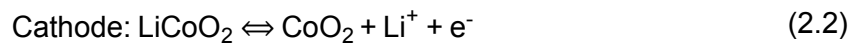
2 Theoretical Concepts

2.1 Fundamental thermodynamics

To provide a theoretical foundation for the understanding of the present work, this chapter will describe the fundamental thermodynamic and electrochemical relationships which are important to discuss Si/C-based anodes and Li-Ion batteries. This chapter aims at demonstrating how electrochemical parameters of Li-Ion batteries like cell voltage or energy density depend on and are influenced by thermodynamics and electrochemistry.

2.1.1 Cell Voltage

In a typical Li-Ion battery cell consisting of graphite and LiCoO_2 as anode and cathode active material the electrochemical reactions during the charging process can be written as follows:



The driving force in this electrochemical reaction is the difference of the electrochemical potential of the Li^+ (lithium ions) in the two electrodes. The difference in the chemical potential $\Delta\mu$ can also be described as the difference in the GIBBS FREE ENERGY (ΔG) of the formation of the products and reactants which can be written as:

$$\Delta\mu = \Delta G \quad (2.3)$$

The electrostatic energy of the charged species is given by $-z \cdot F \cdot U$ where z is the charge number of the ionic species ($z=1$ in case of Li^+), F is the FARADAY-CONSTANT (96485 C mol^{-1}), and U is the voltage or potential difference between the anode and the cathode [4, 5]. Under equilibrium or open circuit conditions, the chemical driving force equals the electrostatic driving force and no net current is flowing:

$$\Delta G = -z \cdot F \cdot U \quad (2.4)$$

$$U = \frac{-\Delta\mu}{z \cdot F} = \frac{-\Delta G}{z \cdot F} \quad (2.5)$$

Equation (2.5) displays that the equilibrium cell voltage is given by the differences in the chemical potentials of Li^+ in the anode and cathode. For a standard Li-Ion battery cell with $\text{LiCoO}_2/\text{LiC}_6$, the reduction potentials are 0.7 V and -2.9 V in reference to the standard hydrogen electrode (H_2/H^+). The resulting overall equilibrium cell voltage can be calculated:

$$U = -(-2.9 \text{ V} - 0.7 \text{ V}) = 3.6 \text{ V} \quad (2.6)$$

Apart from its influence on the equilibrium cell voltage, the chemical potential is also related to the activity of the ionic species in a Li-Ion battery cell where R is the gas constant ($8.314 \text{ J mol}^{-1} \text{ K}^{-1}$), a the activity of the ionic species, and μ_0 the standard chemical potential:

$$\mu = \mu_0 + R \cdot T \cdot \ln a \quad (2.7)$$

From this equation, the differences in the chemical potential of the two electrodes can also be related to the activity of the ionic species:

$$\mu_{\text{cathode}} - \mu_{\text{anode}} = R \cdot T \cdot \ln \left(\frac{a_{\text{cathode}}}{a_{\text{anode}}} \right) \quad (2.8)$$

With help of equation (2.8) and balancing with the electrostatic energy it becomes obvious that the equilibrium cell voltage is related to the activity of the Li^+ in the cathode and anode through the NERNST EQUATION:

$$U = - \left(\frac{R \cdot T}{z \cdot F} \right) \cdot \ln \left(\frac{a_{\text{cathode}}}{a_{\text{anode}}} \right) \quad (2.9)$$

Moreover, it results that the equilibrium cell voltage is also influenced by the temperature due to entropy changes at different temperatures. This relation is generally described by the GIBBS-HELMHOLTZ EQUATION [6]:

$$\Delta G = \Delta H - T \cdot \Delta S \quad (2.10)$$

$$\frac{dU}{dT} = -\frac{1}{z \cdot F} \left(\frac{d\Delta G}{dT} \right) = -\frac{1}{z \cdot F} \cdot (-\Delta S) = \frac{\Delta S}{z \cdot F} \quad (2.11)$$

The above presented equation describes the cell voltage under equilibrium conditions when there is no current flow and limits the maximum theoretical energy of a Li-Ion battery cell. Nevertheless, the situation changes if a current starts to flow. A flowing current leads to losses in the cell due to polarization effects accompanied by overpotentials which can mainly be divided in four different mechanisms [6]:

- *Ohmic drop* due to the internal resistance of the cell which is given by the sum of the internal resistances of the electrolyte, the electrodes, the resistances (R) at the electrode/electrolyte interfaces, and the contact resistances at the current collectors. The Ohmic drop is therefore proportional to the applied current and is described by $I \cdot R$. Additionally, the $I \cdot R$ drop leads to Joule heating of the cell.
- *Charge transfer polarization* which mainly occurs at the electrode/electrolyte interface
- *Concentration polarization* arising from the mass transport or diffusion limitation in the bulk electrolyte and electrodes. This leads to concentration differences between the reactants and products.
- Finally, the real cell voltage has to consider the different overpotentials at both electrodes arising due to mass transport limitations, charge transfer limitations, and ohmic drop. Therefore, the real cell voltage differentiates from the maximum theoretical cell voltage U_0 by:

$$U = U_0 - (\eta_{\text{cathode}} + \eta_{\text{anode}}) - (\eta_{\text{cathode}} + \eta_{\text{anode}})_{\text{mass transport}} - I \cdot R \quad (2.12)$$

In the following, the basic relationships between current and voltage in electrochemical systems will be described:

A simplified redox reaction always involves oxidized (O) and reduced (R) species.

The current-voltage relationship can be described by the TAFEL EQUATION where a and b are constants and η is the resulting overpotential:

$$\eta = a + b \log i \text{ and } i = \exp\left(-\frac{a}{b}\right) \exp\left(\frac{\eta}{b}\right) \quad (2.13)$$

In this equation, the current of the forward and backward reactions of the following redox reaction can be related to the concentration of the electroactive species through a geometric factor (A is the surface area of the given electrode) and rate constant for both reaction pathways (k_f and k_b):



$$i_f = n \cdot F \cdot A \cdot k_f \cdot C_O \quad (2.15)$$

$$i_b = n \cdot F \cdot A \cdot k_b \cdot C_R \quad (2.16)$$

Moreover the different rate constants can be written in the ARRHENIUS form as follows:

$$k_f = k_f^0 \cdot \exp\left(\frac{-\alpha \cdot n \cdot F \cdot \eta}{R \cdot T}\right) \quad (2.17)$$

$$k_b = k_b^0 \cdot \exp\left(\frac{(1-\alpha) \cdot n \cdot F \cdot \eta}{R \cdot T}\right) \quad (2.18)$$

The rate constants include the overpotential η that is relative to a general reference point. This means that k_f and k_b are rate constants that are related to the activation barrier for the oxidation and reduction process respectively. The factor α symbolizes the transfer coefficient which is between 0 and 1 and is directly related to asymmetries in the activation barrier of the standard free energies for electrochemical oxidation and reduction [6].

To estimate the rate constants, one can look at the equilibrium conditions with $\eta = 0$ and no net current flow ($i_f = i_b$). Moreover, the concentrations of the oxidized (C_{ox}) and reduced (C_{red}) species at equilibrium can be considered as equal. These boundary conditions lead to the following relationship for the rate constant and the standard rate constant (k^0):

$$k_f^0 \cdot C_{ox} = k_b^0 \cdot C_{red} \text{ or } k_f^0 = k_b^0 = k^0 \quad (2.19)$$

The situation changes under non-equilibrium conditions and the net current can be calculated by the BUTLER-VOLLMER EQUATION which is given by:

$$i = i_f - i_b \quad (2.20)$$

$$i = n \cdot f \cdot A \cdot k^0 \left(C_{Ox} \cdot \exp\left(\frac{-\alpha \cdot n \cdot F \cdot \eta}{R \cdot T}\right) - C_{red} \cdot \exp\left(\frac{(1-\alpha) \cdot n \cdot F \cdot \eta}{R \cdot T}\right) \right) \quad (2.21)$$

In the non-equilibrium case, the concentrations C_{ox} and C_{red} depend on the mass transport which is given by migration, convection, and diffusion due to concentration gradients. In the case of Li-Ion batteries with liquid electrolytes, the most important mass transport phenomenon is diffusion (with the diffusion coefficient D). It can therefore be described by FICK'S SECOND LAW [6]:

$$\frac{\delta C}{\delta t} = D \cdot \frac{\delta^2 C}{\delta x^2} \quad (2.22)$$

2.1.2 Capacity

The theoretical molar capacity of a Li-Ion battery and every other battery type is given by the quantity of electricity involved in the electrochemical reaction, where x is the number of moles of the electroactive species, n is the number of electrons transferred per mole during the reaction, and F is the FARADAY-CONSTANT (96485 C mol^{-1}):

$$Q_{\text{charge}} = x \cdot n \cdot F \quad (2.23)$$

The capacity is usually expressed by the specific weight or mass of the electroactive component (gravimetric capacity). In case of the gravimetric capacity, the mass of the electroactive component can be calculated and is given by the following equation

$$M = x \cdot M_r \quad (2.24)$$

M denotes to the mass of the electroactive species in the cell and M_r to the molecular mass of the same species. The unities of the gravimetric capacity are normally given by Ah kg⁻¹ or mAh g⁻¹ and are often called the specific capacity [4, 6]:

$$C_{\text{specific}} = \frac{n \cdot F}{3600 \cdot M_r} \quad (2.25)$$

The denoted mass may refer to the final Li-Ion battery mass including all inactive components as e.g. packaging, electrolyte, binder, current collectors etc. Nevertheless, in this work the specific capacities will always refer only to the mass of the electroactive species alone. By multiplying the specific capacity with the actual mass of the electroactive component, the so called “rated capacity” of a given Li-Ion battery cell is obtained. In a real Li-Ion battery cell, it is impossible to realize the theoretical full capacity due to the mass contributions of the before mentioned inactive components. Moreover, the electrochemical reactions taking place in the Li-Ion battery cell are always accompanied by losses due to unavailability of some active material, side reactions especially at the electrode/electrolyte interface, and losses along the electron conduction pathways.

Finally, it is worth mentioning that the capacity can strongly depend on the current rate applied for charging and discharging the Li-Ion battery cell due to the before mentioned overpotentials and ohmic losses which become more severe at higher current rates.

2.1.3 Energy density in Li-Ion batteries

In case of energy storage devices the term energy density refers to the energy per weight (gravimetric energy density) or energy per volume (volumetric energy density). The volumetric energy density is the energy that can be obtained per unit volume of the cell and is mostly given in Wh L⁻¹. The energy density strongly depends on the density of the components inside a Li-Ion battery cell as well as the design by which the different components and materials are assembled. The goal especially in consumer electronics or electric vehicles is an optimized energy density for a given volume and geometry while keeping the weight of the battery as low as possible. Another way to define the term energy density is through the so called “specific energy density” which is mostly denoted by Wh kg⁻¹. It can be described as the energy that can be achieved per unit mass of a cell. The “specific energy density” is the product of the operating cell voltage and the specific capacity and can be calculated by inte-

grating the product of the current I and voltage U over time:

$$E_{\text{specific}} = \int U \cdot I \cdot dt \quad (2.26)$$

The discharge time t is related to the maximum and minimum voltage threshold and strongly depends on these specific parameters: characteristics of the materials, the mixing properties, side reactions, irreversible processes, and availability of the active materials inside the electrode [6].

2.1.4 Power density in Li-Ion batteries

Besides the energy density another very important parameter of a battery cell, especially for automotive applications is the power density, which can also refer to the specific weight or volume. The gravimetric power density is the power that can be obtained per unit mass of the cell and is mostly presented in W kg^{-1} . The power of a battery itself can be calculated by integrating the cell voltage over current [6]:

$$\text{Power} = \int U \cdot dI \quad (2.27)$$

2.1.5 Current rate

The current rate (also known as C-rate) is defined as the current needed to fully charge or discharge a battery's nominal capacity in a certain amount of time. For example, in a battery with 1 Ah a current of 0.1 A is defined as C/10, because the battery needs ten hours to be fully charged or discharged. Higher C-rates are usually needed to achieve high power densities but at the same time the specific energy density is decreasing rapidly due to smaller capacities at higher C-rates. Mathematically, the C-rate can be described by the following equation [6]:

$$\frac{C}{x} = \frac{\text{Full capacity (Ah)}}{\text{hours}} = \text{current (A)} \quad (2.28)$$

2.1.6 Efficiency in Li-Ion batteries

In Li-Ion batteries, two different types of efficiencies can be defined: the energy efficiency and the coulombic efficiency (CE) [4, 6]. The energy efficiency is given by the fact that the energy needed to charge a Li-Ion battery can never be smaller than the amount of energy released by the battery during the discharge process which is a direct consequence of the second law of thermodynamics. The reason can be found in the presence of different overpotentials and side reactions (e.g. the formation of passivation layers like the SEI (Solid Electrolyte Interphase) on the electrode surface). The energy efficiency is defined as follows:

$$\text{Energy Efficiency} = \frac{\int U_{\text{dis}} \cdot dq_{\text{dis}}}{\int U_{\text{ch}} \cdot dq_{\text{ch}}} \quad (2.29)$$

The second important efficiency in Li-Ion batteries is the coulombic efficiency (CE) which is defined by the proportion of the charge Q transferred during the charge (Q_{ch}) and discharge (Q_{dis}) process. The CE is in most cases much closer to 100 % compared to the energy efficiency because it does not take the cell voltage and possible overpotentials into account:

$$\text{Coulombic efficiency} = \frac{Q_{\text{dis}}}{Q_{\text{ch}}} \quad (2.30)$$

The CE is an important parameter in the evaluation of new battery components like active materials, binders, or electrolytes since it displays the efficiency of a battery cell to reversibly store Li^+ and, in addition, it effectively shows the consequences of side reactions or other irreversible processes [6].

2.2 Graphite, the state of the art anode material

Today's commercial Li-Ion batteries often vary in the choice of the cathode active material e.g. there are companies which prefer LFP (Lithium-Iron-Phosphate), NMC (Lithium-Nickel-Manganese-Cobalt-Oxide), NCA (Lithium-Nickel-Cobalt-Aluminum-Oxide), or LiCoO_2 (Lithium-Cobalt-Oxide), depending on the area of application [7]. In contrast almost all suppliers choose graphite or graphitic carbon as the anode active material for secondary Li-Ion batteries. In the following, I will describe the reasons why graphite is commonly used as anode

material. Moreover, an insight in its chemical lithiation behavior is provided. Prior to the description, I will shortly point out the three main requirements a material should possess to be considered as a good candidate as an anode material in Li-Ion batteries:

- The potential of the lithiation and delithiation should be very low against Li/Li^+ to achieve a high cell voltage
- The number of Li^+ that can be reversibly stored should be high in order to achieve a high gravimetric and volumetric capacity
- The material should be structurally stable for a large number of lithiation and delithiation cycles in order to assure a long-lasting battery cell.

Until today, graphite is the material which properties and characteristics show the best agreement with the above mentioned requirements. There are hundreds of known carbon modifications like natural and synthetic graphite's, active carbons, glassy carbons, or cokes. Dahn et al. have distinguished different classes of carbons which can be used in Li-Ion batteries. Moreover, a description of the advantages of graphitic carbon as the anode active material is given [8]. In short, the main reason for graphite to be the anode material of choice can be found in its structure: Graphite crystallizes in a layered lattice consisting of sp^2 hybridized C atoms which form a planar network with hexagonal symmetry [9]. A schematic graphite structure can be seen in Figure 1.

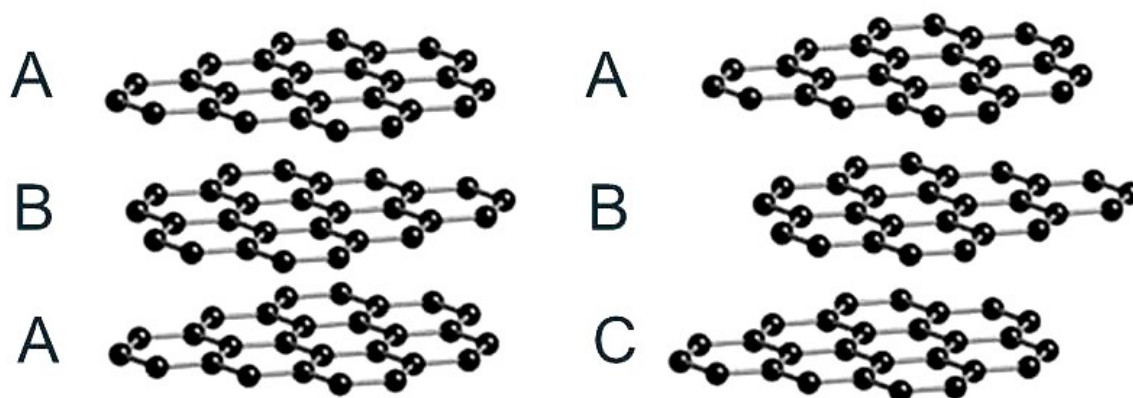


Figure 1: Comparison between the hexagonal (ABA) and rhomboedric (ABC) modification of graphite with the respective stacking order of the graphene layers (adapted and modified from [9]).

Under and above the planar layers, delocalized p_z -orbitals have a maximized charge density which leads to a three dimensional configuration of interacting π -electrons and VAN-DER-WAALS interactions [10]. Figure 1 additionally depicts the two naturally abundant graphite

modifications. Especially the hexagonal modification is strongly used as the active material in anodes for Li-Ion batteries. The differences between the two modifications can be found in the stacking order of the different graphene layers. In addition to the before mentioned hexagonal modification in which the different graphene layers following an alternating ABA stacking order, one can also find graphite with a rhomboedric structure. This modification has an additional C layer that is shifted from A and B and leads to an ABC stacking order [11, 12]. Both structures enable graphite to reversibly store Li^+ between the different graphene layers which is often described as ROCKING-CHAIR mechanism in the literature [13].

During the electrochemical intercalation of Li^+ between the different graphene layers different, specific LiC_y -compounds are formed, with the highest lithiated phase being LiC_6 . Simultaneously, the layer distance between the different graphene layers increases during the lithiation process about ~10 %. The lithiation and delithiation process only takes place via the prismatic plane (arm-chair and zig-zag faces) and leads to changes in the stacking sequence from ABA to AAA which means that in the case of the lithiated graphite the different graphene layers are not shifted against each other, which can be seen schematically in Figure 2 [14].

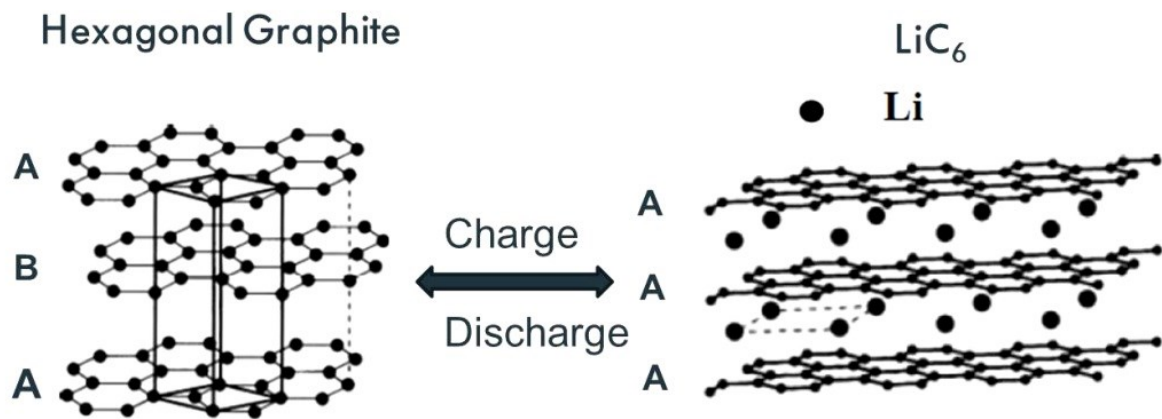


Figure 2: Change of the ABA stacking order in hexagonal graphite to an AAA stacking order due to the intercalation of Li^+ [14].

A significant phenomenon during the electrochemical Li^+ intercalation in graphite is the step-wise formation of periodic alignments of unoccupied graphene layers. In the literature, this phenomenon is described as stage formation [15]. The stage formation is a thermodynamic process which depends on the energy required to expand the VAN-DER-WAALS-GAPS and to overcome the repulsive interaction of the different Li_xC_6 -layers [14]. The stage formation can

be observed during the electrochemical reduction of graphite in a Li-Ion containing electrolyte. Figure 3 shows the relationship between the electrochemical potential and the formation of the different intercalation steps (compounds) during the galvanostatic reduction of graphite to LiC_6 .

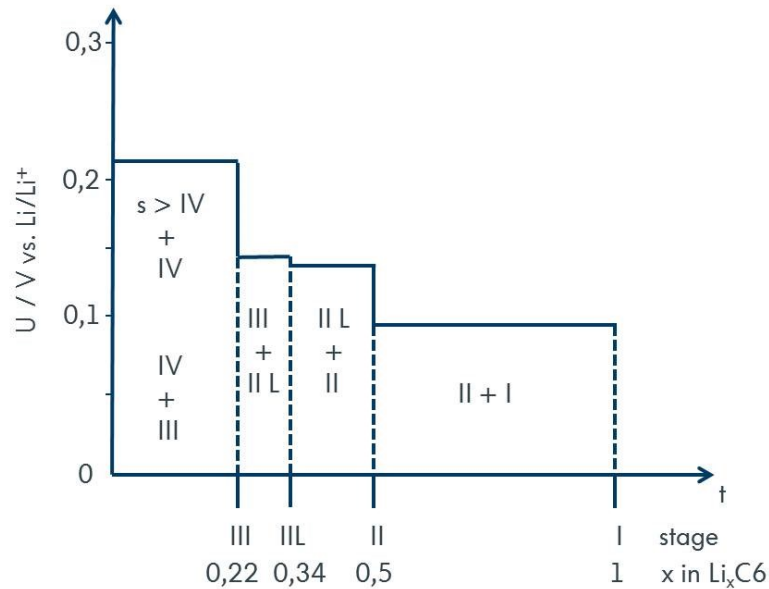


Figure 3: Schematic representation of the different intercalation steps of Li^+ into graphite depending on the potential U vs. Li/Li^+ and the molar fraction x of Li in Li_xC_6 (adapted and modified from [14]).

The different plateaus describe two coexisting Li_xC_6 phases which resemble the different intercalation steps and Li_xC_6 compounds. During the electrochemical intercalation of Li^+ into graphite, four different steps are known which are labeled as $s = \text{I, II, III, and IV}$. The first step starts at a potential of ~ 0.21 V vs. Li/Li^+ until the complete transformation to $\text{Li}_{0.22}\text{C}_6$ has occurred. In the following, three different steps with different Li_xC_6 composition can be observed until the final LiC_6 compound is formed at potentials of < 0.1 V vs. Li/Li^+ . The phenomenon can be experimentally observed during galvanostatic and potentiostatic measurements of the Li^+ intercalation into graphite electrodes. However, one should mention, that usually no sharp boundary between the different stages can be observed, because the packing densities of the different Li_xC_6 compounds are slightly different. Experimentally, the complete lithiation of graphite will not be reached at potentials < 0.1 V vs. Li/Li^+ which is due to side reactions that increase the resistance of the anode e.g. the SEI formation [16, 17].

One of the main reasons for the stability of the graphite anodes over thousands of

charge/discharge cycles is the relatively small volume expansion of only ~10 %, which enables the graphite to be mechanically stable during the repeating cycling steps. Furthermore, the low Li^+ intercalation potential leads to the formation of a SEI on the graphite surface. In the following cycles, the SEI protects the graphite from solvent cointercalation which can lead to the exfoliation of graphite [18-20]. Moreover, a stable SEI slows down the proceeding decomposition of the electrolyte due to reduction reactions at the graphite surface at low potentials [21].

2.3 Silicon: the new anode material of choice?

In order to increase the capacity and energy density of future Li-Ion batteries, there is a great demand of new anode and cathode materials that are able to store more Li^+ reversibly and have a good cycling stability at the same time. One material that shows promising characteristics to replace graphite as the anode material in Li-Ion batteries is Si. The comparison of the main parameters of different possible anode materials is summarized in Table 1.

Table 1: Comparison of the different characteristics between different possible active materials in anodes for Li-Ion batteries (adapted from [22]).

Material	Li	Si	C	Sn	Ge	Al	Sb	Bi	Mg
Density	0.53	2.33	2.25	7.29	5.32	2.7	6.7	9.78	1.3
Lithiated phase (Li_xM)	-	3.75	0.167	4.4	4.4	1	3	3	3
Volumetric capacity (mAh cm^{-3})	2047	8336	837	9786	8639	2681	7246	3765	4355
Specific capacity (mAh g^{-1})	3862	3578	372	994	1624	993	660	385	3350
Potential (U vs. Li/Li^+)	0	0.4	0.05	0.6	0.3	0.3	0.9	0.8	0.1
Volume Change (%)	100	280	12	260	300	96	200	215	100
Abundance in Earth crust	34 th	2 th	10 th	47 th	51 th	3 th	62 th	68 th	7 th

Si is the second most abundant element in the earth crust with a portion of ~26 wt. %. The high availability together with its exceptional volumetric and specific capacity as well as its relatively low insertion and deinsertion potential vs. Li/Li^+ make Si a promising candidate in replacing graphitic carbon as a future anode material in rechargeable Li-Ion batteries [22-26]. The replacement of graphitic carbon or at least the addition of a certain percentage of high capacity Si materials to obtain Si/C-anodes would considerably increase the capacity of future Li-Ion batteries [23]. Moreover, the low working potential would lead to an increase in gravimetric and volumetric energy density which is needed to increase the driving range of electric vehicles or the run duration of consumer electronics (laptops, selfphones, etc.). In this PhD thesis, the focus lies on the investigation of Si/C-based anodes for Li-Ion batteries. In the following chapters, the electrochemical alloying and dealloying process of Si with Li as well as the drawbacks and problems that have to be overcome to incorporate Si/C-based anodes into Li-Ion batteries for commercial applications will be described.

2.3.1 Electrochemical formation of lithium-silicon alloys

The reaction of Li to form various Li/metal alloys is a well-known process and has been reported for several different elements. However, only five of them have been intensively studied: Si, Sn, Sb, Al, and Mg. The main reasons for the focus on these materials are their low cost, abundance, and environmental compatibility (compare Table 1) [22, 27, 28].

In 1976, Sharma et al. demonstrated for the first time that Si can electrochemically form alloys with Li at higher temperatures [22]. In later works, Huggins and Wen showed that during this lithiation process several crystalline lithium silicides ($\text{Li}_{12}\text{Si}_7$, Li_7Si_3 , $\text{Li}_{13}\text{Si}_4$, and $\text{Li}_{22}\text{Si}_5$) are formed. These compounds follow a distinctive Li-Si (lithium-silicon) equilibrium phase diagram. According to the phase diagram and coulometric titration experiments at 415 °C, $\text{Li}_{22}\text{Si}_5$ is the highest lithiated phase, with a calculated theoretical capacity of ~4200 mAh g^{-1} [29, 30]. However, several studies have revealed that the formation of Li-Si alloys at room temperature show different results compared to the results obtained at higher temperatures and it is an open debate, if $\text{Li}_{15}\text{Si}_4$ is the highest lithiated phase with a specific capacity of 3578 mAh g^{-1} [31-33].

2.3.2 Lithiation and delithiation process of silicon at room temperature

Generally the reaction of Li with a metal like Si is divided into two different groups which differ in their reaction mechanism: a.) *solid-solution reactions* and b.) *addition reactions* [34-36]. In both types of chemical reactions, the reaction equation can be generally expressed as:



In the case of a *solid-solution reaction*, no phase or structural change of the reacting metal framework occurs during the reaction with Li. In an *addition reaction*, the phase structure of the lithiated metal is different from the phase structure of the unreacted metal. This means that the reaction includes a phase change from M to LiM_x .

The lithiation and delithiation process of crystalline Si or other metals such as crystalline Sn, Al, or Sb can be considered as an *addition reaction* [37, 38]. In the case of crystalline Si the electrochemically induced lithiation takes place via a two-phase mechanism in which pure crystalline Si is consumed to form amorphous lithiated Si. Both phases are separated by a reaction front of a few nanometers [37-39]. This two-phase reaction mechanism is due to the high activation energy needed to break the very stable Si framework. To weaken the strong Si-Si bonds, a high concentration of Li at the reaction front is needed which additionally leads to an enhanced reaction kinetic [40]. The described amorphous Li_xSi_y -phase has a very high lithium content with $x=3.4 \pm 0.2$ Li atoms per Si atom. This leads to very high capacities but is also the main reason for the high volume expansion of the material during the electrochemical reaction. An additional effect of the massive volume changes is a high gradient and transformation strain of the material which weakens the structural integrity of the Si [41].

At room temperature the first electrochemical lithiation of crystalline Si follows a two-phase reaction. This behavior can also be observed in the voltage profile of a Si/Li half-cell in Figure 4 (solid line). The voltage profile shows a relatively flat and long plateau starting around ~0.1 V vs. Li/Li^+ which results from the long coexistence of the amorphous lithiated Si-phase ($\text{a-Li}_x\text{Si}_y$) and the still unlithiated crystalline Si-phase. This behavior differs strongly from the voltage profile which can be observed at higher temperatures. Figure 4 displays that significant Li_xSi_y -phases are present which result in different sharp steps in the voltage profile (dashed line). The reason for the different voltage profiles lies in the electrochemically induced solid-state amorphitization of the crystalline Si which results in metastable $\text{a-Li}_x\text{Si}_y$ -phases instead of the distinctive equilibrium Li_xSi_y -phases which are kinetically hindered to form at room temperature due to a higher GIBBS FREE ENERGY [29, 30, 38].

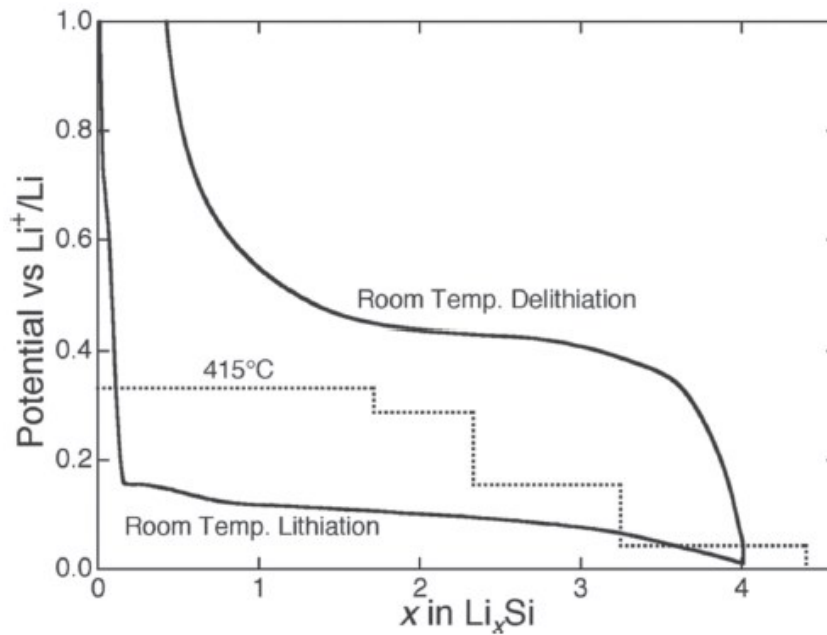


Figure 4: Voltage profile vs. Li/Li^+ for the first electrochemical lithiation and delithiation of crystalline Si at room temperature and its influence on the formation of different Li_xSi compounds (solid line). For comparison reason the dashed line indicates the formation of the different Li_xSi compounds at 415 °C (sharp steps indicating the phase transitions) [38].

From the equilibrium phase diagram proposed by Wen and Huggins, $\text{Li}_{22}\text{Si}_5$ should be the highest lithiated phase. However, as mentioned above until today it is not fully clarified if this phase can be formed during an electrochemically induced lithiation process at room temperature. For example, Weydanz et al. found by X-ray diffraction (XRD) experiments at room temperature $\text{Li}_{21}\text{Si}_5$ to be the highest lithiated phase which corresponds to $\sim 4020 \text{ mAh g}^{-1}$ [42]. These findings are inconsistent with results of Obravac et al. who also studied the structural changes during the lithiation process of crystalline Si by ex-situ XRD and Hatchard et al. who conducted in-situ XRD measurements [31, 43]. They found that at potentials below 50 mV vs. Li/Li^+ the highly lithiated $\alpha\text{-Li}_x\text{Si}_y$ phase suddenly crystallizes to a crystalline $\text{Li}_{15}\text{Si}_4$ phase and no higher lithiated phases like $\text{Li}_{22}\text{Si}_5$ or $\text{Li}_{21}\text{Si}_5$ could be observed. Furthermore, they found that this phase was formed even if they use amorphous Si as the anode active material. It is important to mention that this crystallization could only be observed for micrometric particles and films $> 2 \mu\text{m}$ and is not reported for thin films or Si nanoparticles which have been used in this work [43, 44].

Different Solid-State-NMR studies of Key et al. helped to gain more insight into the structural modifications of the Si during the lithiation and delithiation process [40, 41]. By analyzing the changes of the ^7Li -NMR shifts at different potentials vs. Li/Li^+ , they were able to draw conclu-

sions concerning the chemical environment of the Li^+ in the vicinity of different Si atoms. They proposed that the beginning of the lithiation process occurs at around ~ 0.11 V vs. Li/Li^+ and as the lithiation process proceeds, different Si-clusters, Si-chains, Si-rings, and Si-dumbbells form (details shown in Figure 5)

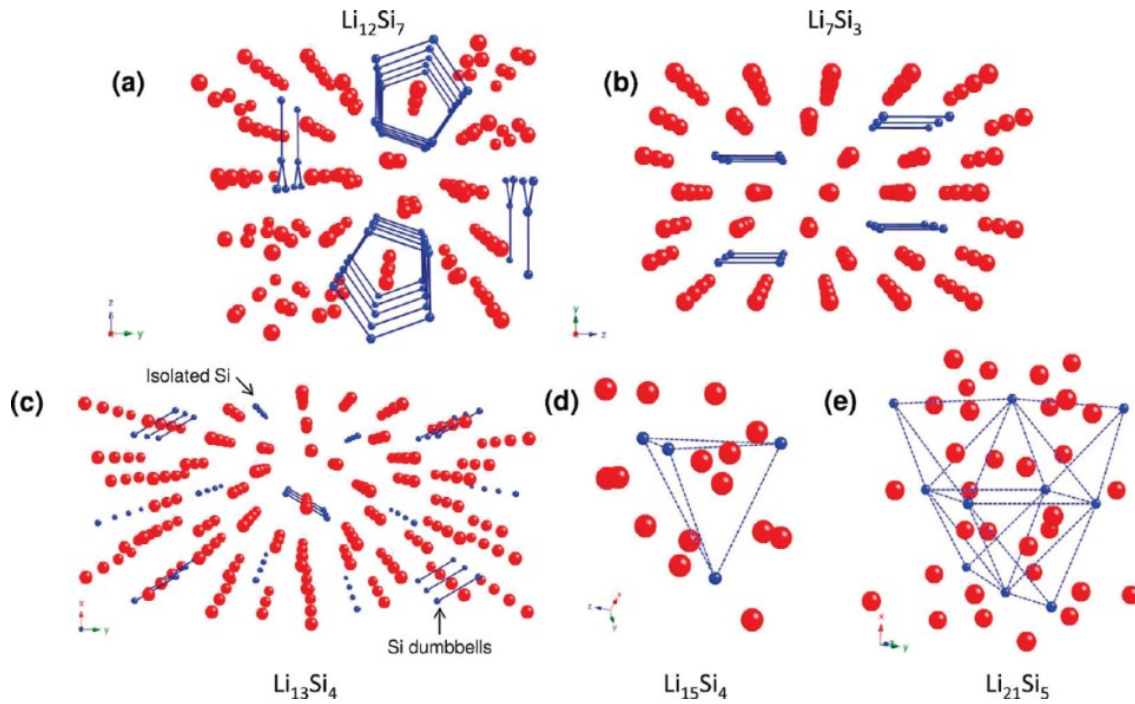


Figure 5: The different phases and structures proposed during the lithiation of Si. The structures were concluded from ^7Li -NMR measurements and include Si-clusters, chains, rings, and dumbbells [41].

As mentioned in chapter 2.3.2, during the lithiation process of Si the tetrahedral Si-network is destroyed and Si-bond breaking occurs. Density functional theory (DFT) calculations of Kim et al. explain the destruction of the originally intact diamond structure of Si by an energetically more favorable negative mixing enthalpy for Li_xSi_y alloys. They additionally calculated a Li-Si alloy with ~ 70 atm. % Li to be the most stable. Moreover, they found that the state of charge of the Li-atoms during the whole lithiation process is almost constant (+0.8) while the state of charge of the Si-atoms strongly varies during the lithiation process (between -0.5 and -3.3) [45]. These theoretical results are an explanation for the formation of different amorphous Li_xSi_y phases during the lithiation and delithiation process with ZINTL-character which have been observed and reported by several research groups [46, 47].

In addition, Wan et al. performed first-principles-calculations which showed that higher lithiated Si ($x > 0.1875$ in Li_xSi) lead to the permanent breaking of several Si-bonds. Consequently, the permanently broken Si-bonds are responsible for the amorphitization of the Si during the first lithiation process [48]. Furthermore, it has been reported that during the delithiation

process from Li_xSi to pure Si no reconversion to crystalline Si occurs which means that the Si remains amorphous after the first lithiation. Figure 6 schematically shows the different structural changes that occur during the first and second lithiation and delithiation of micrometric Si [49].

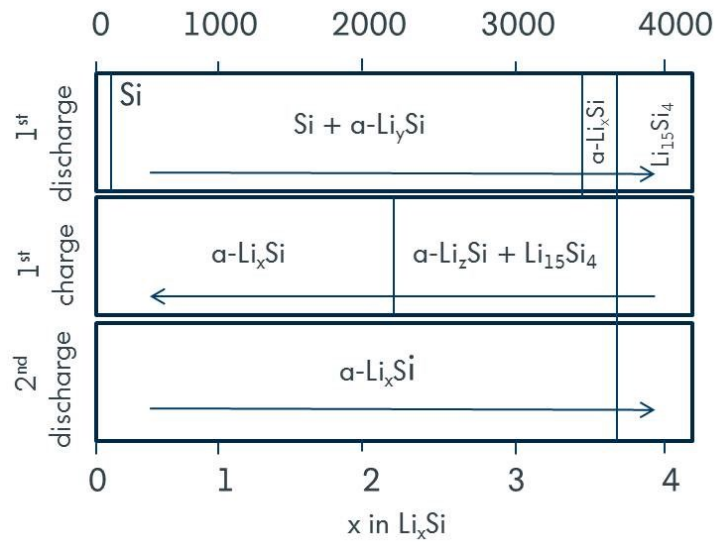


Figure 6: Schematic representation of the structural changes and existing and co-existing phases that occur during the lithiation of micrometric Si (adapted from [49]).

2.3.3 Volume changes of silicon

In the literature, it is assumed that the main problem in using Si-based active materials in anodes for Li-Ion batteries is the enormous volume change of the Si during the lithiation and delithiation. This volume change can be up to 280 % and may result in the pulverization of the electrode, electrical insulation of certain electrode areas, and contact loss to the current collector [26, 50-53]. The continuous volume changes of the Si do not only have an influence on the stability of the electrode framework but also have an influence on the stability of the before mentioned SEI on the surface of the anode. Li is taking part in the formation of the SEI which means that during this process some of the Li is irreversibly consumed [32, 54]. Furthermore, the continuous volume change of Si can cause the formation of new uncovered surface area due to cracks, pulverization, or morphology change of the Si accompanied by additional SEI formation leading to an increased irreversible capacity of the battery [55].

2.3.4 Approaches to improve silicon containing active materials

It is expected that the high volume change of Si during the lithiation and delithiation is the main reason for the strong capacity decay and low cycling stability of pure Si. In the following, different approaches that have been reported in the literature to address this problem will be presented:

The positive effect of Si nanoparticles with particle sizes <100 nm have been reported by Li et al. in the late 1990s [44]. The improved results for nanoparticles on the cycling performance and capacity retention, compared to micrometric particles may be explained by two major reasons:

- a.) The diffusion length of Li^+ is much shorter in Si nanoparticles which leads to a faster lithiation and delithiation and also to a better charge transport [22, 54].
- b.) Nanoparticles can mitigate effects of the volume expansion more effectively compared to bulk materials because they can sustain higher stress and strain and do not crack as easily as micrometric particles. Liu et al. described a critical size of <150 nm under which no fracture of the particles could be observed [56].

Kim et al. made experiments on the optimized particle size for Si nanoparticles. They found that the reversible specific capacity of Si nanoparticles with an average particle size of ~10 nm showed the best results compared to Si particles with 5 nm and 20 nm average particle sizes. However, the highest coulombic efficiency (CE) was found for the 20 nm Si nanoparticles. One explanation for the results is that nanoparticles ≤ 5 nm have a stronger tendency to form agglomerates. The reason for the better CE of the 20 nm particles compared to the 10 nm particles could be explained by the smaller specific surface area of the 20 nm particles [57]. The smaller surface area leads to less SEI formation on the surface of the Si during the cycling process.

Another improvement could be achieved by using amorphous Si nanoparticles instead of crystalline Si particles because amorphous Si materials do not undergo the irreversible phase transition during the first lithiation and delithiation cycle. Additionally, amorphous Si nanoparticles show an isotropic volume expansion compared to the anisotropic volume changes in crystalline Si materials which is also believed to have a positive effect on the morphological stability of Si during the lithiation and delithiation process [58, 59].

Excellent results for Si-containing anodes have been reported by using Si thin films which can be produced by e.g. Chemical Vapor Deposition (CVD) or RF-magnetron sputtering.

Takamura et al. were able to deposit a 50 nm Si thin film on Ni-foil that retained a specific capacity of $\sim 2000 \text{ mAh g}^{-1}$ for more than 1000 cycles. However, they also found that an increase in the film thickness leads to a rapid decay in the cycling stability (Si films with $1.8 \mu\text{m}$ thickness could retain 2000 mAh g^{-1} only for 50 cycles) [60]. The poor performance of thicker Si films can be explained by longer Li^+ -diffusion path length, an increased electrical resistance, and an increased mechanical strain during cycling.

Moreover, it is reported that also the roughness of the current collector has a big influence on the performance of thin films. Lee et al. reported that rough Cu-foil show better results compared to flat and smooth Cu-foil due to a better adhesion between the thin films or active particles and the current collector [61].

Another successful approach to improve the performance of Si materials is to nanostructure the morphology. For example, Cui et al. investigated the effects of Si nanowires and nanofibers. These materials allow a fast Li^+ -transport and an anisotropic volume change due to its one-dimensional morphology [52, 62, 63].

The same group reported results of hollow Si nanofibers which have been prepared by electrospinning of a Polyacrylonitril solution (PAN) followed by a carbonization step of the PAN and subsequently CVD deposition of Si. After this procedure, the inner C-core was removed due to another annealing step. This procedure leads to an additional formation of SiO_x on the Si outer surface which afterwards forces the volume expansion into the hollow space of the nanofibers leading to an excellent cycling performance of 6000 cycles [64]. Unfortunately, one-dimensional materials are usually very expensive to manufacture and additionally show only a moderate volumetric energy density.

Another promising material design has been reported by Yao et al. who synthesized hollow interconnected Si nanospheres which show a good performance of 700 cycles with a high capacity of 1387 mAh g^{-1} and a high CE. The good results have been explained by a better compensation of the volume expansion of the Si due to the hollow structure of the material [65].

In summary, all the described Si nanostructures still show a volume expansion which affects the overall performance of the battery. However, it is proposed that due to the different nanostructures the volume changes can be better controlled and active pulverization and contact loss can be slowed down. Nevertheless, the drawbacks in nanostructuring active materials are that they are usually expensive to manufacture and that they exhibit a high overall surface area which leads to the formation of more SEI and consequently to higher irreversible capacity especially in the first few battery cycles. Moreover, the volumetric energy density is reduced because only a small portion of the given volume is filled out with active material and a lot of space is empty to compensate the volume changes [66].

Another approach to enhance the performance and cycling stability of Si containing anodes is to use matrix materials in which Si is dispersed. The role of the matrix material is to minimize or to buffer the volume change during the electrochemical reaction of Si with Li. A positive effect could be a decreased agglomeration of the active material, especially when nanoparticles are used [67]. Essential properties of the matrix material should be a fast transport of electrons and Li^+ as well as a stabilizing effect on the electrode framework. Matrix materials can be divided between inactive and active materials which differ in the ability to additionally store Li^+ reversibly during the charging and discharging process.

Anodes containing inactive matrix materials usually consist of active particles (e.g. Si particles) and electrochemical inert matrix materials like metals (e.g. Fe, Cu, and Ni), metal oxides (e.g. Al_2O_3 and Co_3O_4), or ceramics (e.g. TiC) [67-75]. The application of matrix materials shows a positive effect on the volume expansion and a more stable cycling performance due to the buffer effect. Additionally, an increased electronic conductivity of the anodes can be achieved depending on the matrix materials applied. The main disadvantages are usually the decreased gravimetric as well as volumetric specific capacity which leads to a minor energy density of the battery. Therefore, it is very important to use an inactive matrix material which is light, mechanically stable, and ionically and electronically conductive, to increase the kinetics of the electrochemical processes [67, 68].

In anodes containing active matrix materials, both, the active material (e.g. Si particles) and the matrix material can reversibly store Li^+ during the charging and discharging process of the anode. The basic idea of this concept is to minimize the effects of the volume changes during the lithiation and delithiation process while maintaining as much gravimetric and volumetric capacity as possible. Practically, this can be achieved by using a material combination with different lithiation and delithiation potentials. For example, Yan et al. report that a Mg_2Si -system has a positive effect on the cycling performance due to a lithiation and delithiation at different potentials vs. Li/Li^+ [76]. Nevertheless, most investigations focus on active materials containing Sb and Sn as the primary component [77-81].

An approach that has often been described is the incorporation of C into the electrode. In the literature, a variety of different Si/C materials are presented that range from C coated with Si, Si coated with C, and mechanically mixed Si and C powders [44, 82-85]. To obtain the different Si/C materials, different techniques have been applied as e.g. CVD with SiH_4 , carbonization of different organic precursors, ball-milling, and the mixing of pure powders to obtain the electrode slurry [86-90].

The development of the discussed anode materials targets an increased electrochemical performance, an enhanced electronic conductivity of the total electrode composite, and a positive effect on the stability of the electrodes due to an effective compensation of

the volume changes during charging and discharging.

A different approach to increase the cycling stability of Si-based anodes that goes without a change to the different components in the electrode is to control the charge and discharge potential range in which the Si-based anodes are cycled. By controlling the charge and discharge cut-off voltages, one has the ability to control the depth of lithiation and delithiation.

In the case of Si-based anodes this method has the advantage that the degree of volume changes and particle agglomeration can be controlled simultaneously by adjusting the cut-off voltage [44, 91]. The positive effect of a higher cut-off voltage during the lithiation of Si on the anode cycling stability has been reported by several research groups. Results by Obravac et al. lead to the conclusion, that cut-off voltages <50 mV vs. Li/Li^+ result in a spontaneous transformation of the amorphous Li_xSi_y -phase to a crystalline $\text{Li}_{15}\text{Si}_4$ -phase. This transformation leads to a strong increase of the internal stress inside the material which consequently results in a decreased cycling stability [51]. Nevertheless, recent studies suggest that this transformation only occurs in micrometric particles and not in nanoparticles with particle sizes <150 nm [56].

Moreover, Li et al. could show a strong improvement of their Si-based anodes by lowering the delithiation cut-off voltage from 2 V to 0.8 V vs. Li/Li^+ . The drawback of this approach is that lowering of the cut-off voltage decreases the specific capacity of the used active material because the depth of lithiation and delithiation is significantly reduced [49]. For example Jung et al. reported a decrease of the specific capacity of the Si-based anode from 3000 mAh g^{-1} to 400 mAh g^{-1} by changing the lithiation cut-off voltage from 0 V to 0.2 V vs. Li/Li^+ [58].

Nevertheless, the approach seems to be promising especially for materials like Si which exhibit a high specific capacity going hand in hand with a high volume expansion. The reason for this is that only a fraction of the theoretically available capacity can still lead to a significant increase of the overall capacity of the battery cell (see Figure 7 [26]). However, it is important to emphasize that the restriction of the cut-off voltages will lead to a smaller overall cell voltage of the battery which results in a smaller energy density. This makes clear, that adjustments of the cut-off voltages have to be done carefully to find a good compromise between increased cycling stability and decreased energy density.

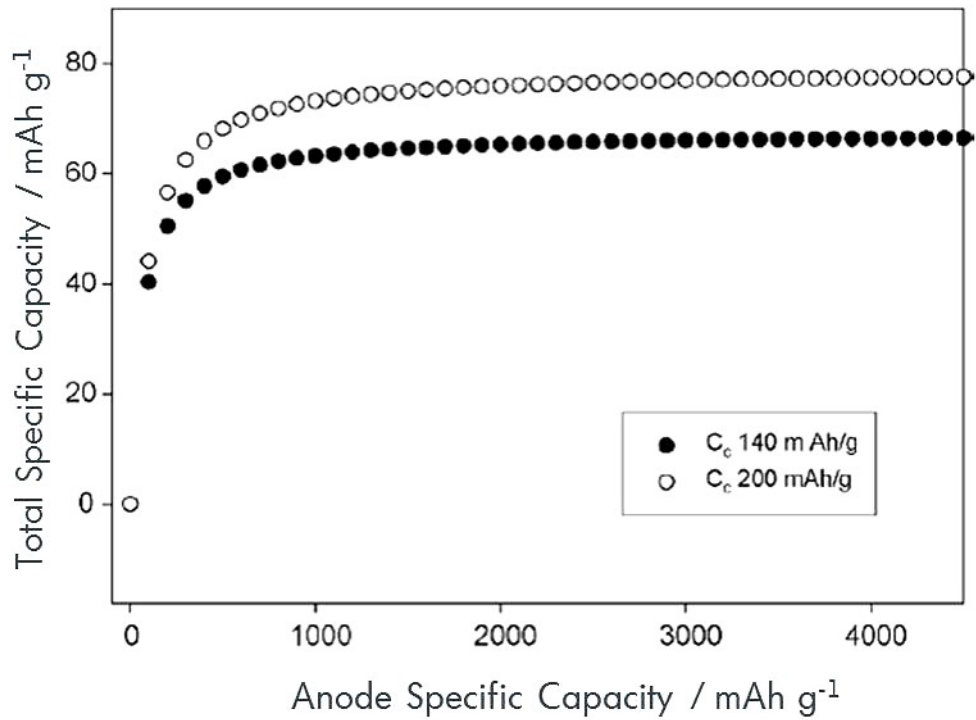


Figure 7: Relationship of the total specific capacity of a Li-Ion battery cell with a constant cathode specific capacity as a function of the specific anode capacity [26].

2.4 Electrolyte

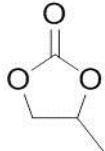
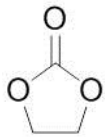
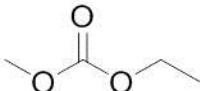
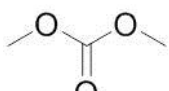
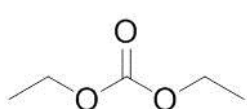
The electrolyte is the connecting component between the anode and the cathode in a Li-Ion battery. Most electrolytes used in commercial Li-Ion battery cells are liquid in the temperature range of operation. In this work, liquid electrolytes are used exclusively. Therefore, the following specifications are mainly valid for liquid electrolytes. However, it is worth mentioning that also polymer or solid-state Li^+ -conductors exist.

The main task of the electrolyte is to ensure the conduction of Li^+ between both electrodes. Moreover, the electrolyte provides the separation between the negative and positive electrode (together with the separator). The chemical and physical properties of the electrolyte have a strong influence on the battery performance and, in particular, on the electrode/electrolyte interface characteristics. Most electrolytes that are currently in use are liquids and consisting mainly of two parts: the solvents and the solved Li-salt. An ideal solvent should possess the following properties [92, 93]:

- The ability to dissolve the Li-salt in high concentrations (high dielectric constant ϵ)
- A low melting point (T_m) and a high boiling point (T_b), to be liquid in a wide temperature range
- A low viscosity which enables a faster Li^+ -transport
- Nontoxic, economically friendly, and a high flash point (T_f) for a safe and nonflammable battery cell

Until today, the solvents, which meet the requirements to a large extent, are cyclic or linear carbonates like propylene carbonate (PC), ethylene carbonate (EC), diethyl carbonate (DEC), dimethyl carbonate (DMC), or ethylmethyl carbonate (EMC). The different specific physical and chemical characteristics of the most commonly used solvents for battery electrolytes are given in Table 2.

Table 2: Structure and physical and chemical properties of typical solvents in liquid electrolytes for Li-Ion batteries [92].

Solvent	Structure	η (cP) (25 °C)	ϵ (F m ⁻¹)	T_m (°C)	T_b (°C)	T_f (°C)	ρ (g cm ⁻³)
PC		2.53	64.92	-55	240	132	1.200
EC		1.9 (40 °C)	89.78	37	248	160	1.321
EMC		0.65	2.958	-14.5	107	23	1.006
DMC		0.59	3.107	-2-4	90	18	1.063
DEC		0.75	2.805	-43	126	31	0.969

The characteristic properties of the solvents clarify that one solvent alone cannot fulfill all the requirements needed such as high conductivity, low viscosity, and acceptable T_m , T_b , and T_f . Therefore, battery manufactures and electrolyte producers prefer mixtures of different solvents. These mixtures mainly consist of a cyclic carbonate (e.g. EC) and one or more linear carbonates (e.g. DEC, DMC, or EMC) to combine the high dielectric constant of cyclic carbonates with the low viscosity of linear carbonates [92].

The other important component of a battery electrolyte is the dissolved Li-salt. The Li-salt should have a high solubility and a high mobility of the solvated ions in the solvents. The most commonly used Li-salts for Li-Ion batteries are aprotic compounds such as Lithiumhexafluorophosphate (LiPF_6), Lithiumtetrafluoroborate (LiBF_4), Lithiumhexafluoroarsenate (LiAsF_6), or Lithiumperchlorate (LiClO_4). From these salts, LiPF_6 is the most commonly used salt in commercialized Li-Ion batteries. The reason for this does not lie in its outstanding conductivity or thermal stability but in the best combination of the above mentioned properties [94, 95]. The most important physical and chemical characteristics of typical Li-salts are presented in Table 3.

Table 3: Physical and chemical properties of certain Li-salts for application in electrolytes for Li-Ion batteries [92].

Salt	M (g mol ⁻¹)	T _m (°C)	σ^*	T _{decom.} (°C)
			(mS cm ⁻¹) in EC/DMC	
LiPF₆	151.9	200	10.7	65-80
LiBF₄	93.9	293	4.9	>100
LiAsF₆	195.9	340	11.7	>100
LiClO₄	106.4	236	8.4	>100

The mixture of the Li-salt with the solvent(s) forms the actual electrolyte being responsible for the transport of Li^+ between the electrodes. An important requirement of such an electrolyte solution is a wide electrochemical window which can be understood by an energy diagram of a Li-Ion battery cell. In Figure 8 the schematic energy diagram of a Li-Ion battery cell is shown. The chemical potential of the Li^+ in the cathode and anode are given by $\mu_{\text{C(Li)}}$ and $\mu_{\text{A(Li)}}$ respectively and are noted against the Li/Li^+ reference potential. E_C and E_A are the redox potentials of the electroactive species in the cathode and anode and ΔE is the energetic bandgap between the HOMO (Highest Occupied Molecular Orbital) and LUMO (Lowest Unoccupied Molecular Orbital) of the electrolyte. To avoid a continuous decomposition of the

electrolyte during the operation, ideally the redox potential of the anode (E_A) and the cathode (E_C) fall in the window or bandgap between the HOMO and LUMO of the electrolyte. On the anode side, the chemical redox potential (E_A) is typically very close to the reference energy level of Li/Li^+ which is necessary to obtain a high overall cell voltage. On the cathode side, the chemical redox potential is strongly dependent on the applied cathode material. An ideal electrolyte should have its LUMO level at ~ 0 V vs. Li/Li^+ and its HOMO level higher than the chemical redox potential of the cathode material in order to provide a high stability throughout a wide potential range of the Li-Ion cell [92]. This relationship for an ideal electrolyte can be described by the following equation:

$$\text{OCV} = \mu_{\text{C(Li)}} - \mu_{\text{A(Li)}} \leq \Delta E \quad (2.32)$$

In real batteries, the HOMO requirements are most often fulfilled since the cathodic limit is generally around 4.5 V vs. Li/Li^+ . Only for new high voltage materials, the electrolytes can be oxidized at potentials > 4.5 V vs. Li/Li^+ [96].

The situation differs at the anode where the LUMO of the electrolyte is mostly around 1.4–0.8 V vs. Li/Li^+ [92]. From this it follows that E_A is lower in energy or higher in potential than the LUMO of the electrolyte which results in the reductive decomposition of the electrolyte at the interface between the anode and the electrolyte [92, 97]. This process and its consequences will be discussed in more detail in chapter 2.5.

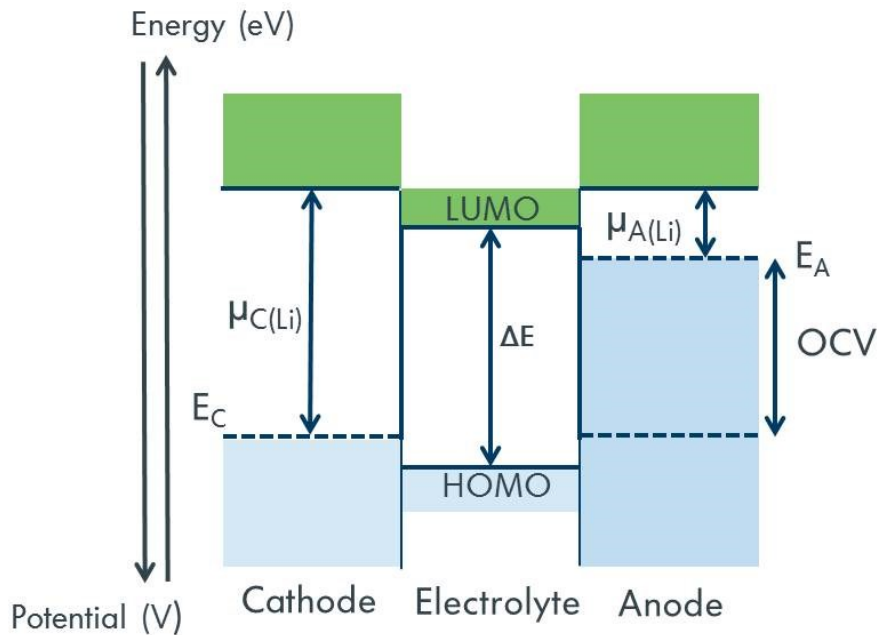


Figure 8: Energy and potential diagram of the electronic HOMO and LUMO states in the cathode, electrolyte, and anode of a schematic Li-Ion battery cell (adapted from [93]).

In addition to the thermodynamic requirements, a good electrolyte should have low toxicity, low cost, almost no electronic conductivity, a high Li^+ -conductivity, stability at extreme conditions (thermal abuse, mechanical, and electrical stability), and the feature of being chemically inert towards other cell components like current collectors, separators, or the packaging material. Ideally, the reaction products of the electrolyte components are not flammable to increase the safety of a Li-Ion battery cell [98, 99].

2.5 The electrode/electrolyte interface

In the previous chapter 2.4, the characteristics and requirements for electrolyte solutions in Li-Ion batteries were discussed and, moreover, the possible decomposition of the electrolyte was described with respect to the working potential of the electrodes being either higher or lower than the HOMO or LUMO of the electrolyte. Nevertheless, even though the Li-Ion cell is thermodynamically not stable at certain conditions, a standard Li-Ion cell still achieves several years of service life. This leads to the conclusion that the electrodes possess a certain kinetic stability towards the electrolyte solution. The main reason for the kinetic stability in Li-Ion batteries is the formation of a solid layer at the surface of both electrodes (anode and cathode). Its formation normally takes place during the first few charging and discharging cycles of the Li-Ion cell due to the decomposition of the electrolyte. It is believed that some products of these reactions are not soluble in the electrolyte and precipitate at the surface of the respective electrode. The formed layer was first described by Peled et al. in 1979 and is called the Solid Electrolyte Interphase (SEI). It is believed to be electronically insulating and ionically conducting which leads to a slowdown of the electrolyte decomposition in the following cycles [100]. Furthermore, the charge and discharge processes are not significantly inhibited because Li^+ can still diffuse through the layer into the respective electrode. The formation of such a stable interface layer proved to be crucial in Li-Ion battery cells for the proper operation over several years.

The SEI on graphite-based anodes gained much attention in recent years and has been intensively studied. The research mainly focused on the formation mechanism, the morphology, and composition [101-103]. The analytical investigation proved to be difficult as its sensitivity towards air and water make it difficult to handle the samples properly. Nevertheless, it was tried to analyze the SEI by several analytical tools such as X-ray Photoelectron Spectroscopy (XPS), Fourier Transformation Infrared Spectroscopy (FTIR), Secondary Electron Microscopy (SEM), Energy Dispersive X-ray Diffraction (EDX), Transmission Electron Mi-

croscopy (TEM), Solid-State-NMR, Raman Spectroscopy, or Mass Spectroscopy (SIMS, TOF-SIMS). Based on these analyses, the SEI is mainly composed of carbonates, lithium salts, lithium oxides, polymeric compounds, and lithiumalkoxides [104-107]. Generally, the SEI formation process at the C/electrolyte interface starts during the first Li^+ -insertion into the anode host. As mentioned above, during this first charging process, the anode reacts with the electrolyte which subsequently decomposes and thereby forms the solid passivation layer on the surface of the C-based electrode. The instability of the electrolyte results from the very low operating voltage of the C-based anode in Li-Ion cells and it is generally reported that the formation process starts at potentials $<1.4\text{-}0.8\text{ V vs. Li/Li}^+$ [92].

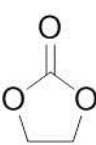
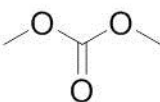
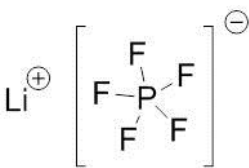
For C-based anodes it is reported, that the SEI covers the electrode completely and, gradually, it reaches a certain critical thickness during the first few battery cycles that leads to a good electronic insulation between the electrode and the electrolyte resulting in an improved electrolyte stability in the following cycling. The continuous dissolution/deposition of the SEI especially during the charge and discharge step has often been reported [104, 105]. In case of anodes containing graphite or graphitic carbon, the SEI is a crucial component since it prevents the cointercalation of solvent molecules as well as solvated Li^+ between the graphite sheets. The solvation shell is stripped off at the SEI during the Li^+ -intercalation. The cointercalation of solvent molecules and solvated Li^+ has to be prevented because it can lead to the exfoliation of graphite [108, 109].

The composition of the SEI on the surface of the C-based anodes result from three different reaction categories: reduction of the solvents, reaction of the Li-salt, and side reaction with impurities of the electrode and electrolyte. As described above, the composition of the SEI has been characterized by a variety of different analytic techniques. Yet, the difficulties in the sample preparation as well as the difficulties in studying the SEI formation in-situ lead to a great uncertainty in the exact composition of the SEI. Furthermore, the composition strongly depends on parameters like temperature, storage time, cycling parameters, formation process, electrolyte composition, type of C, type of conductive additive, the binder used in the electrodes, and the impurity concentrations [104, 106]. Hence, the observed deposition and dissolution as well as the reported changes in the SEI thickness and composition after a different number of cycles or storage time state that the SEI is a very complex and dynamic system, which need further investigation.

In chapter 2.4, it was described that the main solvents in electrolytes for Li-Ion batteries are either cyclic or linear carbonates. The following Table 4 displays examples for possible proposed reaction schemes for EC and DMC as an example for cyclic and linear carbonates and possible reactions for the Li-salt LiPF_6 [105, 107, 110, 111]. These components are used in commercially available Li-Ion batteries and give an overview on the variety of proposed

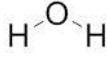
SEI products and were also applied in the electrolytes of the PhD thesis.

Table 4: Possible reactions taking place for EC, DMC, and LiPF₆ during the SEI formation process at the anode/electrolyte interface [105, 107, 110, 111].

 <p>EC</p>	$(\text{CH}_2\text{O})_2\text{CO} + 2\text{e}^- + 2\text{Li}^+ \rightarrow \text{Li}_2\text{CO}_3 + \text{C}_2\text{H}_4$
	$2(\text{CH}_2\text{O})_2\text{CO} + 2\text{e}^- + 2\text{Li}^+ \rightarrow (\text{CH}_2\text{OCO}_2\text{Li})_2 + \text{C}_2\text{H}_4$
 <p>DMC</p>	$\text{CH}_3\text{OCO}_2\text{CH}_3 + \text{e}^- + \text{Li}^+ \rightarrow \text{CH}_3\text{OCO}_2\text{Li} + \text{CH}_3^\bullet$
	$\text{CH}_3\text{OCO}_2\text{CH}_3 + \text{e}^- + \text{Li}^+ \rightarrow \text{CH}_3\text{OLi} + \text{CH}_3\text{CO}_2^\bullet$
 <p>LiPF₆</p>	$\text{LiPF}_6 \rightarrow \text{LiF} + \text{PF}_5$
	$\text{LiPF}_6 + n\text{e}^- + n\text{Li}^+ \rightarrow \text{LiF} + \text{Li}_x\text{PF}_y$
	$\text{LiPF}_6 + \text{Li}_2\text{CO}_3 \rightarrow 3\text{LiF} + \text{POF}_3 + \text{CO}_2$

The reactions displayed in Table 4 show only a small portion of possible and reported reactions forming the SEI and do not include secondary reactions or side reaction with impurities. The most common and influential impurities in Li-Ion batteries are hydrofluoric acid (HF) which is a byproduct of the LiPF₆-synthesis process and a byproduct of certain primary reactions taking place with LiPF₆, and water (H₂O). The impurities can induce a variety of possible reactions with either the original electrolyte components or with the SEI components formed during primary reactions. Table 5 displays a few examples of proposed reactions taking place with the impurities HF and H₂O [21, 104, 112]. Note that the proposed reaction table and the resulting SEI components are not complete. Table 5 provides an overview about the possible reaction types and resulting SEI components.

Table 5: Possible reactions of H₂O and HF in Li-Ion battery cells which could contribute to the SEI formation on the anode surface [21, 104, 112].

	$\text{LiPF}_6 + \text{H}_2\text{O} \rightarrow \text{LiF} + \text{POF}_3 + 2\text{HF}$
	$\text{H}_2\text{O} + \text{Li}^+ + \text{e}^- \rightarrow \text{Li}_2\text{O} + \text{H}_2$
	
H₂O	$\text{H}_2\text{O} + \text{Li}^+ + \text{e}^- \rightarrow \text{LiOH} + \frac{1}{2} \text{H}_2$
	$\text{ROCO}_2\text{Li} + \text{H}_2\text{O} \rightarrow \text{Li}_2\text{CO}_3$
<hr/>	
	$\text{Li}_2\text{CO}_3 + \text{HF} \rightarrow 2\text{LiF} + \text{H}_2\text{CO}_3$
	$\text{ROCO}_2\text{Li} + \text{HF} \rightarrow \text{LiF} + \text{ROCO}_2\text{H}$
HF	$\text{Li}_2\text{O} + \text{HF} \rightarrow 2\text{LiF} + \text{H}_2\text{O}$

2.6 SEI in silicon-based anodes

In the previous chapters, the possible problems and challenges resulting from the huge volume changes during the alloying and dealloying of Si with Li were described. The volume changes do not only increase the requirements for the material stability but they also affect the SEI stability formed at the Si/electrolyte interface. As described in chapter 2.5, the electrolyte is continuously reduced if the SEI has not grown to a certain thickness or the SEI is not dense enough. The continuous electrolyte decomposition can lead to a growth of the SEI which in turn could result in slower Li⁺-diffusion. It can be noted that a mechanically stable SEI is favorable for a good cycling performance of Si-based anodes. Yet, it is believed that the large volume changes drastically raise the stability requirements of the SEI formed at the Si/electrolyte interface. However, despite the huge impact of the interface in Si-based an-

odes on the cycling performance, the investigations of the formation process, composition, and morphology of the SEI are rare. Most studies concerning the SEI in Li-Ion batteries are conducted on either C or Li surfaces.

The difficulties in characterizing the SEI are comparable to those described in chapter 2.5. Consequently, the analytic methods to gain more insights into the SEI on Si are basically the same (FTIR, XPS, TOF-SIMS, NMR, SEM, and EIS) [113, 114]. These characterization techniques do not give the exact composition of the SEI which leads to the conclusion that the SEI formation, morphology, and composition are even less understood than the SEI on C or Li. The SEI compounds reported at the Si/electrolyte interface are Li_2CO_3 , Li_2O , LiF , Phosphates, Alkoxides (ROLi), lithium alkyl-carbonates (ROCO_2Li), Poly(ethylene oxides) (PEO), Oxalates and, Fluorophosphates (Li_xPF_y) [115-117]. It should be emphasized that this list only provides an overview of the reported species of the SEI in Si-based anodes and is not a general and conclusive list.

The results of these studies show similar SEI compositions on Si compared to the SEI compositions on pure C or Li. Nevertheless, Chan et al. and Kasavajjula et al. suggest that the SEI on Si-anodes should be significantly different from the SEI formed on graphite negative electrodes. They describe two main reasons for the proposed differences [26, 116]:

- The Si surface is believed to be more reactive than graphite resulting in a different SEI composition including hydrocarbons or Li-silicates
- The huge volume change of Si during alloying and dealloying with Li causes crack formation in the SEI which results in the exposure of uncovered Si surface to the electrolyte. This process is again accompanied by further undesired electrolyte degradation and side reactions.

The existing results led to a proposed model of the SEI which depicts an inner inorganic and an outer organic layer, which is schematically shown in Figure 9 [112, 114]. Additionally, it was reported that the SEI on Si strongly depends on the applied voltage with an increased SEI growth at lower potentials [114]. In general, the SEI composition will be influenced by the same factors described in chapter 2.5. It is important to note that the effects of the huge volume expansion on the morphology of the SEI or possible side reactions are so far not fully understood.

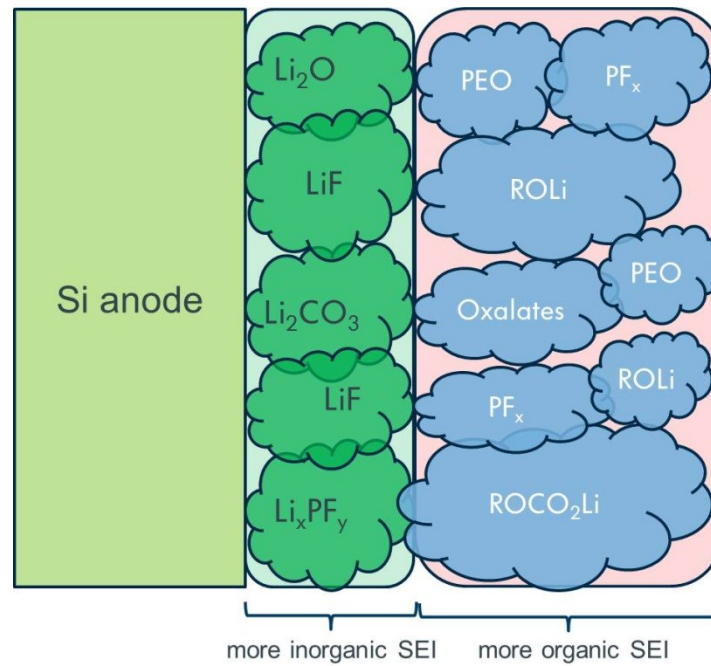


Figure 9: Schematic representation of the proposed SEI model in Si-based anodes, consisting of an inner part which is more inorganic and an outer part which is more organic [116, 118].

Another aspect that is still under debate in the description of the SEI on Si-based anode systems is the role of the SiO_2 or SiO_x native layer on the surface of the Si materials and the effect of surface functional groups (e.g. Si-OH) on the reactions and formation of the SEI on Si surfaces. The reaction of SiO_2 with Li during the first lithiation step has been described and investigated in several studies but it is not clear how these reactions influence the SEI or if these reactions can be described as part of the SEI formation process on Si surfaces. The following reaction equations give an overview about the reported reactions taking place between SiO_2 and Li during the first lithiation process [119-121]:



The above mentioned aspects can be crucial for a profound understanding of Li-Ion batteries with Si or Si/C-based anodes and need further investigation.

2.7 Electrolyte additives

Electrolyte additives are chemical compounds added to the electrolyte solution. The amounts are typically in the range of 0 to 20 wt. %. The aims of electrolyte additives in a battery cell are usually improved cycling performance, enhanced lifetime, reduced impedance as well as higher safety. Broussely et al. investigated the long-term stability of Li-Ion cells that were tested over several years [122]. Their findings reveal that detrimental reactions at the anode due to an unstable and growing SEI lead to an increased impedance followed by a severe ageing of the cells. Moreover, the results display that the use of certain additives (in this case vinylene carbonate (VC)) can drastically improve the cycling performance of the cell. Furthermore, Zhang reviewed the different functionalities of electrolyte additives and classified the additives in the following categories [123]:

- *SEI forming additives* should facilitate the formation of the SEI on the surface of the negative electrode
- *LiPF₆-salt stabilizer* should enhance the thermal stability of LiPF₆ against the organic electrolyte solvent
- *Cathode protection agents* should effectively passivate the surface of the positive electrode to inhibit oxidative electrolyte decomposition and active material dissolution
- *Safety protection agents* should lower the flammability of organic electrolytes and provide overcharge protection, and terminate the battery operation in abuse conditions
- *Li-deposition improver* should reduce the Li-plating especially on the anode surface
- *Other* not classified additives can also have the aim to enhance the ionic solvation, reduce the Al-corrosion of the cathode current collector, or act as wetting agent and viscosity diluter for the electrolyte

In chapter 2.5 and 2.6, the needs for a stable SEI have been explained in detail. One way to influence the stability of the SEI is the addition of certain chemical compounds to the electrolyte solution which influence the SEI formation at the anode/electrolyte interface.

Generally, these additives can be described as compounds producing either a polymeric film or insoluble byproducts during their decomposition which finally can precipitate at the anode surface. It is assumed that one requirement for a good SEI forming additive is a higher reduction potential compared to the solvents reduction potential used in the electrolyte since this will lead to an increased reactivity of the additives at the anode surface [92, 123].

In the literature, a variety of chemical compounds have been proposed as SEI forming additives [124, 125]. In case of Si-based anodes the most prominent are vinylene carbonate (VC) and fluoroethylene carbonate (FEC). In case of VC, several studies reported improvements of the cycling performance of graphite systems and suggested that the decomposition of VC can lead to the formation of polymeric chains by a radical polymerization process which involves its double bond [126]. The resulting SEI is assumed to have a better mechanical stability and a more effective protection of the electrolyte from the electrode. Moreover, Dalavi et al. stated that the amount of LiF (lithium fluoride) on the anode surface is decreased if VC is used as an additive [124]. Finally, Chen et al. described the resulting SEI to be more uniform [127].

Another prominent film forming agent for Si-based anodes is FEC. The resulting SEI is reported to be thinner, smoother, and mechanically and chemically more stable compared to the SEI formed without FEC. Moreover, it was confirmed that a thinner SEI with a high amount of LiF is formed which contradicts the before mentioned results from Dalavi et al., who proposed a more stable SEI if less LiF is present [125, 128, 129]. Etacheri et al. describe a strong formation of polycarbonates in the presence of FEC formed by HF elimination and polymerization [115]. The contradictory results point out that the exact functionalities of the additives are not fully understood. Nevertheless, Figure 10 presents the two most commonly accepted decomposition reaction pathways for FEC.

Finally, both, VC and FEC, have shown to form a more stable SEI which directly leads to an increased cycling performance for Si-based anodes in Li-Ion batteries. In the literature, a variety of chemical compounds have been investigated as SEI forming additives [124, 130]. However, since the variety of possible compounds is almost endless, this chapter focuses on the most prominent and effective additives described in the literature.

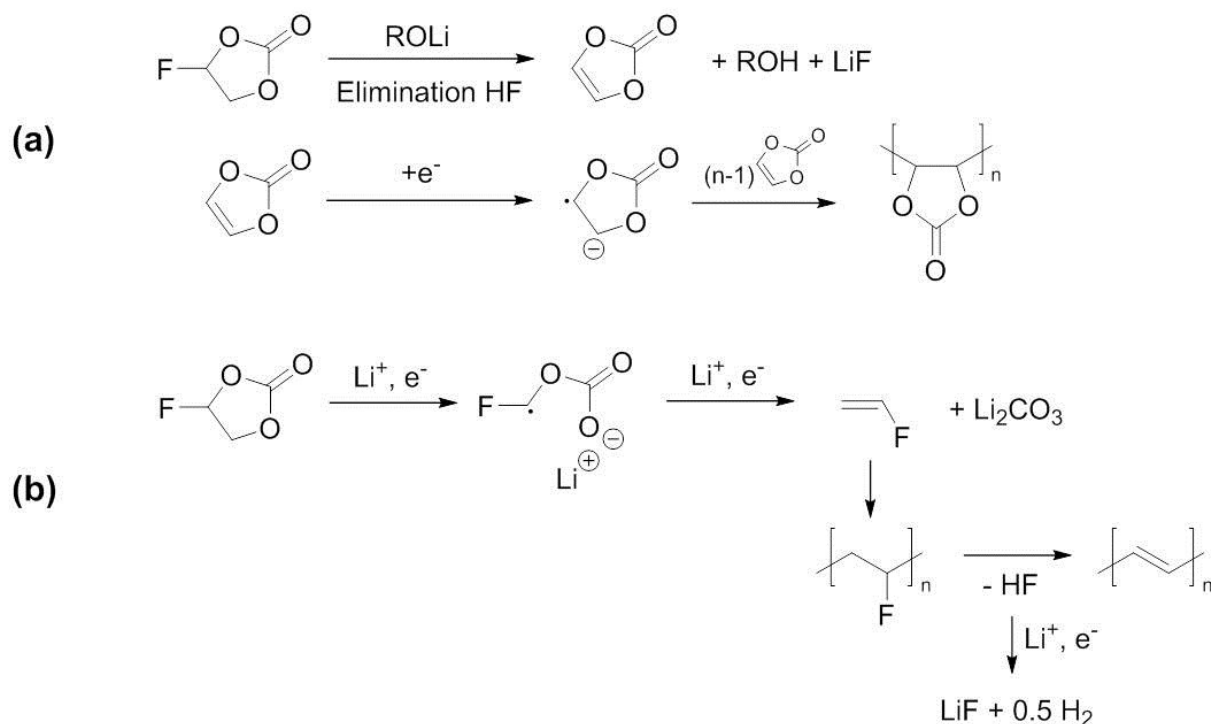


Figure 10: Proposed decomposition reaction of FEC in Li-Ion battery cells, during the SEI formation process [128].

Besides using VC and FEC as film forming additives another way to improve the SEI formation is to use a different Li-salt or a mixture of two different Li-salts. Lithium(bis)oxalate borate was proposed by Choi et al. and Dalavi et al. to improve the capacity retention and cycling performance of Si-based anodes [124, 131]. The resulting SEI is reported to be less porous and has a higher content of semi-carbonates which should lead to an improved passivation of the anode surface. Figure 11 displays the proposed reductive reaction pathway by Xu et al. of LiBOB to form more stable SEI on anodes in Li-Ion batteries [92]

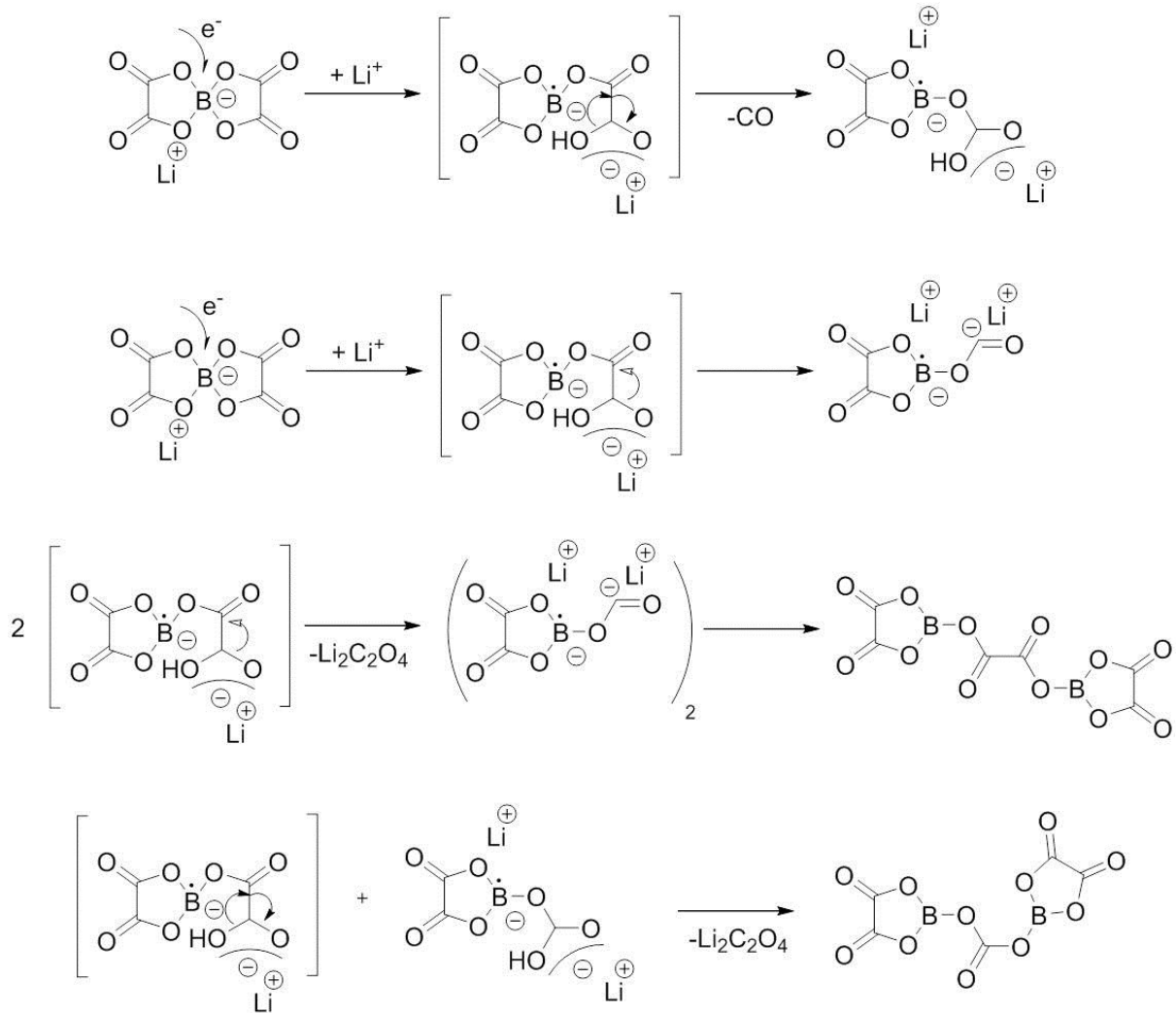


Figure 11: Proposed decomposition process of LiBOB during the SEI formation process on the surface of the anode in Li-Ion batteries [92].

2.8 Binder

Another important parameter which can influence the performance of Si-based anodes is the type of binder used in the electrode framework. Results from the literature lead to the assumption that the requirements for a binder in Si-based anodes are dramatically raised due to the high volume changes of the Si-active material during charging and discharging. The repeating volume changes of the Si can cause the binder to fail, resulting in a loss of electronic contact and a drastic increase in impedance and decrease in capacity retention [132, 133]. In graphite anodes, usually polyvinylidene fluoride (PVDF) is the binder of choice. However, a first study by Liu et al. in 2005 showed the failure of the conventional PVDF binder in Si-based anodes. In this study, they introduced a mixture of styrene butadiene

rubber (SBR) and sodium carboxyl methyl cellulose (CMC) as a binder system which demonstrated significantly superior results compared to the PVDF binder [134]. Choi et al. proposed polyamide imide as a new binder for Si-based anodes and demonstrated an improved cycling stability and coulombic efficiency compared to PVDF [135]. In the literature, the superior performance of these binders is often explained by increased mechanical and thermal properties as well as a stronger interaction between the binder and the Si-OH groups on the native SiO_x surfaces of the Si materials.

Two different mechanisms for the interaction between the binder and the Si material are mentioned:

- Hochgatterer et al. describe the binding process as a condensation reaction between the binder and the Si particles by esterification [136].
- Birdel et al. display results which lead to a different interaction model explained by hydrogen bonding between the Si-OH groups on the Si surfaces and the carboxyl functional group of CMC [137].

It is assumed that these processes strongly depend on the pH-value of the solution and an increased reaction rate will take place in a more acidic pH. The latter process implies a self-healing binding process in which the broken hydrogen bonds can reform at a different place of the Si surface. The proposed interaction between the Si surface and the binder functional group could explain the enhanced ability of these binders to withstand the strong volume changes of Si much better than PVDF binders [137-139].

The assumption that a chemical bonding between the active material and the binder has a positive influence on the cycling stability, cycle life, and the specific capacity of an electrode led to the development of new binder materials such as Polyacrylicacid (PAA) [140]. It is assumed that the above described binding to the active material is also valid in the case of PAA-based binders. The results support this assumption and the PAA increased the performance of Si or Si/C-anodes.

Another work by Kovalenko et al. underlined the positive effect of a higher concentration of carboxyl functional groups. In this study, the authors were able to extract sodium-alginate and use this compound as a binder in Si-based anodes. The prepared electrodes showed an excellent cycling stability of ~2000 mAh g⁻¹ for 100 cycles [141].

A different approach that was described in the literature is the development of electronically conductive binder materials in order to reduce the necessary amount of conductive additives inside the electrode which would result in lower weight and higher gravimetric capacity and energy density of the cells [142]. Liu et al. developed three polymers which were electronical-

ly conductive even at very low potentials <1 V vs. Li/Li^+ . The goal of this work was to control the LUMO-energy of the polymer by the addition of certain functional groups. The presented binders were based on a fluoropolymer and the developed structures were PFFO (poly-9,9-dioctylfluorene) and PFFOMB (poly-(9,9-dioctylfluorene-co-fluorene-co-methylbenzoic-acid)). The two functional groups influencing the electronic LUMO-states of the polymers are C=O and methylbenzylester- PhCOOCH_3 -groups. The presented results showed an increased performance, especially for Si/PFFOMB composite electrodes with a specific capacity of 2000 mAh g^{-1} after 650 cycles at a low charge and discharge current of $\text{C}/10$ [142].

In conclusion, the reported results from the literature show a strong influence of an adequate binder system in Si-based anode materials on the overall performance of the battery cell. The application of PVDF, which is the standard binder system in graphite electrodes, failed to be suitable for Si-based anodes. Binders with carboxylic functional groups seem to stabilize the performance by a direct interaction between the Si surface and the binder functional groups. Hence, in this work all the presented results are based on Si/C-anodes using a PAA-binder.

3 Aim of the current work

The aim of this thesis is to provide new insights on the improvement of the cycling stability and capacity retention in Si/C-anodes for Li-Ion batteries and to gain a better understanding of the main degradation processes. Moreover, this thesis tries to present new approaches to influence the anode/electrolyte interface and to increase the performance of Si/C-based anodes. The following chapters will describe the experimental measurements and results to reach the above mentioned goals.

Chapter 4 describes the systematic creation of a new electrolyte formulation for Si/C-based anodes with higher specific capacity, better capacity retention, and higher cycling stability. The new electrolyte shows an impeded SEI growth throughout cycling compared to the SEI formed in a standard electrolyte solution which is assumed to be a key parameter in obtaining higher performances in Si/C-anodes. Other aspects that are analyzed in this chapter are:

- The comparison of the cycling stability of various electrolyte compositions with a reference electrolyte solution and development of a new electrolyte formulation with enhanced cycling stability and specific capacity
- Microstructural characterization of the interface morphology and composition by a detailed SEM- and EDX-analysis on the Si/C-anode surfaces cycled in the new and the reference electrolyte after a different number of cycles as well as the correlation of these results with the electrochemical performance

Chapter 5 describes a new pretreatment method for Si/C-based anodes prior to the actual cycling process to form a primary SEI on the Si/C-anode surface upon the actual cycling procedure. This chapter displays the importance and positive effect of a stable SEI on the long term cycling stability of Si/C-based anodes. It investigates the effects of this method on the SEI growth, cycling stability, and the capacity retention. Finally, this chapter deals with the following aspects:

- Differences in the charge/discharge performance for long-term cycling in the same electrolyte solution for pretreated and non-pretreated Si/C-anodes
- Analysis of the effects of the pretreatment procedure on the SEI growth and composition by SEM, EDX, and FTIR measurements.

Chapter 6 discusses the obtained results and gives an outlook for possible future research topics to improve the performance of Si/C-based anodes in Li-Ion batteries.

4 A new LiNO_3 based electrolyte formulation for Si/C-anodes with enhanced performance in Li-Ion batteries

Authors: Janis Dölle, Mirko Herrmann, Gisela Weinberg, Nicole Giliard, Julian Tornow, Robert Schlögl

Abstract

We present a new electrolyte formulation for lithium-ion batteries (Li-Ion) which leads to a significantly improved cycling stability of silicon/carbon-based (Si/C) anodes. The electrolyte consists of Lithiumhexafluorophosphate (LiPF_6), ethylene carbonate (EC), diethyl carbonate (DEC), dimethyl carbonate (DMC), fluoroethylene carbonate (FEC), and lithium nitrate (LiNO_3). We compared the electrochemical results to a commercial reference electrolyte (LP 71) and found a significant increase in both, specific capacity and cycling stability. The initial capacity of the Si/C-anodes cycled in the new electrolyte is $\sim 1100 \text{ mAh g}^{-1}$ and after 900 cycles still $\sim 585 \text{ mAh g}^{-1}$ remain which is 36% higher than the theoretical capacity of conventional graphite based anodes in Li-Ion batteries ($\sim 372 \text{ mAh g}^{-1}$). We investigated the morphological and electrochemical properties of the anodes cycled in the new and reference electrolyte by scanning electron microscopy (SEM), energy dispersive X-ray spectroscopy (EDX), cyclic voltammetry, and charge/discharge measurements. The obtained results show that the new electrolyte forms a rather stable electrode while a continuously growing Solid Electrolyte Interphase (SEI) forms on the electrode cycled in the standard electrolyte

4.1 . Introduction

In recent years one could observe an increased interest in new Li-Ion battery technologies which are used in microelectronics, transportation, and electric grid. The applications drastically raised the requirements especially in volumetric and gravimetric energy density (Wh l^{-1} and Wh kg^{-1}). To improve the energy density of Li-Ion battery cells, new anode, cathode and, electrolyte materials are needed. As a potential anode material, silicon (Si) stands out due to its high theoretical specific capacity of $\sim 3578 \text{ mAh g}^{-1}$ which is nearly ten times higher than the theoretical capacity of graphite ($\sim 372 \text{ mAh g}^{-1}$) currently used as state of the art anode

material in Li-Ion batteries [22, 26, 27, 143]. However, the Si-based anodes suffer from poor cycling stability that is assumed to be related to the high volume changes of up to $\sim 280\%$ (for the $\text{Li}_{15}\text{Si}_4$ phase) during lithiation and delithiation compared to $\sim 10\%$ in conventional graphite electrodes [26]. These volume changes may lead to several degradation processes e.g. pulverization, electrical insulation of Si in the electrode framework, and contact loss from the current collector [49, 50]. To solve these problems, nanosized Si materials are more and more investigated because recent studies assume that a small particle size of nanostructured Si slows down the degradation of Si and Si/C-based anodes induced by the detrimental effects of the volume changes [22, 56]. Besides the particle size, also the electrolyte composition strongly influences the cycling stability of Si-based anodes in Li-Ion batteries [113-115]. The electrolyte usually consists of one or more Li-salts dissolved in a mixture of carbonate-based solvents [92-94]. These electrolytes are usually electrochemically reduced at potentials $< 0.8\text{ V vs. Li/Li}^+$ which means that they are not stable in the operating voltage regime of C, Si, and Si/C-based anodes [124]. The decomposition products of the electrolyte can precipitate on the surface of the anode and form a passivating layer at the anode/electrolyte interface called Solid Electrolyte Interphase (SEI) [100]. In graphite-based electrode systems the SEI protects the electrolyte from the direct contact with the anode surface which slows down the continuous decomposition of the electrolyte in the following cycles and moreover, prevents the intercalation of solvated Li^+ into the graphite. This could lead to its exfoliation and the destruction of the anode active material [101]. An ideal SEI should allow a fast Li^+ -transport from the electrolyte through the SEI into the Li-storage material and at the same time should exhibit a negligible electronic conductivity to prevent the electrolyte from further decomposition and the SEI from continuous growth [117, 118]. In Si-based anode materials it is believed that the requirements on a stable SEI are significantly increased due to the high volume expansion of Si during charging and discharging. The continuous volume changes could lead to cracks inside the SEI layer accompanied by an irreversible Li consumption due to continuous electrolyte decomposition resulting in a low cycling stability [64, 116, 129]. The composition and structure of the SEI strongly influences the performance of the anode and mainly depends on the electrolyte formulation. One way to influence the SEI formation and composition is to add film forming additives to the electrolyte which alter the SEI characteristics due to different decomposition products. For example the addition of fluoroethylene carbonate (FEC) or vinylene carbonate (VC) proved to have a positive effect on the cycling stability of Si-based anodes [123, 127, 128]. Another interesting additive for electrolytes in Li-Ion batteries is lithium nitrate (LiNO_3) which is well known to have a positive effect in sulfur-based electrode systems where non carbonate-based electrolytes are used [144]. Therefore, this work presents for the first time a new electrolyte formulation using LiNO_3 as an additional

additive in carbonate based electrolyte solutions.

We systematically studied the effects of the two additives FEC and LiNO₃ on the cycling stability of Si/C-anodes and compared the results to the cycling stability in a conventional and commercially available reference electrolyte. Furthermore, we systematically developed an enhanced electrolyte formulation using both FEC and LiNO₃ as additives resulting in a significantly increased cycling stability and capacity retention. Moreover, we investigated the effects of the new electrolyte on the electrochemical properties of the Si/C-anodes by charge/discharge measurements and cycling voltammetry (CV) measurements. Finally, the differences in the morphology and surface composition of the Si/C-anodes cycled in the new electrolyte formulation and the reference electrolyte were studied by scanning electron microscopy (SEM) and energy dispersive X-ray spectroscopy (EDX). All the measurements were compared to the reference electrolyte.

4.2 . Experimental

The Si/C-based anodes were conventionally prepared by mixing 20 wt. % Si (MK Nano, ~60 nm), 60 wt. % graphite (Timcal, SFG-6), 12 wt. % conducting carbon additive (Timcal, C 65), and 8 wt. % PAA-binder (Polyacrylic acid, M_w ~450.000, Sigma Aldrich) in ethanol (Sigma Aldrich, 99 %) for 1 hour using a dissolver at 600 rpm. Afterwards, the obtained slurry was casted on 9 μ m Cu-foil which served as the current collector. The whole process was carried out in an Ar-filled glovebox (MBraun, H₂O < 0.1 ppm, O₂ < 0.1 ppm) to exclude any contamination during the preparation process. Subsequently, the casted electrode was predried at 80 °C overnight inside the glovebox. Afterwards several anodes (\varnothing 12 mm; material load ~2 mAh cm⁻²) were cut out and dried for 5 hours at 120 °C under vacuum without being exposed to air.

To develop a new electrolyte formulation we used the commercially available electrolyte LP 71 (1 M LiPF₆ in EC/DEC/DMC; 1:1:1 wt. %, BASF) as the reference electrolyte solution. We prepared different electrolyte formulations by adding 1 wt. %, 5 wt. %, 10 wt. %, and 20 wt. % FEC (Sigma Aldrich) to the standard electrolyte to measure the effects of the FEC concentration on the cycling stability in Si/C-anodes. In the next step, we investigated the effects of LiNO₃ as an additive by adding 0.1 wt. %, 0.3 wt. %, and 0.5 wt. % LiNO₃ (Sigma Aldrich) to the reference electrolyte. Finally, we investigated the synergetic effects of the additives FEC and LiNO₃ by preparing electrolytes with 10 wt. % FEC as well as 0.1 wt. %, 0.3 wt. %, and 0.5 wt. % LiNO₃ respectively.

After the electrode and electrolyte preparation several customized half cells for electrochemical charge/discharge experiments were assembled, using pure Li metal (Alfa Aesar) as the counter electrode and the prepared Si/C-based anodes as the working electrode. Between the electrodes two sheets of a Celgard 2500 separator were placed and the cells were filled by 300 μL of the respective electrolyte.

Charge/discharge experiments were carried out in a conventional CC-CV-mode (constant current constant voltage) at a Basytec CTS battery cycler. The first two cycles were conducted with a C/10 rate between 0.01 V and 0.9 V. After reaching the respective potential limits the voltage was held constant for 1 h. For the following cycles a 1C charge/discharge current was applied and the potential limits were changed to 0.04 V and 0.9 V. To investigate the effects of the different electrolytes on the rate capability we cycled the anodes with different C-rates (C/10, C/2, 1C, 5C, and C/10) for ten cycles respectively. Moreover, we conducted cyclic voltammetry measurements (CV) in a 3-electrode setup. Therefore, several Swagelok cells were assembled using Li metal as both, the counter and the reference electrode. The CV measurements were performed after a different number of charge/discharge cycles (1, 2, 15, and 100 cycles) using 0.1 mV s^{-1} as scan rate and potential limits of 0.01 V and 1.25 V in order to study the effects of the different electrolytes on the reversible redox processes of the Si/C-anodes.

The morphological properties of the pristine Si nanomaterial were characterized by transmission electron microscopy (TEM) measurements. The TEM measurements were conducted at a Philips CM 200 TEM with LaB₆ cathode and an acceleration voltage of 150 kV. The Si nanopowder was transferred into the TEM without air contact in a vacuum transfer holder. The morphology and composition of the prepared anodes cycled in the new and reference electrolyte for a different number of cycles (before cycling, after 1, 15, and 100 cycles) were analyzed by SEM and EDX (Hitachi S-4800 and EDAX Genesis 4000). SEM images were recorded from a mixed signal of secondary and backscattered electrons. For the EDX measurements 5 kV and 15 kV were used as accelerating voltages. To exclude the effects of air, the battery cells were disassembled in the glovebox and the Si/C-anodes were thoroughly washed with DMC and afterwards transferred to the SEM by an air tight sample holder. Note that for each analytical investigation new Si/C-anodes were cycled and prepared.

4.3 . Results

Figure 12a shows the specific charging capacities of three different Si/C-based anodes all cycled in the reference electrolyte LP 71. The results display the reproducibility of the investigated reference system. The characteristic cycling behavior of the Si/C-anodes cycled in LP 71 display a relatively stable capacity for the first ~15-20 cycles followed by a rapid capacity decrease in the following cycles. The specific charging capacity at 1C from the 3rd to the 20th cycle is around ~850-900 mAh g⁻¹ and only reaches ~280 mAh g⁻¹ after 100 cycles. The charging current was 1C except for the first two cycles which were performed at a current of C/10. This SEI formation step is conducted to form a more robust SEI. Note that the lower charging rate and the pronounced SEI formation at the beginning of the cycling procedure results in significantly higher charge capacities for the first two formation cycles.

To characterize the effects of FEC as an electrolyte additive on the cycling stability as well as the capacity retention of Si/C-anodes we prepared electrolytes with different FEC additive concentrations. The results for the Si/C-anodes are shown in Figure 12b. We measured the best cycling stability and highest specific capacity for the electrolyte with 10 wt. % FEC. The cycling stability and specific capacity increases stepwise with the addition of 1 wt. %, 5 wt. %, and 10 wt. % FEC. A higher concentration of FEC results in a decreasing cycling performance that can be observed for the results of the electrolyte with 20 wt. % FEC shown in Figure 12b. Hence, we conclude that ~10 wt. % FEC is an optimum concentration for this additive at these experimental conditions. The specific capacity at the beginning of the 1C cycling procedure is ~990 mAh g⁻¹ which is significantly higher compared to the results for the anodes cycled in LP 71. Moreover, the specific capacity after 100 cycles is drastically increased with ~817 mAh g⁻¹ compared to ~280 mAh g⁻¹. To study the effects of LiNO₃ as an additive in carbonate-based electrolyte solutions we characterized three different additive concentrations. The results for the addition of LiNO₃ are presented in Figure 12c. Note that it was only possible to solve up to 0.5 wt. % due to the low saturation limit of LiNO₃ in the respective solvents. The results for the addition of LiNO₃ display improved cycling stability and a higher specific capacity compared to the anodes cycled in LP 71 especially for the highest concentration of LiNO₃. However, the performance increase due to the addition of LiNO₃ is lower compared to the addition of FEC.

To investigate possible synergetic effects of both additives on the performance of the Si/C-anodes we developed new electrolyte formulations by systematically adding 10 wt. % FEC and 0.1 wt. %, 0.3 wt. %, and 0.5 wt. % LiNO₃ to the LP 71 electrolyte solution. The results on the Si/C-anodes are shown in Figure 12d. We find that the addition of 10 wt. % FEC and

0.5 wt. % LiNO₃ leads to the best cycling stability and capacity retention with ~1042 mAh g⁻¹ at the beginning of the 1C cycling procedure and ~922 mAh g⁻¹ after 100 cycles which is ~70 % higher compared to the results obtained for the Si/C-anodes cycled in LP 71 and ~12 % higher compared to the electrolyte with only 10 wt. % FEC. For a better comparison the results obtained for the different electrolyte formulations are shown in Figure 13a. The comparison displays the stepwise increase in cycling stability and specific capacity due to the addition of the different additives. Moreover, the positive effect of the new electrolyte formulation is clearly visible.

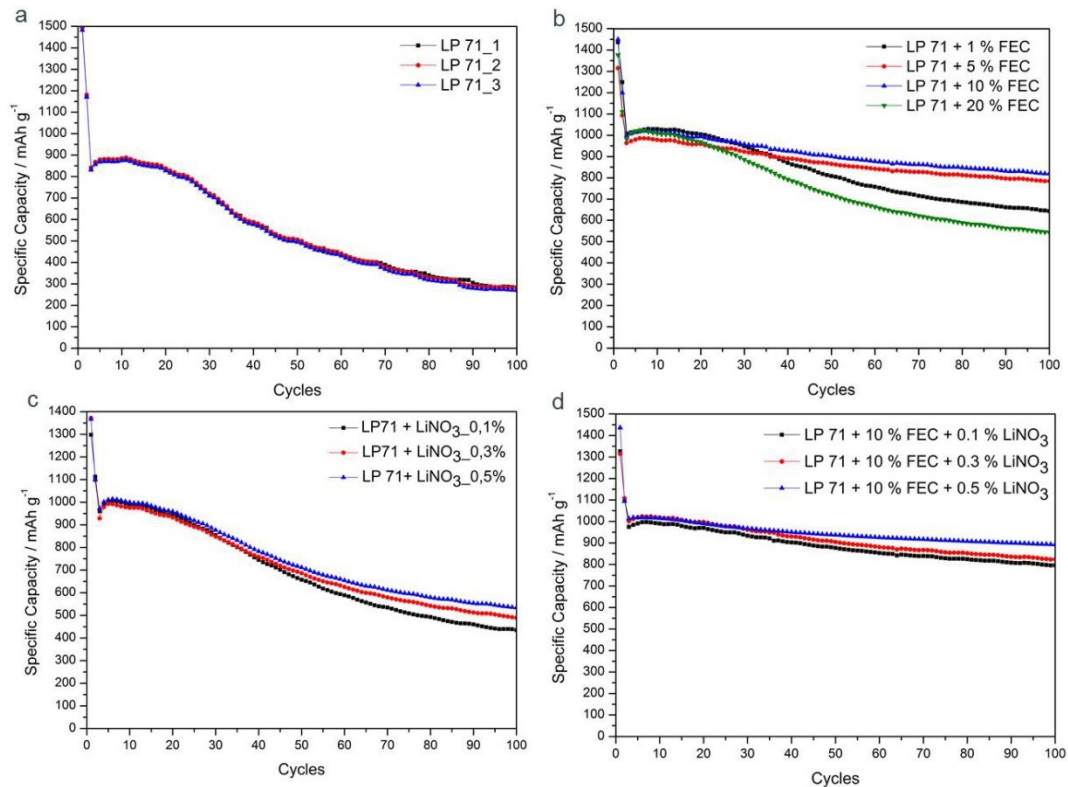


Figure 12: Charging capacities with different electrolytes to optimize the cycling stability of Si/C-anodes: a.) reference electrolyte LP 71 b.) 1 wt. %, 5 wt. %, 10 wt. %, and 20 wt. % FEC additive c.) 0.1 wt. %, 0.3 wt. %, and 0.5 wt. % LiNO₃ additive d.) new electrolyte formulation with 10 wt. % FEC and 0.5 wt. % LiNO₃ as well as LP 71 + 10 wt. % FEC + 0.1 wt. % LiNO₃, and LP 71 + 10 wt. % FEC + 0.3 wt. % LiNO₃.

To analyze the effect of this new electrolyte on the long term cycling performance we conducted charge/discharge measurements at 1C for 900 cycles. Figure 13b displays that even after 900 cycles the specific capacity of the anode is still ~585 mAh g⁻¹ which is about ~36 % higher than the theoretical specific capacity of graphite (372 mAh g⁻¹). Moreover, we obtained a very low average capacity loss of only ~0.05 % per cycle and a high coulombic efficiency (CE) of ~99.5 %.

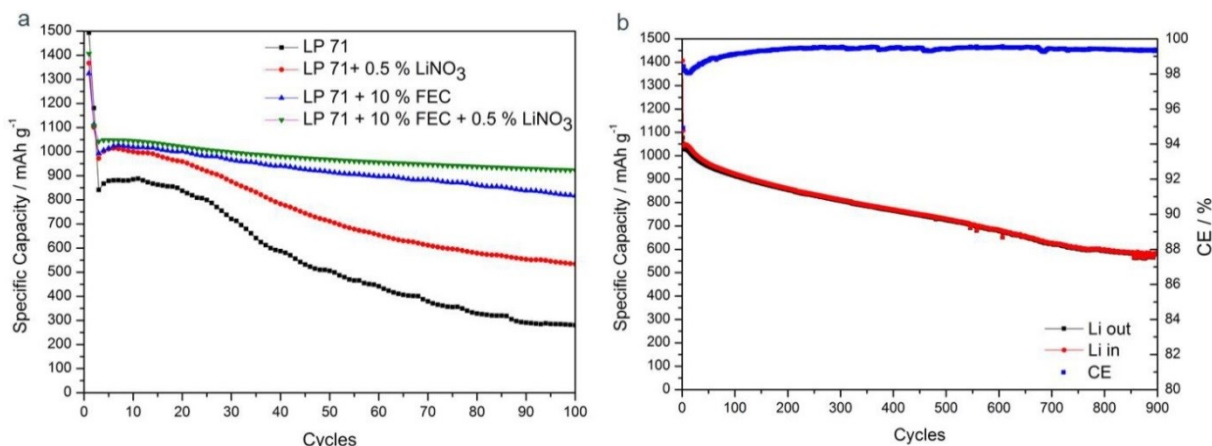


Figure 13: a.) Charging capacities to compare the cycling stability of Si/C-anodes cycled in the different electrolyte solutions b.) Long term cycling stability of a Si/C-anode cycled in the new electrolyte formulation

Differences in the charge/discharge process for the different electrolytes should also become visible for the reversible redox processes of the Si/C-anodes in the different electrolytes. For the following, a more detailed analysis of the influence of electrolytes on Si/C-anodes, we compare an electrolyte showing the most stable cycling stability with one having a low cycling stability. Hence, we analyze the anode using the new and the LP 71 electrolyte.

In Figure 14, cycling voltammograms show the influence of the different electrolytes to the reversible redox processes. These experiments were performed at one electrode after a different number of charge/discharge cycles between 0.01 V and 1.25 V vs. Li/Li^+ . The respective redox peaks are indicated according to the literature [20, 145]. The CV's for the LP 71 electrolyte in Figure 14a show the highest redox activities for Li^+ -insertion and -deinsertion into C and Si after 15 cycles. This correlates well with the charge/discharge curves in Figure 12, showing an initial increase of the charging capacity up to about the 15th cycle. While the CV after the second cycle shows the same redox peaks after 15 cycles, but with lower intensities, there is no Li^+ -insertion/deinsertion peak into C visible after only one cycle. This is generally correlated to the formation of a SEI in the first cycles which usually stabilizes the electrode against further formation. However, the strong dependency of the redox activity with cycling indicates that no stable SEI forms on the Si/C-anodes. Hence, the anode is in a dynamic formation state with continuously changing electrode properties leading to the complete absence of activity for Li^+ insertion/deinsertion after 100 cycles. In contrast with the new electrolyte formulation, the CV after the first cycle exhibits already similarities to the one after 15 cycles in its deinsertion behavior. Besides slight deviations in the activities of the redox processes the general activities and shapes of the CV's after 2, 15, and 100 cycles are pretty

similar. Hence, with the new electrolyte the electrode formation is predominantly performed in the first cycle which results in a relatively stable performance for the succeeding cycles.

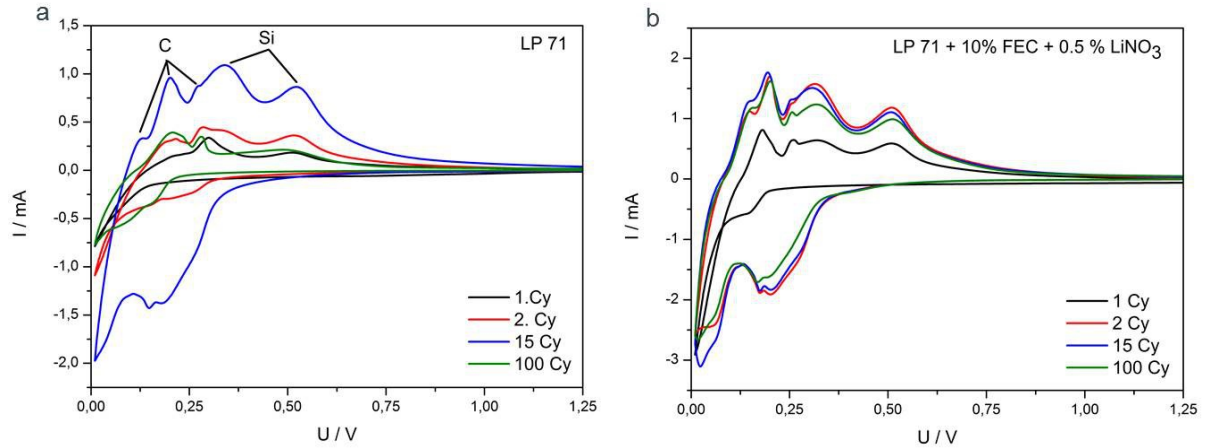


Figure 14: a.) Cyclic voltammetry measurements of Si/C-based anode between 0.01 V and 1.25 V in the standard reference electrolyte (LP 71) using a scan rate of 0.1 mV s⁻¹ b.) Cyclic voltammetry measurements using the new electrolyte formulation.

A similar trend of the electrode formation is observed from cycle dependent charging and discharging measurements. The results shown in Figure 15 are correlated to the charging and discharging of the Si/C-anodes. The experiment in Figure 15a is performed with a constant C-rate (except for the two initial cycles) while the measurement in Figure 15b differs from this by applying different C-rates. To understand Figure 15a, it is important to note that the charge/discharge experiment shown in Figure 12 is performed for each cycle by initially applying a constant current (CC) until a voltage of 0.04 V and 0.9 V is reached for charging and discharging respectively. Subsequently, the potential is kept at these constant voltages (CV) to compensate for any non-equilibrium effects. The higher the ratio of the capacity obtained in this subsequent CV-step to the total capacity the lower is the ratio of the capacity which can be exhibited during the CC-process. This can be explained by a higher ratio between side reactions e.g. due to electrolyte decomposition to the overall capacity of the Si/C-anode. This ratio is plotted in Figure 15a for the charging and discharging of the two electrolytes. For both electrolytes, the first two cycles were measured with a C-rate of C/10 while the following cycles were conducted with 1C. The ratio of the CV-capacity during the first two cycles is significantly smaller because the system is given more time during the CC-step to reach nearly full lithiation/delithiation. The results for the succeeding cycles shown in Figure 15a generally display that for the charging process of Si/C-anodes, the CV-ratio is significantly higher compared to the discharging process. This can be understood because during the

charging process the Si/C-anodes are kept at a very reductive potential of 0.04 V, which results in a continuous reduction of the respective electrolyte solution. Contrarily, during the discharge process the anodes are kept at 0.9 V which is a much less reducing potential resulting in a lower CV-ratio to the overall CC-CV capacity due to less electrolyte decomposition. Another effect could be that enhanced electrolyte decomposition could lead to a thicker SEI or to SEI components allowing only slower Li⁺-transport through the SEI into the anode resulting in lower capacities.

Furthermore Figure 15a shows the differences between the standard electrolyte solution and the new electrolyte formulation. Using the new electrolyte results in a relatively constant ratio for the CV-step during the charge and discharge process, indicating only little electrolyte decomposition throughout the cycling process. The behavior with the LP 71 standard electrolyte is significantly changed and the ratio for the CV-capacity is only stable for about the first 20 cycles correlating well with the stable cycling behavior of the anodes for about the first 20 cycles in Figure 12. Subsequently, the CV-ratio during the charge and discharge process increases drastically and reaches roughly 95 % of the total capacity after 100 cycles for the charging step, indicating a continuous decomposition of the reference electrolyte or an impeded Li⁺-transport into the anode throughout the whole cycling process.

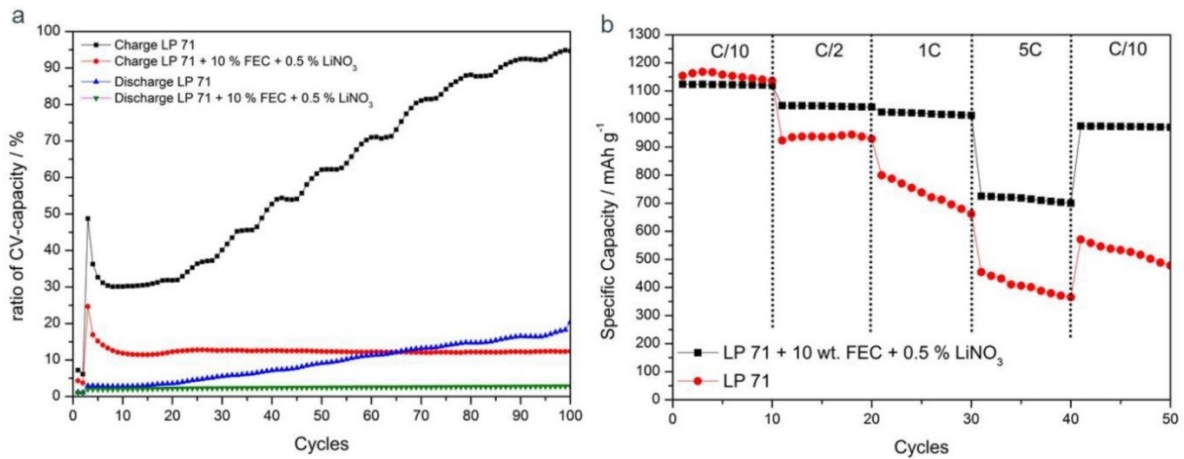


Figure 15: a) Ratio of the constant voltage step (CV-step) capacity compared to the total capacity (CC-CV-step) b) Rate capability and specific capacities at C/10, C/2, 1C, 5C, and again C/10 for 10 cycles respectively.

Further, a significant dependency of the charging velocity to the applied charging rate is observed in Figure 15b for the two different electrolytes. Cycling experiments were conducted at C/10, C/2, 1C, and 5C. At the beginning of the measurements, a low C-rate of C/10 was applied resulting in a slightly higher specific capacity for the Si/C-anodes cycled with LP

71. However, the degradation over cycling and the capacity loss per cycle is already more severe compared to the new electrolyte. With higher C-rates the Si/C-anodes cycled in the new electrolyte formulation clearly outperform the anodes in the standard electrolyte and only at high currents of 5C ($\sim 5,3 \text{ A g}^{-1}$) and already ~ 30 -40 cycles we could observe a considerable capacity decay. Finally, the C-rate was again reduced to C/10 to investigate the capacity retention at low currents. The results display that the specific capacities are considerably higher for the Si/C-anodes cycled with the new electrolyte and show that the addition of the two additives FEC and LiNO₃ not only influence the long term cycling performance but also has a positive impact on the performance at different C-rates.

The above described electrochemical measurement methods indicate a dynamic electrode formation with the LP 71 electrolyte which could be stabilized with the addition of FEC and LiNO₃. Hence, we will analyze if these findings from the electrochemical data can be observed and related to the microstructure of the electrode. We investigate the electrode morphology and composition by a SEM- and EDX-analysis. Before discussing the cycled electrodes, the morphology and composition of the pristine Si/C-anode are displayed in Figure 16. In the SEM images (Figure 16a+b) one can clearly identify the micrometer sized graphite-particles by their flake-like morphology while the Si and the conductive C (carbon) are both round shaped nanoparticles and can only be distinguished by the material contrast. The Si nanoparticles appear significantly brighter compared to the conductive C nanoparticles which is visible in such a high resolution due to the mixed SEM signal of secondary and backscattered electrons. This procedure is validated by the EDX-analysis on the related spots shown in Figure 16c. From the material contrast a generally broad dispersion of Si particles over the electrode is seen in Figure 16a however, the particles do not cover the electrode homogeneously but agglomerate (Figure 16a+b) instead.

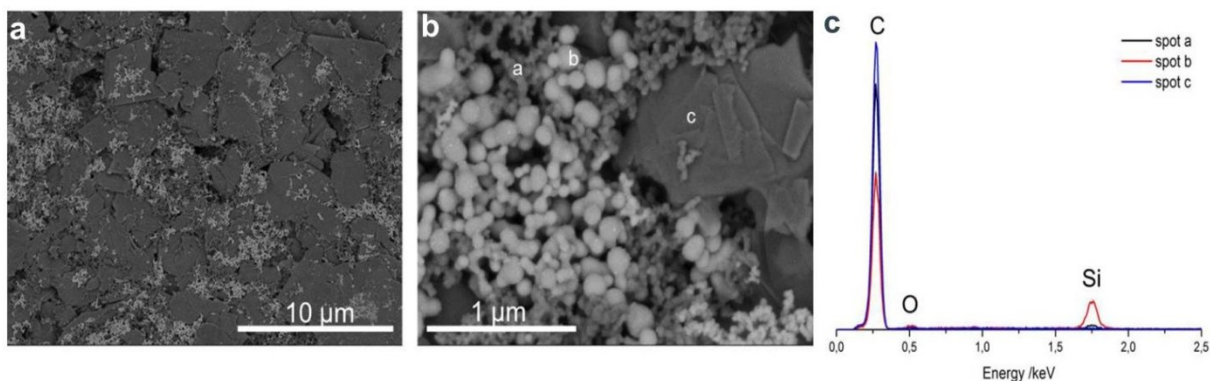


Figure 16: a) Overview SEM image of the fresh, uncycled anode surface b.) Higher magnification SEM image of the fresh and uncycled Si/C-anode indicating the different anode components: conductive C (spot a), Si (spot b), and graphite (spot c) c.) EDX-spectra's of the spots in Figure 16b.

The results of the EDX measurements in Figure 16c show that the pristine Si/C-anode consists predominantly of C and Si with traces of oxygen (O). The O probably originates from the binder as well as the native oxide layer on the Si-nanoparticles which was found by TEM measurements on the Si raw material shown in Figure 17. The TEM measurements reveal that the Si-nanoparticles consist of a crystalline Si-core and a very thin amorphous SiO_x -shell of about 1-2 nm.

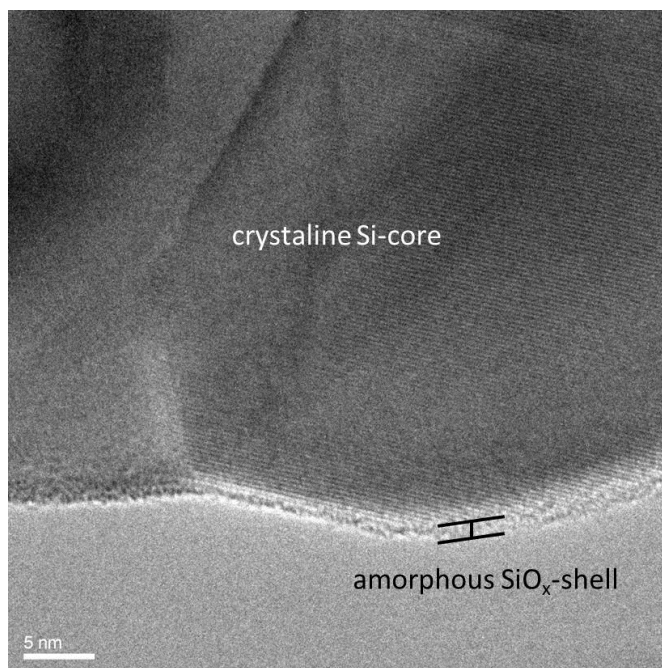


Figure 17: TEM image of the pristine Si nanoparticles. The image displays the characteristic crystalline Si-core of the Si nanoparticles which is surrounded with a ~1-2 nm thin amorphous SiO_x -shell

The Si/C-anode morphology and composition significantly changes after cycling in the LP 71 electrolyte. Figure 18 shows SEM images representing the anode morphology after a different numbers of cycles. After the first cycle a new structure has formed which can be observed as the fluffy agglomerated component in Figure 18d. After 15 cycles (Figure 18b+e) further changes in the electrodes surface morphology are visible by the strong contrast change in the SEM images.

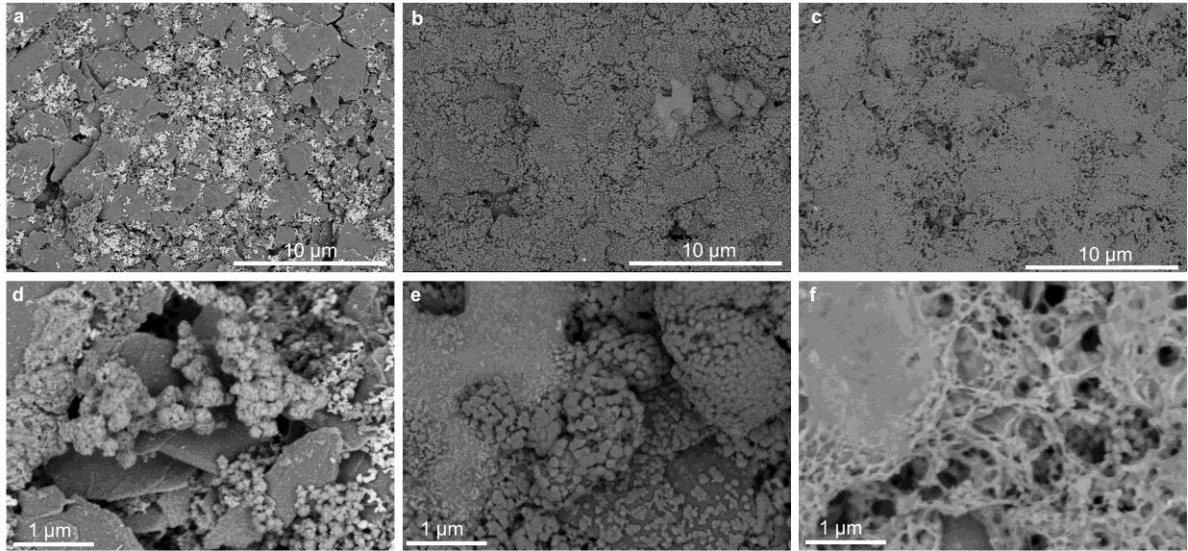


Figure 18: a-c.) Overview SEM images of the anodes cycled in the standard electrolyte after 1 (a.), 15 (b.), and 100 cycles (c.) d-f) Higher magnification SEM images of the anode surfaces after 1 (d.), 15 (e.), and 100 cycles (f.).

A magnified SEM image of the Si/C surface morphology after 15 cycles in Figure 19 shows that a formation of fiberlike or netlike structures begins. After 100 cycles the formation of the fiberlike and netlike morphology of the Si/C-anode becomes even more enhanced (Figure 18f). Yet, with cycling in the LP 71 electrolyte the Si/C-anode is subject to a continuous change of the electrode structure.

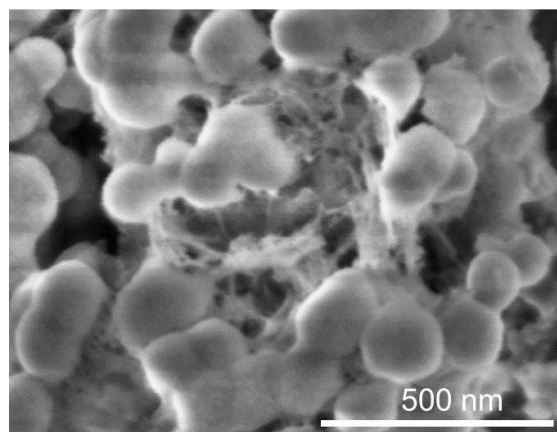


Figure 19: Magnified SEM image of the Si/C-anodes after 15 cycles cycled in the LP 71 reference electrolyte, showing the beginning formation of fiberlike and netlike structures due to enhanced SEI growth.

The cycle dependent morphology evolution for the Si/C-anodes with the new electrolyte formulation is significantly stabilized compared to the results for the Si/C-anodes cycled in the LP 71 electrolyte and is shown in Figure 20a-f. In Figure 20a we already find a contrast change of the anode after 1 cycle compared to the uncycled Si/C-anode (compare Figure 16a). The Si appears less bright compared to the Si after 1 cycle with the LP 71 electrolyte (compared to Figure 18a) indicating that the microstructure of the Si has changed already after one cycle. Moreover, a new structure has formed consisting of different elements C, O, N (nitrogen), and the main component F (fluorine) which is indicated as spot a in the higher magnification image in Figure 20d and the EDX measurement in Figure 21b. The new structure is visible in all samples and already forms during the 1st cycle.

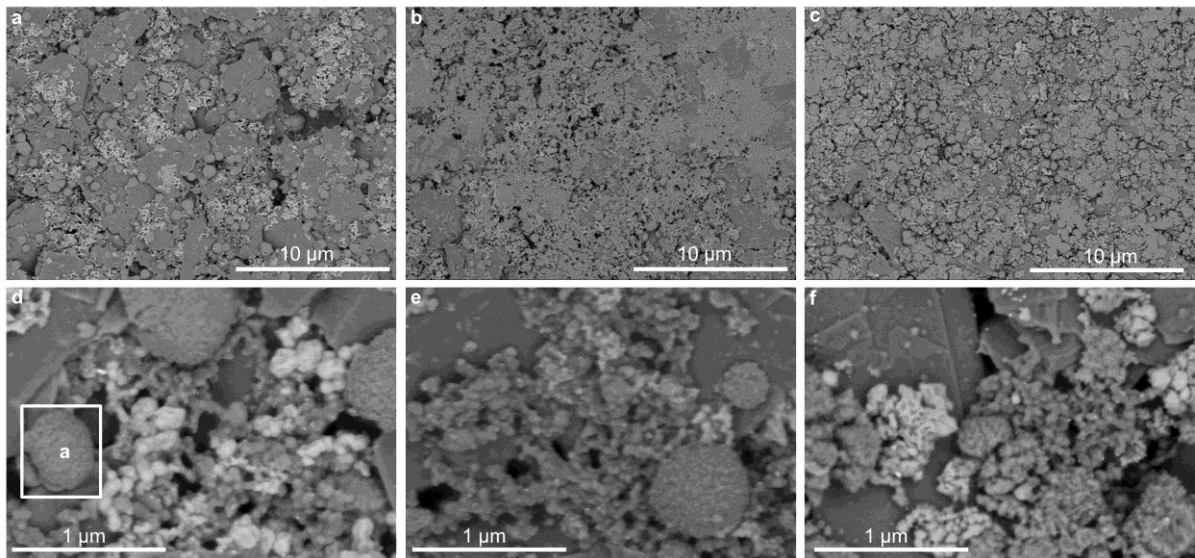


Figure 20: a-c.) Overview SEM images of the anodes cycled in the new electrolyte after 1 (a.), 15 (b.), and 100 cycles (c.) d-f) higher magnification SEM images of the anode surfaces after 1 (d.), 15 (e.), and 100 cycles (f.).

The high F and small N content leads to the conclusion that the structure is formed due to the additives FEC and LiNO_3 and may be related to the SEI formed on the anodes with the new electrolyte formulation (details shown in Figure 21a+b). However the effects and nature of the newly formed structure need further investigation.

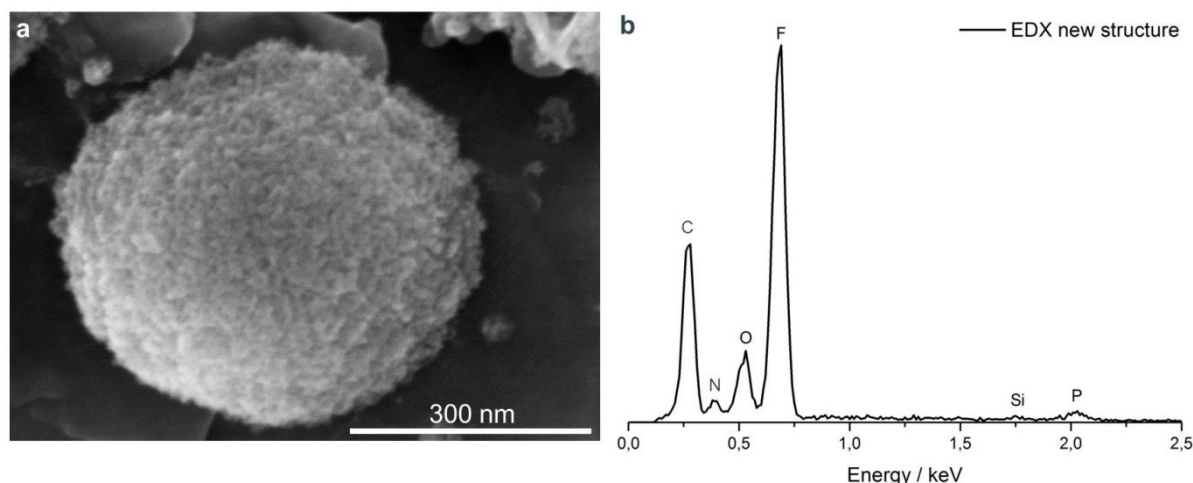


Figure 21: a.) In-detail SEM image of the new structure formed during cycling in the new electrolyte indicated as spot a (framed) in Figure 20d b.) EDX-spectra of the new formed structure shown in Figure 21a.

Besides the formation of a new structure the SEM images in Figure 20 display slight changes in contrast and morphology with increased cycle number indicating a slight change in the electrodes microstructure. However, compared to the anodes cycled in the LP 71 electrolyte the effect appears much less severe with the new electrolyte. In Figure 20e and f the different Si particles can still be distinguished. Furthermore, the fiberlike or netlike morphology, visible after 15 and 100 cycles for the anodes cycled in the LP 71 electrolyte, seems to be absent. These findings lead to the assumption that the new electrolyte formulation effectively stabilizes the formed anode which results in an enhanced cycling stability of the Si/C-anodes.

To further characterize the differences in the surface composition we conducted cycle-dependent EDX measurements for the Si/C-anodes in the two different electrolyte solutions. The results shown in Figure 22a+b indicates that the electrode formation starts during the first few cycles. Compared to the EDX results for the pristine electrode in Figure 16c we observe an increase of the O and F content for the anodes cycled in both electrolytes which can be assigned to the electrode formation induced by the decomposition of the electrolyte during the cycling process. With the LP 71 electrolyte we observe a continuous decrease of the C and Si signal but a continuous increase of the O signal upon cycling. This supports again the dynamic formation process of the Si/C-based anode in the LP 71 electrolyte. Furthermore, the EDX measurements also allow to identify the location of the electrode formation by applying a higher acceleration voltage of the incident electron beam and hence, a deeper information depth. Figure 23 shows the EDX-spectra of a Si/C-anode after 100 cycles in the standard electrolyte with 15 kV instead of 5 kV used for Figure 22a. Figure 23 shows that the Si signal strongly increases with higher accelerating voltage while the O to C ratio

stays rather unaffected. Yet, the O to C ratio does not depend strongly on the depth of information while Si is obviously located in a deeper distance from the electrodes surface. This leads to the conclusion that Si is buried under a layer containing C, O, F, and P (phosphate). Such a layer growing on top of the electrodes surface is known as the Solid Electrolyte Interphase (SEI). Therefore, from the electrochemical and microscopic study we can conclude that the SEI on a Si/C-based anode is continuously growing using the LP 71 electrolyte.

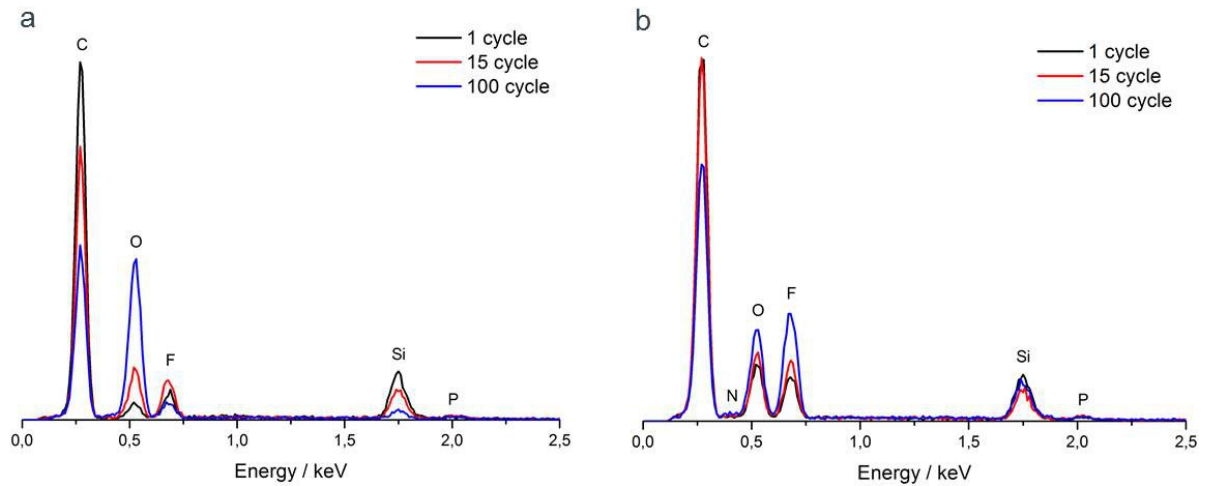


Figure 22: a.) Overview EDX-spectra of the anodes cycled in the new electrolyte for 1, 15, and 100 cycles
b.) Overview EDX-spectra of the anodes cycled in the standard electrolyte for 1, 15, and 100 cycles.

The EDX measurements with the new electrolyte are shown in Figure 22b for different cycles. Compared to the pristine electrode, the O and F components are increased already after the first cycle and a slight P signal is detected. In contrast to the LP 71 electrolyte the succeeding changes with cycling are much less pronounced. Especially the Si signal is not decreasing with higher cycle numbers. Hence, also the EDX measurements show the stabilization of the electrode formation process. From the electrochemical and microstructural investigations we cannot clearly separate if the electrode formation is just the growth of a stable and very thin SEI on the electrode surface or if the formation builds up the active phase for the Li^+ -insertion/deinsertion.

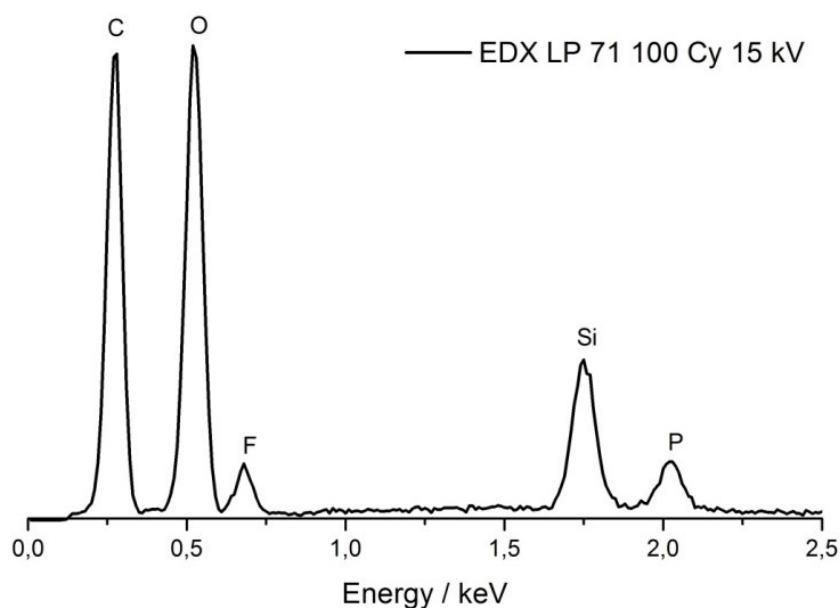


Figure 23: EDX measurement of a Si/C-based anode after 100 cycles in LP 71 standard electrolyte and an increased accelerating voltage of 15 kV. The increased Si signal indicates that the Si is not dissolved during the cycling process but rather buried under a thick SEI layer.

4.4 Discussion

The results in this work display that the addition of certain additives and the combination of different electrolyte components can lead to an increased performance of Si/C-anodes in Li-ion batteries. The LP 71 electrolyte has an inferior battery performance and from electrochemical methods a continuous change of the electrodes redox processes is observed. Hence, with the LP 71 electrolyte no stable Si/C-anode forms. These dynamic variations of the electrochemical electrode properties correlate well with a continuous growth of a SEI on the electrodes surface which is observed by the microstructural analysis. A reasonable explanation for the degradation of the battery performance with cycling is the continuous growth of the SEI which buries the active phase for Li^+ -insertion/deinsertion and hence electronically insulates the Si-active material from the electronically conducting carbon framework if the SEI growth to a certain thickness. An enhanced SEI growth is a result of a continuous electrolyte decomposition which could be observed in the increasing ratio of the CV-capacity to the overall capacity in the CC-CV cycling procedure throughout cycling. Furthermore a growing SEI could also lead to an impeded Li^+ transport throughout the SEI into the anode, resulting in less capacity. Moreover, the results of the cycle dependent SEM and EDX measure-

ments additionally point out the importance of controlling the interface chemistry in Si/C-anodes to impede the continuous electrolyte decomposition and SEI growth. However, it is important to note that this is only one possible degradation mechanism and that the results of the electrochemical and microstructural measurements are a summation of a various number of sub-steps taking place in the respective Li-Ion battery cell and are until now not completely understood or even faultlessly defined. There are a various number of sub-steps which could all significantly change the performance of a Si/C-anode e.g. the formation of the SEI, the transport of Li^+ in the electrolyte solution, the transport of Li^+ through the formed SEI layer, the absorption of Li at the anode surface, the diffusion of Li^+ in the different anode components, or consecutive reactions which can take place due to the continuous growth of the SEI layer. All these sub-steps could be influenced and changed due to the application of the new electrolyte formulation and therefore it is still not very well understood how to systematically influence the performance of an anode by certain changes in the electrolyte formulation.

Furthermore, the above mentioned mechanisms might be partly correct but do not fully describe the battery performance. Interestingly, for the LP 71 electrolyte one observes an improvement of the battery performance within about the first 15 cycles. Hence, the continuous electrolyte decomposition and growth of a SEI cannot explain this effect completely. Obviously the pristine electrode requires a certain activation to gain its full activity. One could also say that the really active electrode is not the pristine one but needs to be formed during the first cycles. This formation requires only one cycle with the new electrolyte. Moreover, with the new electrolyte only slight dependencies on the cycle number are observed by electrochemical as well as microstructural measurements. We observed an improved cycling performance going hand in hand with only a slight modification of the microstructure especially for higher cycles. Unlike for the LP 71 electrolyte, with the new electrolyte it could not be distinguished between an active phase and a SEI. Hence, it cannot be excluded that the real active phase for Si-based battery anodes is not Si alone but a composite containing Si, F, and O. However, the selected system for this work contains too many initial components like Si, SiO_x , binder, conductive C, and graphite-flakes and therefore it is too complex to elucidate the phase responsible for charge storage.

This argumentation should point out that the addition of certain additives is not simply a change of the electrolyte composition but it is more importantly a change of the complete “reaction network” possibly resulting into a completely new material and reaction system, or in other words to a new active electrode. In this case the term “reaction network” can be defined as the combination of different single reactions like electrolyte decomposition, secondary reactions of these decomposition products, or possible reactions with the binder or C materials. The possible single reactions form a complex “reaction network” which itself can

be strongly influenced by other parameters like e.g. temperature, voltage, or applied current and its different dependencies are until now not completely understood.

To further investigate the effects of additives we think it will be essential to separate the different components of the system and additionally try to isolate the different sub-steps taking place in a Li-Ion battery system and thoroughly investigate the elemental steps. These experiments are necessary to gain a more fundamental understanding about how the different components influence the different sub-steps during the battery operation and the “reaction network” of the system. Furthermore we think it should increase the ability to systematically raise the performance of a Li-Ion battery in the future.

4.5 Conclusion

We demonstrated the enhancing effect of the new electrolyte composition 1 M LiPF₆ in EC/DEC/DMC (LP 71) + 10 wt. % FEC + 0.5 wt. % LiNO₃ on the cycling performance and capacity retention of Si/C-based anodes by comparing the results with the reference electrolyte solution LP 71. Si/C-based anodes cycled with the new electrolyte show an exceptional cycling performance and still exhibit more than 585 mAh·g⁻¹ after 900 cycles which is significantly higher than the theoretical capacity of conventional graphite anodes. We compared the new electrolyte composition with electrodes cycled in a standard reference electrolyte (LP 71). Electrochemical and microstructural measurements for anodes cycled in the two electrolytes for a different number of cycles lead to the conclusion that the SEI continuously grows in case of the reference electrolyte LP 71. Furthermore, the charging/discharging performance decreases with higher cycle numbers which can be linked to enhanced electrolyte decomposition with the standard electrolyte resulting in a continuous SEI growth.

Finally, we observed that the SEI formation is significantly slowed down in the new electrolyte going hand in hand with a more stable long time cycle performance. The thick SEI is obviously inferior for the battery performance so we assume that a denser and more stable SEI forms on Si/C-anodes with the new electrolyte formulation.

5 Solid Electrolyte Interphase in a beaker– New pretreatment method for improved Si/C-anodes in Li-Ion batteries

Authors: Janis Dölle, Gisela Weinberg, Nicole Giliard, Julian Tornow, Robert Schlögl

Abstract

This work presents the results of a new pretreatment method for the direct formation of a Solid Electrolyte Interphase (SEI) layer on silicon/carbon-based anodes (Si/C) in Li-Ion batteries. The pretreatment in a solution containing fluoroethylene carbonate (FEC), lithium nitrate (LiNO_3), and lithiumbis(oxalate) borate (LiBOB) at 0.6 V for ~30 min is conducted inside a beaker and is easily applicable to all kinds of film forming additives. To proof the effect of the preformed SEI layer, the following cycling was conducted using a conventional Lithiumhexafluorophosphate (LiPF_6) and ethylene carbonate-based electrolyte (EC). The pretreatment leads to an improved cycling stability without any additional additives needed. The results display the influence of a more stable SEI at the electrode/electrolyte interface on the cycling behavior. The pretreated Si/C-anodes display a stable cycling behavior for 250 cycles with still $\sim 705 \text{ mAh g}^{-1}$ residual specific capacity and an initial 1C capacity of $\sim 1050 \text{ mAh g}^{-1}$. Moreover, the initial coulombic efficiency (CE) of the pretreated electrodes is significantly improved ($\sim 85 \%$) as well as the CE during the cycling process ($\sim 99.5 \%$). Microstructural characterization by SEM and EDX displays that the good performance is likely due to a stable SEI which forms during the pretreatment procedure. The pretreatment effectively slows down the continuous electrolyte decomposition due to the formation of a more stable SEI resulting in impeded SEI growth throughout cycling.

5.1 . Introduction

Since the early 1990's Li-Ion batteries have been widely used as power sources and energy storage devices for various applications and commodities like portable electronic, electrical

grid, or electric (or hybrid) vehicles [146-148]. The demand for new anode, cathode, and electrolyte materials is still high because the energy and power density is essentially determined by the materials used. In commercialized Li-Ion batteries, the active material of the negative electrode (anode) is usually pure graphite or graphitic carbon (C) which has a relatively low specific capacity of $\sim 372 \text{ mAh g}^{-1}$ [26]. However, the growing demand on advanced Li-Ion batteries with high power and high energy densities especially for electric vehicles needs new materials with higher capacities [149]. One promising anode material for Li-Ion batteries is silicon (Si) due to its high specific capacity of $\sim 3580 \text{ mAh g}^{-1}$ and relatively low working potential of $< 0.5 \text{ V vs. Li/Li}^+$ allowing for large cell voltages. However, a strong volume expansion during lithiation and delithiation of up to 280 % leads to severe stress which forms cracks in the bulk Si and results into a fairly low cycling stability. Nanostructuring Si reduces the crack formation but increases the interface area between Si and the electrolyte; hence the interface properties become more severe for the battery performance. A low working potential leads to the decomposition of the liquid electrolytes commonly used in commercialized Li-Ion batteries which are not stable at potentials $< 0.8 \text{ V vs. Li/Li}^+$ [50-52, 149]. The decomposition products of the electrolyte form the strongly investigated Solid Electrolyte Interphase (SEI) on the negative electrode. It has been reported that the composition and characteristics of the electrode/electrolyte interface strongly influences the performance and stability of a Li-Ion battery [22, 106, 116, 150-152]. The surface films mainly consist of the electrochemical decomposition products of the solvents, salts, and additives of the electrolyte. In the case of carbonate-based solvents with LiPF_6 as Li-salt several studies suggest that the SEI mainly consists of insoluble reduction products such as lithium carbonate, lithium alkyl carbonates, lithium alkoxide, polycarbonates, and ethers [104, 107, 114, 115].

For conventional graphite electrodes these surface films grow to a certain thickness because they are electronically insulating and hence self-passivate a further severe decomposition which leads to a stable cycling [153].

In the case of Si-based anodes the SEI formation is not self passivating, this can either be due to a non-electronically insulating character of the SEI or due to the strong volume expansion of Si [27, 46, 52, 153-155]. In the latter case, the SEI has to withstand large volume changes which can lead to cracks inside the SEI resulting in a continuous electrolyte decomposition and new SEI formation [27]. To tackle the problem of the low SEI stability several approaches have been reported in the literature like mixing the Si particles with conventional graphite powder, coating Si with C, or nanostructuring the Si [31, 140, 156, 157]. A different approach to increase the cycling stability of Si-based anodes is to alter the electrolyte composition to generate a more stable SEI. The most common way is to add certain film forming additives to a standard electrolyte solution e.g. FEC (fluoroethylene carbonate), VC (vinylene

carbonate), or succinic anhydride [127, 130, 158]. Another approach is to replace the commonly used Li-salt LiPF_6 by LiBOB (lithium bis(oxalate)borate) in order to form a more stable SEI on Si-based anodes which afterwards leads to an enhanced cycling stability [124]. Nevertheless, the drawbacks of the addition of certain additives can be a decreased stability at high potentials which are necessary for new high voltage cathode materials like $\text{LiNi}_{0.5}\text{Mn}_{1.5}\text{O}_4$ and $0.5\cdot\text{Li}_2\text{CoO}_3\cdot0.5\text{LiNi}_{0.44}\text{Co}_{0.25}\text{Mn}_{0.31}\text{O}_2$. Another drawback could be safety problems due to a higher flammability of certain additives [159, 160]. Furthermore, it is well known that LiBOB is less conductive in typical carbonate-based solvents and has a lower solubility especially in solvents with low dielectric constants [92].

To overcome these limitations of additives by exploiting their advantages, we report in this work a pretreatment method in order to form a stable SEI. This SEI is electrochemically formed inside a beaker in a solution composed of FEC, LiNO_3 (lithium nitrate), and LiBOB, while the following battery cycling is conducted in a conventional electrolyte solution. The major advantage is an improved cycling stability, while additionally a preformed SEI can also reduce the irreversible Li consumption which is of strong interest for a full battery cell.

5.2 . Experimental

The Si/C-based anodes were prepared by mixing 20 wt. % Si (MK Nano, ~60 nm), 60 wt. % graphite (Timcal, SFG-6), 12 wt. % conducting carbon additive (Timcal, C 65), and 8 wt. % PAA-binder (Polyacrylic acid, $M_w \sim 450.000$, Sigma Aldrich) in ethanol (>99 %, Sigma Aldrich) for 1 hour using a dissolver at 1500 rpm. Afterwards, the obtained slurry was casted on 9 μm Cu-foil which served as the current collector. The whole process was carried out in an Ar-filled glovebox (MBraun, $\text{H}_2\text{O} < 0.1$ ppm, $\text{O}_2 < 0.1$ ppm). Subsequently, the casted electrodes were dried inside a glovebox at 80 °C overnight. Afterwards several anode pieces (~3.38 cm^2) were cut out and dried for 5 hours at 120 °C under vacuum without being exposed to air. The following pretreatment was also conducted inside an Ar-filled glovebox by placing the Si/C-anode as the working electrode and a piece of Li-foil as the counter electrode into a beaker filled with the pretreatment solution consisting of 0.5 wt. % LiNO_3 and 1 wt. % LiBOB dissolved in 20 mL FEC (before the experiment the solution was stirred for ~1 h). A schematic illustration of the experiment is shown in Figure 24a. After placing the two electrodes into the solution a current of C/10 was applied till the Si/C-working electrode reached a potential of 0.6 V vs. Li/Li^+ which subsequently was held constant for 30 min (Biologic VMP 3). After the pretreatment, the Si/C-anode was thoroughly washed with DEC (diethyl carbonate

(DEC), Sigma Aldrich) and dried at room temperature inside the glovebox for several hours. After the drying process several anodes (\varnothing 12 mm; material load $\sim 2 \text{ mg cm}^{-2}$) were cut out and assembled in customized half cells for electrochemical charge/discharge experiments using pure Li metal (Alfa Aesar) as the counter electrode and the pretreated Si/C-based anodes as the working electrode. Between the two electrodes two sheets of a Celgard 2500 separator (PP) were placed which subsequently were wetted by 300 μL of a conventional LiPF_6 and carbonate-based electrolyte (BASF LP 71: 1M LiPF_6 in EC/DEC/DMC 1:1:1). After the assembling, the electrodes were galvanostatically cycled using a conventional CC-CV-method (constant current constant voltage) at a Basytec CTS battery cycler. The first two cycles were conducted with a C/10 rate between 0.01 V and 0.9 V. After reaching the respective potential limit the voltage was held constant for 1 h. For the following cycles a 1C charge/discharge current was applied and the potential limits were changed to 0.04 V and 0.9 V. To investigate the effect of the different electrolytes on the rate capability we cycled the anodes with different C-rates (C/10, C/2, 1C, 5C, and C/10) for ten cycles respectively. To analyze the effects of the pretreatment we additionally conducted measurements on non-pretreated Si/C-anodes.

Moreover, we monitored the differentiated charge (dQ vs. V) during the pretreatment procedure of the Si/C-anodes to investigate the electrochemical decomposition during the pretreatment process (C/10 from open circuit voltage (OCV) to 0.6 V). A microstructural characterization of the pretreated and non-pretreated Si/C-anodes was conducted by SEM and EDX measurements before cycling, after the pretreatment, and after 100 cycles (Hitachi S-4800 and EDAX Genesis 4000). To exclude the effects of air, the cycled cells were opened inside the glovebox and the Si/C-anodes were washed with DEC, dried, and afterwards transferred to the SEM by an air tight sample holder. The SEM-analysis was performed using a mixed signal of the secondary and backscattered electrons to have a good compromise in structural and compositional information. Finally, the effects of the pretreatment method on the composition of the SEI were analyzed by ATR-FTIR measurements (Shimadzu IRPrestige-21; using a Ge-crystal) between 500 cm^{-1} and 3500 cm^{-1} and a resolution of 2 cm^{-1} . Therefore, a non-pretreated sample before cycling was used as a reference system and compared to the ATR-FTIR spectra of the anodes measured directly after the pretreatment procedure and after 100 cycles in the reference electrolyte.

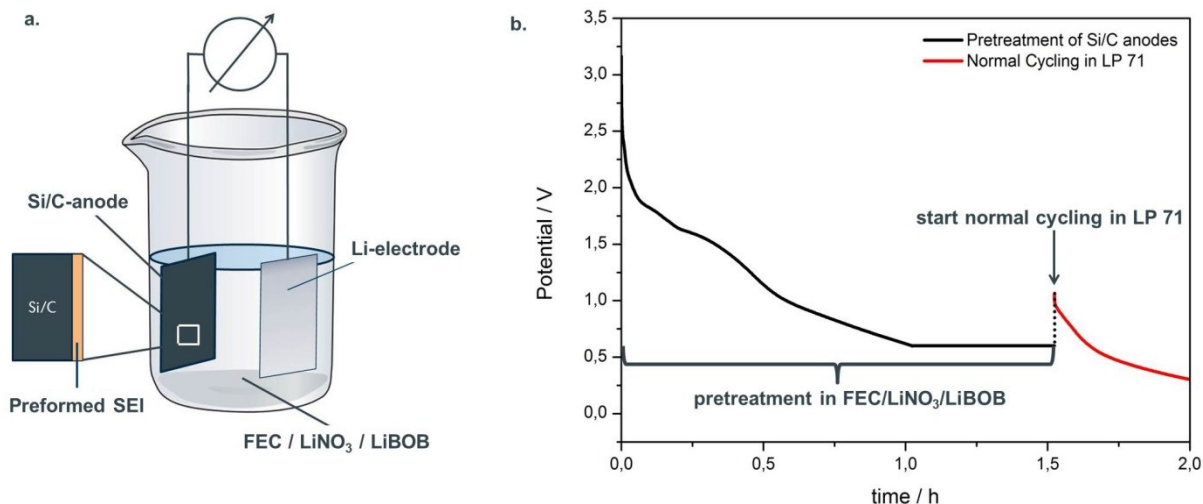


Figure 24: a.) Experimental setup for the pretreatment procedure b.) Potential vs. time plot during the pretreatment process of the Si/C-anodes in the pretreatment solution containing FEC, LiBOB, and LiNO₃.

5.3 . Results

In Figure 24b the potential vs. time behavior is shown for a typical electrochemical pretreatment experiment of the Si/C-based anodes. The potential limit of 0.6 V is reached in ~1h by applying a constant current of C/10. The potential was subsequently held constant for 30 min to form a SEI on the surface of the electrode. The formation of the primary SEI due to the decomposition of the pretreatment solution can be observed in the dQ vs. V plot in Figure 25. The potential range of 2.2 V-1.6 V features three distinctive peaks which indicate the reductive decomposition of the three components FEC, LiBOB, and LiNO₃ of the pretreatment solution. The decomposition of FEC starts at ~1.6 V vs. Li/Li⁺ and the decomposition of LiBOB is in the potential range of 1.7-1.8 V vs. Li/Li⁺ [161, 162]. Therefore, we assume that the small peak at ~2.2 V vs. Li/Li⁺ can be assigned to the reductive decomposition of LiNO₃. Possible reductive decomposition products of LiNO₃ have been described by Aurbach et al. to be Li₂O and Li_xNO_y species which both act as good passivating agents that simultaneously allow a fast Li⁺-transport [115, 163].

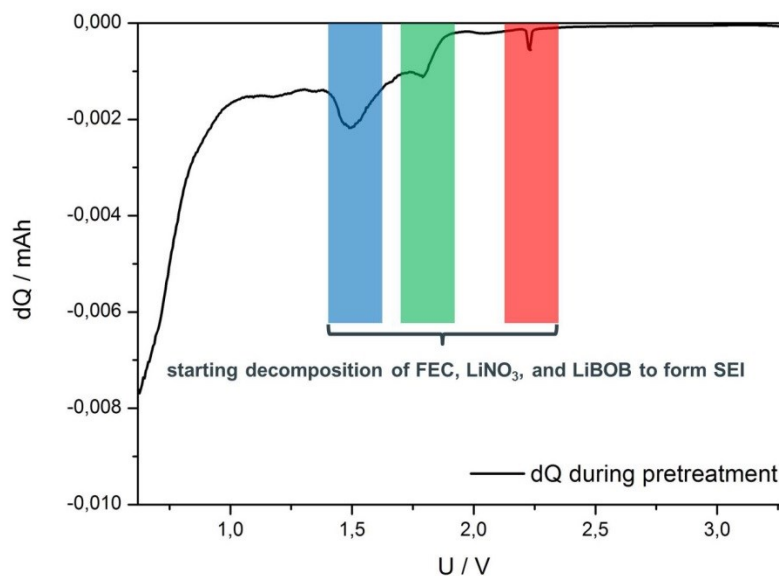


Figure 25: Differential capacity (dQ) vs. potential behavior during the pretreatment process. The peaks indicate the reductive decomposition of the pretreatment solution components

After the primary SEI formation the electrode is newly assembled using the standard electrolyte LP 71 for the succeeding cycles. This is indicated in Figure 24b as starting of the normal cycling where the potential initially rises again to ~ 1 V by an applied current equivalent to $C/10$. In case of a fully passivating SEI, Li^+ -insertion would start immediately and the potential would drop directly to 0.5 V. Since the potential drop is on a timescale of several minutes, the preformed SEI is not fully passivating and additional electrolyte decomposition occurs. However, the electrolyte decomposition is effectively impeded by the preformed SEI resulting in a higher capacity retention, cycling stability, and coulombic efficiency (CE). As a reference system non-pretreated Si/C-anodes in the same standard electrolyte solution (LP 71) are used. In Figure 26, the non-pretreated anodes display a relatively low CE during the first cycle with $\sim 59\%$ which can be explained by the decomposition of the LP 71 electrolyte and the formation of the SEI layer on the electrode surface. In comparison to the non-pretreated anode the already pretreated anode exhibits a significantly higher first cycle CE of $\sim 85\%$ which is believed to be a direct consequence of the primary formed SEI layer during the pretreatment procedure. However, it is important to notice that the CE after the pretreatment is only improved but not reaches close to 100 % which, consistently to the discussion for Figure 24b, indicates that there are still surface reactions taking place and that the SEI formation process is not completed after the pretreatment procedure.

Moreover, Figure 26 displays an increased cycling stability, specific charging capacity, and CE throughout 100 charge/discharge cycles for the pretreated compared to the non-pretreated electrodes. After 100 cycles the non-pretreated anodes achieve only a specific

charging capacity of $\sim 281 \text{ mAh}\cdot\text{g}^{-1}$ compared to $\sim 900 \text{ mAh}\cdot\text{g}^{-1}$ for the pretreated electrodes. Furthermore, the CE reaches $\sim 99.5 \%$ for the pretreated anodes compared to $\sim 90\text{--}95 \%$ in case of the non-pretreated anodes. It is important to emphasize that all the cycling experiments were conducted by using the same electrolyte (LP 71, without any additives) which leads to the conclusion that the improved cycling performance can be attributed to the pretreatment in the specific pretreatment solution.

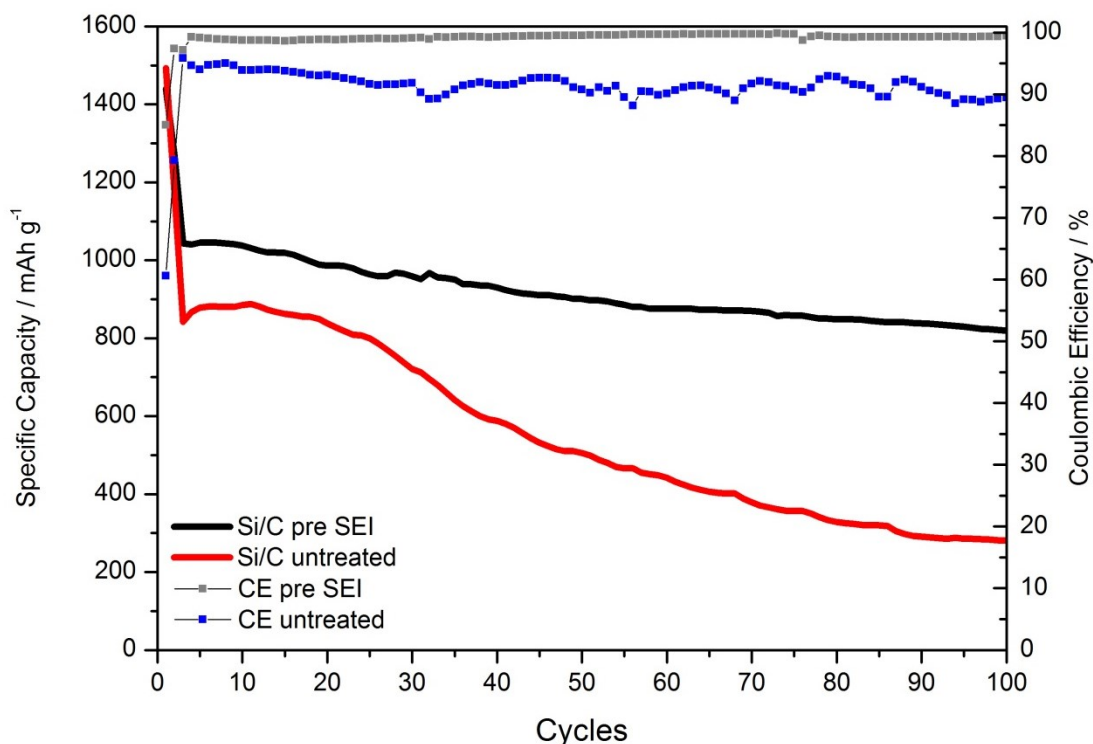


Figure 26: Comparison of the capacity vs. cycling performance between the pretreated and non-pretreated Si/C-anodes for 100 cycles.

To investigate the effect of the preformed SEI on the long term cycling stability we cycled the Si/C-anodes for 250 cycles. The results in Figure 27 point out that the cycling behavior for the charging as well as the discharging process only shows a slow decrease during the long term cycling procedure. After 250 cycles the anodes still display $\sim 705 \text{ mAh}\cdot\text{g}^{-1}$ which is $\sim 71 \%$ of the initial 1C capacity. Moreover, the CE during the 250 cycles is very high with $\sim 99.5 \%$ indicating a good reversibility of the Li^+ -insertion/deinsertion process. Without the pretreatment it was not possible to cycle the cells for this high number of cycles which can be seen in Figure 26.

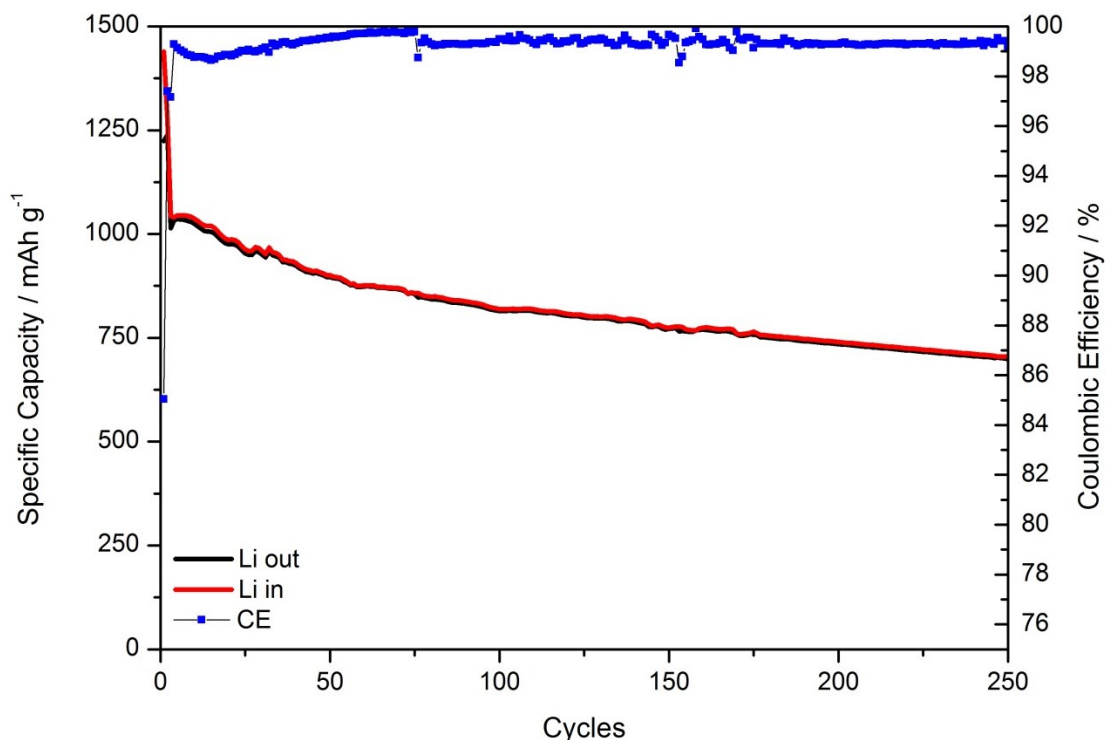


Figure 27: Long term cycling behavior of the pretreated Si/C-anodes using the LP 71 electrolyte without any additives.

The preformed SEI also influences the rate performance of the Si/C-anode. Figure 28 shows the differences between the pretreated and non-pretreated electrodes at different C-rates. The non-pretreated Si/C-anode shows a stable cycling performance only in the first few cycles and at relatively low charging rates of C/10 or C/2 respectively. In the following cycles we observe a strong decrease of the specific capacity especially at higher C-rates of 1C and 5C. In contrast, the pretreated electrodes display only a slight capacity decay for charging rates of C/10, C/2, and 1C and only at a very high rate of 5C (~5 A/g) one observes a significant capacity drop associated with an increased capacity fading over cycling. Since the capacity in the succeeding cycles at a slow charging rate of C/10 almost recovers the initial values received at C/10, the high current do not irreversibly modify the chemical structure of the electrode and the low capacities at high currents result from transport related polarization effects.

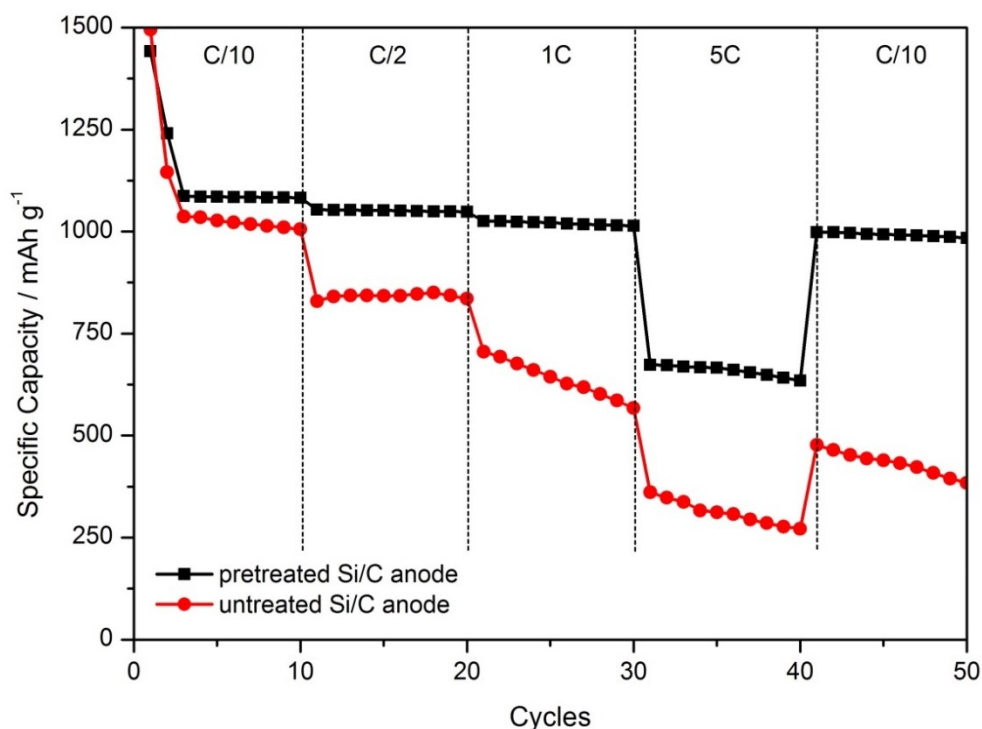


Figure 28: Performance of the pretreated and non-pretreated Si/C-anodes at different C-rates.

An alternative method to determine the rate performance would be to evaluate the remaining charging or discharging current after one hour holding the voltage constant at the respective potential limit. This constant voltage (CV) step allows for a better equilibration of the given battery cell system.

If the remaining current during the CV-step approaches zero it indicates that a complete lithiation/delithiation of the active material took place. On the other hand two possible mechanisms can appear if the current is significantly larger than zero. One possibility is a slow Li^+ -transport which influences the rate performance of the battery. The other possibility is that electrochemical side reactions like e.g. SEI formation due to the continuous decomposition of the electrolyte solution take place. The latter of course does not give any information about the rate performance of the battery cell. Figure 29 displays the current vs. time plot for 100 cycles with the pretreated (Figure 29a) and non-pretreated (Figure 29d) Si/C-anodes. Enlargements of a region at the beginning and one at the end of the cycling process are shown in Figure 29b+c and Figure 29e+f. The remaining current after the CV step is indicated as the blue dotted line for the discharge processes and as the red dotted line for the charge processes. All discharge processes approach a remaining current close to zero after the CV-step, hence the delithiation is completed and no side reactions occur. This is conclusive, since at the 0.9 V vs Li/Li^+ potential of the discharge CV-step the electrolyte is known to be

stable. Therefore, one learns that the Li^+ -transport is fast enough to occur within the given time frame of 1 h. We do expect a similar transport behavior in the charging step and therefore assume that the lithiation of Si is also terminated after the 1 h CV-step. But the remaining charging currents significantly differ from zero. Since the remaining charging current after the CV-step does not origin from the Li^+ insertion, this current can be related to the electrolyte decomposition. The remaining charging current with the pretreated Si/C-electrode is shown in Figure 29b+c for the initial cycles and cycles around the 100th, respectively. Initially the absolute remaining current is 0.038 mA and quickly decreases to a constant value of 0.023 mA with higher cycle numbers. Hence, the electrolyte decomposition occurs each cycle and the SEI is not self-blocking its growth. However, compared to the non-pretreated Si/C-anodes, the pretreated ones are rather stable against electrolyte decomposition which is indicated by the about one order of magnitude larger remaining current for the non-pretreated electrodes. The non-pretreated samples exhibit an initial absolute remaining current of 0.4 mA which decreases to a saturation value of 0.2 mA at around the 15th cycle. This means that the electrolyte decomposition and therewith the continuous SEI growth should occur at a higher rate before. This might explain the capacity increase up to the 15th cycle, observed in Figure 26.

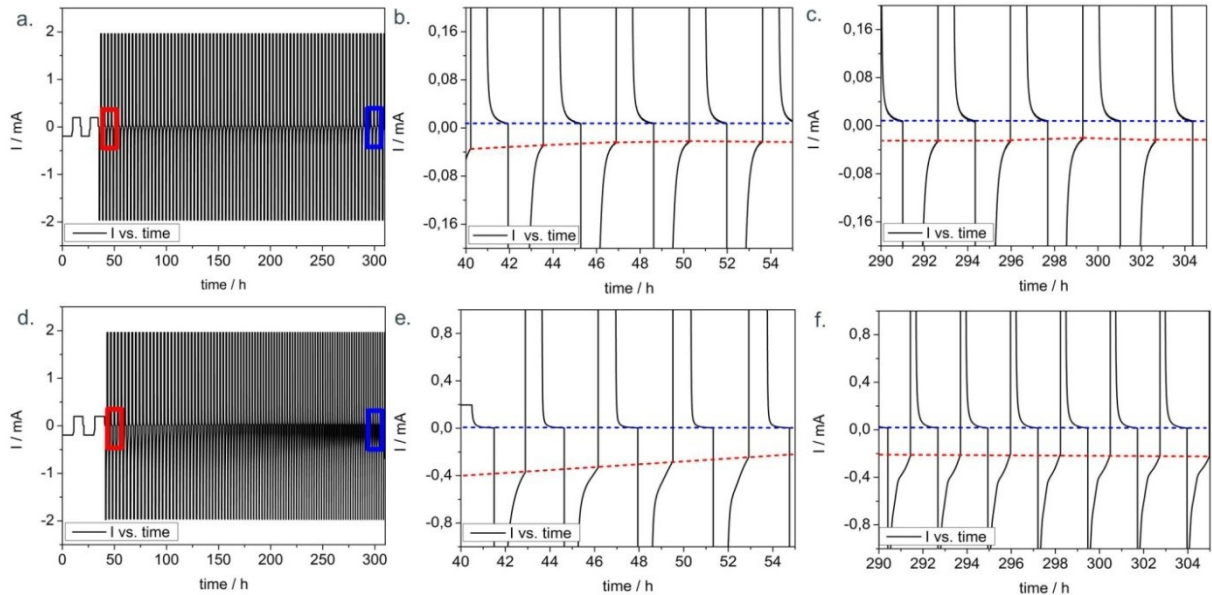


Figure 29: a) Current vs. time plot for 100 cycles of the pretreated Si/C-anode; b) Magnified area for the current vs. time behavior, indicated by the red square in Figure 29a; c) Magnified area for the current vs. time behavior, indicated by the blue square in Figure 29a; d) Current vs. time plot for 100 cycles of the non-pretreated Si/C-anode; e) Magnified area for the current vs. time behavior, indicated by the red square in Figure 29c; f) Magnified area for the current vs. time behavior, indicated by the blue square in Figure 29c

The stabilization of the SEI due to the effective pretreatment is also observed by a morphological analysis with SEM. Figure 30 displays the morphological evolution of the pristine Si/C-anode (Figure 30a+d) and the results after 1 cycle (Figure 30b+e) and 100 cycles (Figure 30c+f) for the non-pretreated Si/C-anodes. The applied SEM mode, mixing signals of secondary and backscattered electrons, results in a good contrast between the Si particles (brighter contrast) as well as the conductive C-nanoparticles (darker contrast). The graphite flakes can be easily distinguished due to its flake-like structure and its dark contrast. After 1 cycle, we observe a slight contrast change for the non-pretreated anode that can be explained by the SEI formation; furthermore, we monitor a beginning coverage with SEI. Moreover, we observe that some particles lose their original shape and getting distorted (indicated by the particles in the area of the black square in Figure 30e.). After 100 cycles the anode is almost fully covered by a thick SEI layer and it is almost impossible to distinguish between the different electrode components. These observations indicate that the SEI formed on the non-pretreated Si/C-anodes still allow intensive electrolyte decomposition accompanied by a continuous growth of the SEI throughout the cycling process.

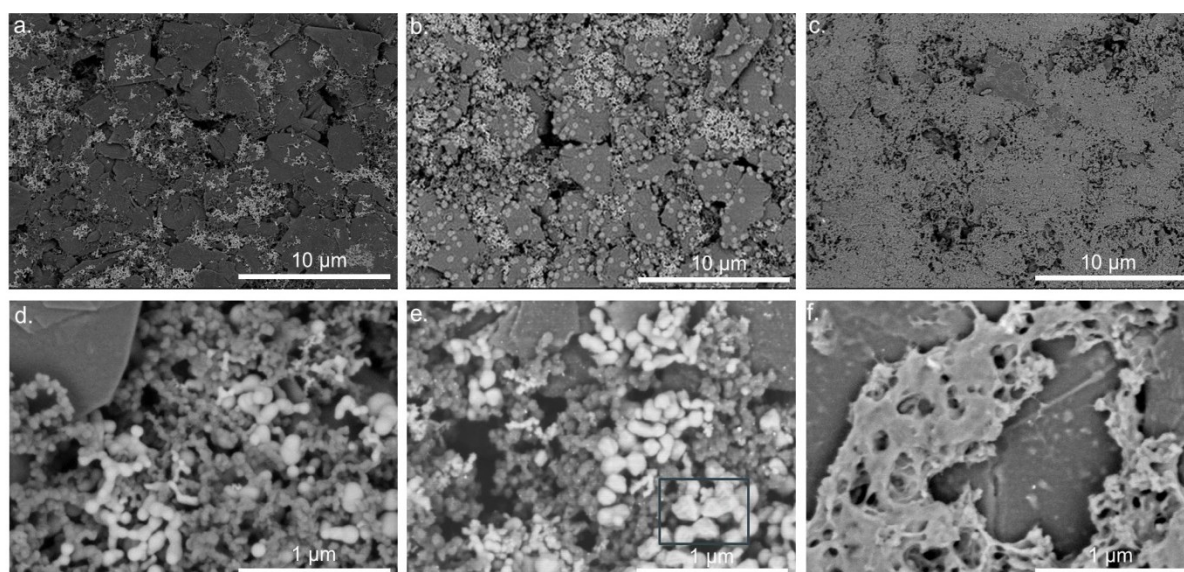


Figure 30 a-f.): SEM images of the non-pretreated Si/C-anode before cycling (a+d), after 1 cycle (b+e), and after 100 cycles (c+f).

The SEM-images for the pretreated electrodes are illustrated in Figure 31. The electrode morphology directly after the pretreatment procedure is shown in Figure 31a+d. By comparing Figure 30a and Figure 31a we find a slightly brighter contrast in case of the pretreated electrode which can be assigned to the formation of a thin SEI layer. Nevertheless, the morphological differences between the uncycled and pretreated electrode are negligible which

can be verified by comparing the magnified SEM images shown in Figure 30d and Figure 31d. Our previous results indicate that the pretreatment strongly influences the growth of the SEI film on the electrode surface which becomes visible due to a less severe coverage of the electrode after 1 cycle (Figure 31b) compared to the results for the non-pretreated electrode (Figure 30b). In fact, after 1 cycle we observe that the surface of the electrode is less covered. After 100 cycles in Figure 31a+f one observes a significant change in the surface morphology, since the surface is now covered with a SEI layer. However this coverage is far less severe compared to the non-pretreated anodes shown in Figure 30 c+f.

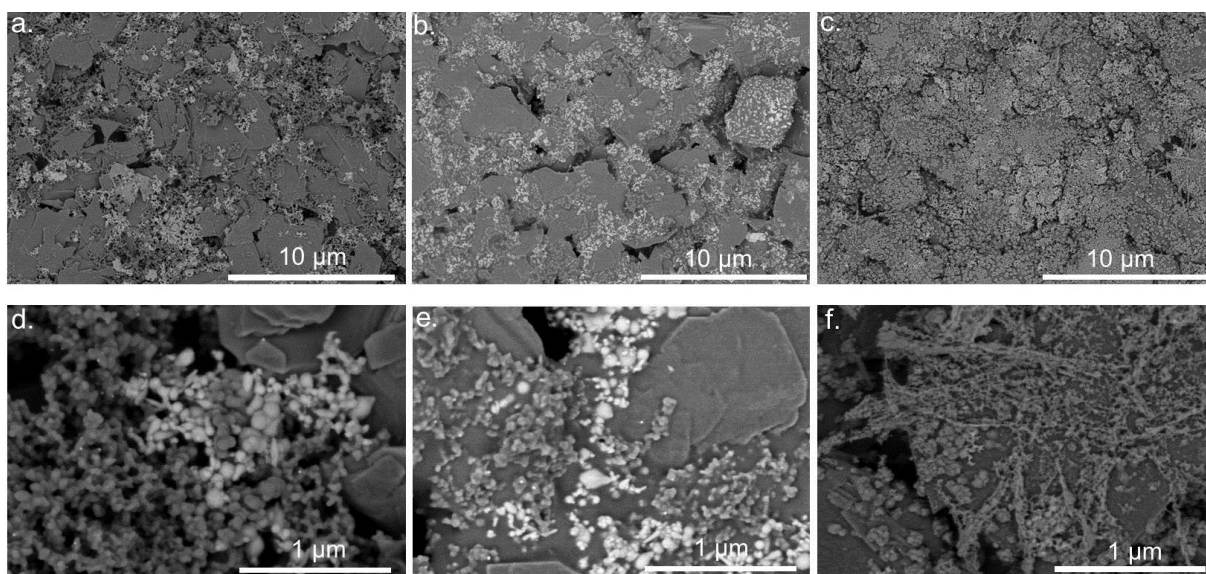


Figure 31 a-f): SEM images of the pretreated Si/C-anodes directly after the pretreatment (a+d), after 1 cycle (b+e) and after 100 cycles (c+f).

Changes in the SEI composition and SEI growth characteristics throughout the cycling for the non-pretreated and pretreated anodes are also visible in the EDX-overview spectra in Figure 32a+b. The results reveal that the Si-signal is strongly decreased throughout the 100 cycles in case of the non-pretreated anode whereas the Si-signal for the pretreated anode only shows a small decay. This result can be explained by a thicker SEI grown on the surface of the non-pretreated electrodes. Moreover, Figure 32b shows that the composition of the SEI still changes with continuous cycling. This is in good agreement with Figure 24, indicating that the SEI formed after the pretreatment is not completely stable, but a different SEI grows on it when cycled in the standard electrolyte. This additional SEI has a significant F (fluorine) content as indicated by the increasing F signal with higher cycle numbers. Further the SEI growing on the pretreated electrode also differs from the SEI growing on the non-pretreated electrode, even though they are both cycled in the same electrolyte solution. As mentioned,

the SEI on the pretreated electrode is strongly F containing, whereas the SEI of the non-pretreated anodes seem to have a major O (oxygen) content. So the chemical composition of the electrolyte strongly influences the electrode composition and therewith also the further SEI growth.

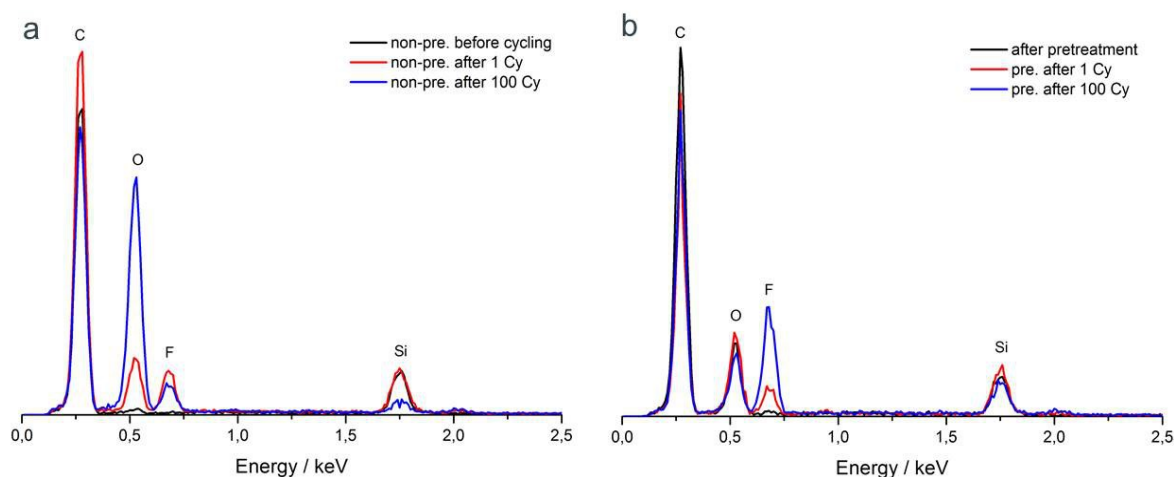


Figure 32: a.) EDX overview spectra's before cycling, after 1 cycle, and 100 cycles for the non-pretreated Si/C-anode b.) EDX overview spectra's directly after the pretreatment, after 1 cycle, and after 100 cycles for the pretreated Si/C-anode.

To investigate the fiberlike structures observed during the cycling procedure in the SEM images we characterized the chemical composition of the white square area in Figure 33a by EDX measurements. The SEM image is a close up of Figure 31f but in the secondary electron mode to better visualize the morphology of the anode components especially the fiberlike structures. First, we performed EDX measurements with 5 kV accelerating voltage, the results of these EDX measurements lead to a first assumption that the fiberlike structure may does not contain Si (see Figure 33b (5 kV)). However, a second investigation with an increased accelerating voltage of 15 kV reveals that the Si seems to be buried under a thick SEI layer which mainly consists of F, O, and P (phosphate).

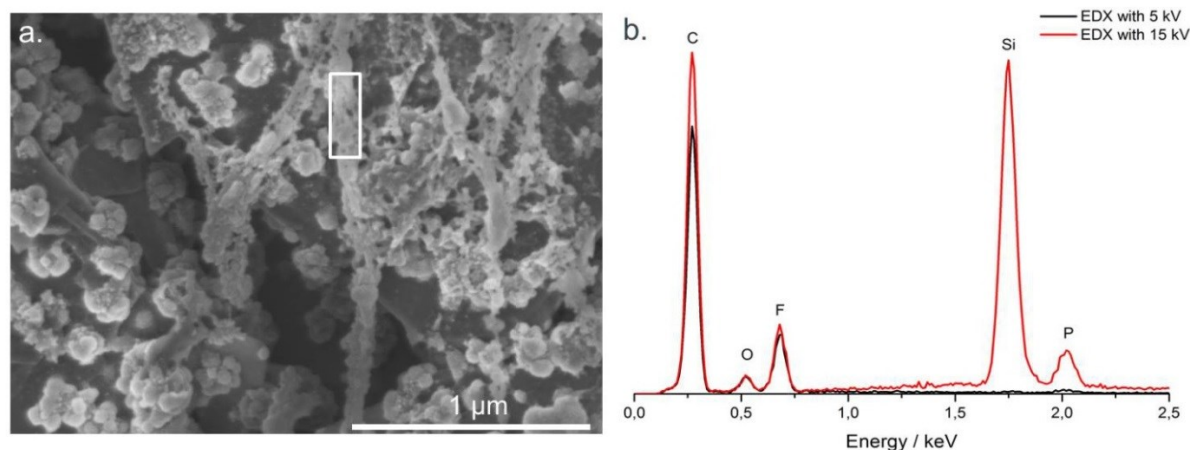


Figure 33: a.) SEM image of the forming fiberlike structures of the pretreated Si/C-anode after 100 cycles in the secondary electron mode to better visualize the morphology of the anode components b.) EDX spectra's of the area indicated with a white square in Figure 33a with 5 kV and 15 kV accelerating voltage

The difference in the chemistry of the SEI on pretreated and non-pretreated Si/C-anodes is also verified by ATR-FTIR measurements. The FTIR-spectra of the pristine electrodes shown in Figure 34a exhibit a broad peak around $900\text{--}1200\text{ cm}^{-1}$ which can be attributed to the Si-O bands of the Si active material of the electrodes. Moreover, a few smaller peaks could be observed which indicate the presence of the PAA-binder with the characteristic COOH-vibration at $\sim 1700\text{ cm}^{-1}$. The other bands are likely due to other vibrations of either the binder or surface groups on the Si, graphite, or conductive carbon (e.g. C-H $\sim 1380\text{--}1480\text{ cm}^{-1}$). After the pretreatment we observe a drastic change of the FTIR-spectra due to the formation of the preformed SEI. The new bands after the pretreatment procedure in the potential range of 3.3-0.6 V vs. Li/Li^+ can be assigned to the preformed SEI on the surface of the anodes which is composed of the reduction products of FEC, LiBOB, and LiNO_3 . For example, the decomposition of the LiNO_3 additive results in N containing groups, hence the characteristic N-O bands at $\sim 1515\text{--}1580\text{ cm}^{-1}$ and $\sim 1350\text{ cm}^{-1}$ as well as the N-H band at $\sim 1650\text{--}1680\text{ cm}^{-1}$ are related to it. Moreover, the bands at 1828 cm^{-1} and 1150 cm^{-1} are likely due to the formation of PEO-like species (poly(ethyleneoxide)) with the characteristic (O-C-O)- and (C-O-C)-vibrations. The formation of PEO-like species must originate from a C containing reactant and is therefore related to the reductive decomposition of FEC. Furthermore, the decomposition of LiBOB and LiNO_3 result in the formation of certain Li containing components such as Li_2CO_3 (OCO $^-$ bending at $\sim 859\text{ cm}^{-1}$) and Li_2O ($\sim 607\text{ cm}^{-1}$). The other components in the primary SEI are very difficult to clarify because of the variety of possible decomposition products with similar characteristic groups. Nevertheless, the FTIR results clearly indicate the differences between the pretreated and the pristine Si/C-anodes. In Figure 34b the preformed SEI is shown after 100 cycles in the standard electrolyte LP 71. Most of the above

discussed FTIR-bands identified directly after the pretreatment are still visible after 100 cycles in the standard electrolyte.

Further Figure 34b shows the FTIR-spectra of non-pretreated Si/C-anodes after 100 cycles in the standard electrolyte. The results clearly show the differences in the SEI composition between the pretreated and non-pretreated anodes after 100 cycles in the same electrolyte. The bands of the non-pretreated electrode significantly differ from those of the pretreated electrode. The different FTIR-bands lead to the conclusion that the pretreatment not only influences the SEI composition of the primary SEI but also has an influence on the SEI composition after 100 cycles. The different SEI formation by cycling in the identical electrolyte solution might either originate from the influence of surface groups formed during the pretreatment or from different potential conditions due to a different voltage drop over the preformed SEI.

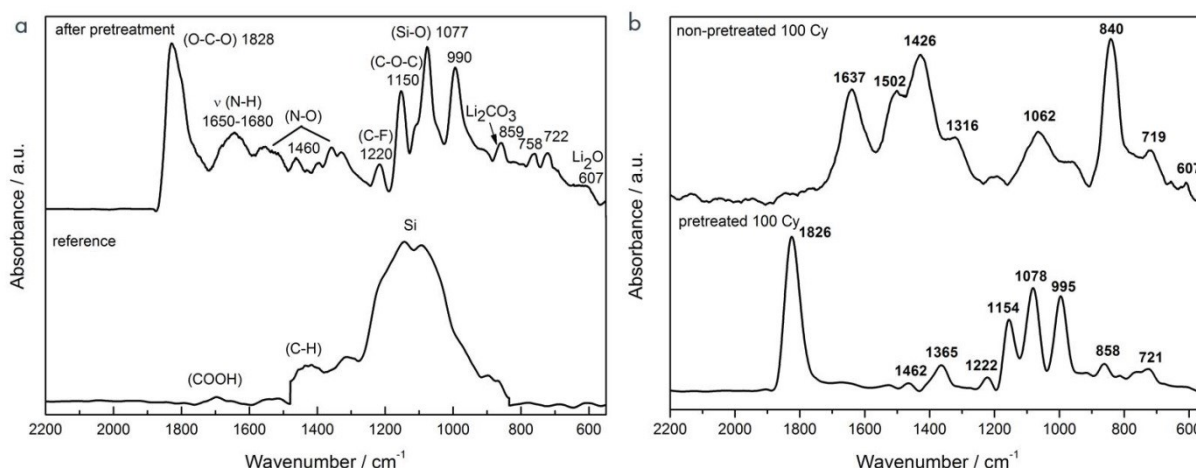


Figure 34: a). ATR-FTIR spectra's are of the pristine Si/C-anode (reference) and directly after the pretreatment process b.) Comparison of ATR-FTIR spectra's of pretreated and non-pretreated Si/C-anodes after 100 cycles in the LP 71 reference electrolyte.

5.4 . Discussion

The above presented study compares Si/C-anodes which were equally prepared except for an additional SEI pretreatment step for one of the electrodes. The electrodes are cycled in the same standard electrolyte after the pretreatment. Since the electrode morphology of the pretreated and the non-pretreated electrode are almost identical, a difference in mechanical stress induced by the large volume expansion of Si can be excluded as origin for the pro-

longed stability of the pretreated anode. This agrees with findings from TEM investigations by other groups, where Si nanoparticles stay mechanically intact if they are below a certain threshold size [56]. But in contrast to the morphology, our spectroscopic analysis identifies that the major changes due to the pretreatment affect the chemical interface of the anode to the electrolyte. The primary SEI formed after the pretreatment of the anodes exhibits different chemical species compared to the non-pretreated anode. This is not surprising, since it was electrochemically pretreated in different initial species. Important is the succeeding cycling in the same standard electrolyte. The CE (coulombic efficiency) in the first cycle of the pretreated anode in the standard electrolyte is with ~85 % too low for a pure reversible Li^+ -insertion and deinsertion and indicates that the pretreatment does not form a completely stable SEI yet. However, the results show that the growth velocity of the further SEI in the following cycles, resulting from the decomposition of the standard electrolyte, is significantly decelerated compared to the SEI growth rate on a non-pretreated electrode. Besides the growth rate, the FTIR results indicate that also the composition of the SEI from the standard electrolyte is not identical for the two initially differently treated electrodes. Hence, the interface chemistry of the electrode and electrolyte influence the growth rate and the composition of the SEI. Overall the SEI formation is significantly dependent on the electrolyte and the electrode surface and has to be taken into account in the discussion of the battery reaction. Therefore, as discussed earlier in chapter 4 the battery electrode of importance is not the pristine, but the electrode which forms under the operation conditions by the interfacial reactions with the electrolyte.

We further observe that the SEI thickness exhibits a certain correlation to the overall battery performance, meaning that for higher cycle numbers a thicker SEI results in lower retained specific capacity. The time dependent measurements show that a transport limitation is unlikely to explain this worse battery performance with a thicker SEI. A possible, but here not completely proven explanation for the influence of the SEI thickness on the rapid capacity decay could be that the SEI overgrows the Si particles and detaches them from the current collecting carbon framework, if the SEI layer reaches a certain thickness. Thereby the active Si material gets electronically insulated and cannot take part in the following lithiation and delithiation processes. In case of the non-pretreated Si/C-anodes the critical thickness seems to be reached after ~15-20 cycles because after this we observe a rapid decrease of the specific capacity (compare Figure 26). The above discussed results allow for the conclusion that the interfacial chemistry between the electrode and the electrolyte is the major factor limiting the stability of Si/C-based anodes for Li-Ion batteries. This finding becomes especially relevant since the nanostructuring of Si, required for a better mechanical stability, results in an enhanced interface area to the electrolyte and therefore induces stability prob-

lems which require an especially stabilized electrode/electrolyte interface. Hence, an effective pretreatment and the formation of a more stable SEI on Si-based anodes significantly helps to increase the cycling stability and capacity retention of future Si-based anodes in Li-ion batteries. Moreover, a preformed SEI prior to the actual formation and cycling would significantly improve the possible energy densities of a battery because the irreversible capacity during the first few cycles of a Li-ion battery is mainly due to the formation of the SEI in which certain amounts of Li are irreversibly consumed. The new pretreatment procedure does not prevent the SEI formation, but significantly reduces the SEI growth in the following cycles as discussed above. This makes the procedure additionally attractive for full cells where only a limited amount of Li is supplied by the battery cathode.

5.5 . Conclusion

This work presents the results for a new pretreatment method of Si/C-anodes for Li-ion batteries prior to the actual charge/discharge experiments in a standard electrolyte solution. The pretreatment is conducted electrochemically inside a beaker using a pretreatment solution containing FEC, LiNO_3 , and LiBOB which are known to be good film forming agents. The results of the electrochemical measurement reveal an increased specific capacity, cycling stability, and coulombic efficiency (CE) for the pretreated anodes. To investigate the differences between the pretreated and non-pretreated Si/C-anodes we monitored the chemical changes taking place at the surfaces during the pretreatment procedure and cycling process by ATR-FTIR measurements. The obtained results reveal a drastic change in the surface composition due to the formation of a thin primary SEI layer on the Si/C-anode. The different effects of the pretreatment on the microstructural characteristics throughout cycling were investigated by SEM and EDX measurements and compared to non-pretreated Si/C-anodes cycled in the same electrolyte. The results illustrate that the SEI growth can be strongly impeded due to the formation of a primary SEI by the pretreatment procedure in the specific pretreatment solution. The irreversible capacity during the formation process is strongly reduced which goes hand in hand with an increased CE during the Li-ion battery cell formation process. In case of the non-pretreated Si/C-anodes we observe an enhanced SEI growth resulting in rapid capacity decay. Our results display that the pretreatment procedure slows down the degradation mechanisms in Si/C-anodes. Hence, we assume the interfacial chemistry to be the dominant factor for the battery degradation and the formation of a stable SEI is the key parameter to achieve a stable cycling performance with Si/C-anodes.

6 Conclusion and outlook

6.1 Conclusion

Increasing the energy density in Li-Ion batteries is crucial for the widespread of electric or partly electrified vehicles, consumer electronics, or stationary energy storage systems. One way to achieve this aim is to change the cell chemistry of a Li-Ion battery cell by substituting the existing anode and cathode active materials. One possible anode material that has the capability to increase the energy densities in future Li-Ion batteries is Si due to its high theoretical gravimetric capacity of $\sim 3580 \text{ mAh g}^{-1}$ which is nearly ten times the theoretical capacity of graphite ($\sim 372 \text{ mAh g}^{-1}$).

This thesis deals with two different approaches to alter and improve the electrochemical and interfacial properties of Si/C-based anodes to increase the specific capacity, the cycling stability, and the capacity retention. Moreover, it should provide a better understanding of possible degradation processes taking place in Si/C-based anodes.

In chapter 4 the first approach is presented and discussed which includes the development and analysis of a new electrolyte formulation. The obtained results for the new electrolyte composition were compared to a commercially available standard electrolyte consisting of the Li-salt LiPF_6 and the solvents EC, DMC, and DEC (LP 71). In the new electrolyte solution 10 wt. % FEC and 0.5 wt. % LiNO_3 were added as additives. The addition of these additives proved to have a beneficial synergetic effect on the performance of Si/C-anodes and significantly increase the specific capacity and cycle life.

To gain more insights into the differences between the reference electrolyte and the new electrolyte a cycle dependent microstructural SEM- and EDX-analysis were conducted. The obtained results lead to the conclusion that the SEI on the Si/C-anodes formed in the new electrolyte is significantly thinner compared to the SEI formed on the Si/C-anodes cycled in the reference electrolyte solution. Furthermore, in case of the LP 71 electrolyte the cycle dependent SEM-analysis revealed that the SEI growth is significantly enhanced throughout the cycling process whereas the SEI growth seems to be slowed down in case of the new electrolyte solution. These results are supported by cycle dependent EDX measurements showing a strongly decreasing Si and C signal with increasing cycle number in case of the reference electrolyte. The obtained results during this study indicate that the Si active materials get likely buried under a thick layer of SEI during the continuous cycling procedure. We assume that the increasing coverage of the Si active material during the cycling process can lead to the electronic insulation from the electronically conducting framework and the cov-

ered Si active material cannot take part in the following lithiation and delithiation processes. In case of the new electrolyte solution, the EDX signals of C and Si are almost constant for 100 cycles which support the results of the SEM analysis indicating a thinner and less growing SEI. These findings can be one possible explanation for the more stable cycling performance of the Si/C-anodes in the new electrolyte.

A stable and thin SEI seems to be crucial for a good performing Si/C-anode. If the SEI is not insulating or dense enough the electrolyte solution is continuously decomposed throughout the cycling process resulting in a fast insulation of the Si-active material due to continuous SEI growth. This process is additionally accompanied by a strong capacity decay and short cycle life. The differences in the two electrolytes have been investigated by analyzing the ratio of the specific capacity during the constant voltage step (CV-step) to the total capacity in the constant current constant voltage cycling procedure (CC-CV). These measurements showed that the CV-ratio is strongly increasing in case of the anodes cycled in the reference electrolyte which can be explained by continuous electrolyte decomposition, due to a less stable SEI formed in the LP 71 electrolyte. In case of the new electrolyte solution, the ratio of the CV-capacity to the overall capacity of the Si/C-anode is almost constant throughout the cycling procedure.

Some of the findings in chapter 4 could also be confirmed in chapter 5, where a new electrochemical pretreatment method for Si/C-anodes was introduced to form a stable, primary SEI on the surface of the anodes prior to the actual cycling procedure. The results of the charge/discharge measurements reveal a significant increase of the cycling stability and specific capacity for the pretreated Si/C-anodes. The pretreatment was electrochemically conducted inside a beaker containing a solution of FEC, LiBOB, and LiNO₃ which are all known to be good film forming agents.

The study compared pretreated and non-pretreated Si/C-anodes in the same standard electrolyte solution. The charge/discharge measurements display a significantly higher CE of ~85% during the formation process in the first cycle for the pretreated anodes compared to the non-pretreated anodes (~59 %). This finding can be explained by the formation of a more stable primary SEI due to the electrochemical pretreatment procedure. However, a value of ~85 % indicates that the primary SEI is not completely protecting the Si/C-anode and still allows some electrolyte decomposition resulting in further SEI growth. Nevertheless, the SEI growth in the following cycles could be significantly slowed down compared to the non-pretreated electrodes which was found by cycle dependent SEM and EDX measurements. These measurements additionally revealed that the SEI is continuously growing in case of non-pretreated electrodes. One possible reason for this was found in the remaining current at the end of the CV step of the CC-CV cycling procedure. This time dependent measurements

showed that the remaining current at the end of the CV-step is about one order of magnitude higher in case of the non-pretreated electrodes. A one order of magnitude higher remaining current throughout the whole cycling process could be explained by enhanced electrolyte decomposition due to a less stable SEI. Transport limitation factors, due to a growing SEI could also add to the remaining current however, if the remaining current is dominated by transport limitation factors it should be significantly smaller at the beginning of the cycling procedure, when the SEI is still rather thin compared to its thickness at the end of the cycling process.

The results in this thesis point out that the SEI growth rate and thickness correlates with the declining overall cycle stability of the Si/C-anodes. A possible explanation for this observation could be that the continuously growing SEI overgrows the Si active material, which was already found in chapter 4. If the SEI is reaching a certain thickness the Si gets detached from the electron conducting carbon framework and gets electronically insulated hence it cannot take part in the following charge and discharge cycles resulting in small specific capacities.

Another result of this study revealed that the pretreatment procedure not only influences the SEI growth characteristics but also the surface composition of the electrodes. This was analyzed by FTIR measurements. The FTIR measurements display that the pretreatment effectively forms a primary SEI on the surface of the Si/C-anodes. Its composition can be linked to the decomposition products of the components of the pretreatment solution. After 100 cycles in the standard electrolyte the pretreated Si/C-anodes show only little differences in the FTIR spectra's. However, the differences to the FTIR spectra after 100 cycles for the non-pretreated Si/C-anodes are significant. Therefore we can conclude that the interface chemistry at the electrode/electrolyte interface influences the growth rate and the composition of the SEI. Hence, the SEI formation process depends on both the electrode surface characteristics and the electrolyte composition and has to be considered in the discussion of the battery reaction processes.

These findings display the importance of a stable SEI on the cycling performance and capacity retention. Since the morphology of the pretreated and non-pretreated Si/C-anodes have been almost identical, we can conclude that the performance differences are more likely linked to differences in the interface chemistry than to differences in mechanical stress induced by large volume expansions of the Si. Additionally the results of this thesis show that the Si/C-anode of importance is not the pristine, but the anode which forms after the formation under operation conditions due to interfacial reactions with the pretreatment solution or the electrolyte solution.

Moreover, another positive aspect of the pretreatment method in general is that the pre-

treatment leads to a significantly higher CE which could be very beneficial for the balancing of the anode and cathode of a Li-Ion battery full cell. In a Li-Ion battery full cell, the Li needed to form the SEI is incorporated into the cell by an excess of Li containing cathode active material. The excess of the cathode material results in a decrease of gravimetric and volumetric energy density.

Finally, the obtained results of this work demonstrate that the performance of Si/C-anodes is strongly linked to the electrolyte solution and the electrode surface chemistry at the electrode/electrolyte interface. Moreover, it points out that the application of different electrolyte compositions drastically influences the SEI formation process and that the SEI growth rate strongly affects the overall performance of the Si/C-anode.

Changes in the electrolyte solution or defined changes in the electrode surface characteristics are a possible way to improve the cycling stability and capacity retention however, the obtained results also make clear that the different sub-steps taking place in a Li-Ion battery are still very little understood. Changing the electrolyte solution or having changes in the anodes surface properties lead to changes in the complete “reaction network” of a Li-Ion battery and can affect not only the electrolyte or surface characteristics but also the SEI formation and SEI growth. Moreover, the effects of different electrolyte compositions on possible secondary reactions in the SEI formation process in Si/C-based anodes need further investigation. The combination of all these sub steps forms a complex “reaction network” which finally decides about the overall performance of the Si/C-anode and hence the Li-Ion battery. Therefore, the obtained results additionally reveal that it is important to gain a better understanding of the different sub-steps taking place in a Li-Ion battery cell and to learn how these sub-steps can be positively influenced by changes of certain battery cell parameters.

6.2 Outlook

The research and the results of this thesis could lead to a variety of future research topics:

- It is suggested to separate the different components of a Si/C-based battery cell to get a more detailed understanding of how different components influence the different sub-steps and the “reaction network” of Si-based anodes. Therefore, it would be necessary to design proper model systems and experiments. One possible research pathway could be the deposition of Si and C thin films to study the effects of different electrolyte solutions at different experimental conditions on the SEI formation process. This could lead to new insights how the SEI affects the cycling stability and may take part in the reversible charge/discharge process; a point which is not totally understood until today and should be addressed in the future to get a better understanding of the actual charge storage mechanism in Si-based anodes.
- The new pretreatment method opens a wide variety of possible research topics by changing the composition of the pretreatment solution and the pretreatment experimental parameters like voltage, current, composition of the pretreatment solution, or the temperature. Moreover, this method is also an easily applicable procedure to thoroughly investigate the influence of the different components and learn more about the degradation processes and the “reaction network” of the given Li-Ion battery cell. Furthermore, by isolating the different components and sub-steps it could lead to a better understanding of the SEI formation process in Si/C-anodes which proved to be crucial for the anode performance.
- In this thesis it was shown that the continuous growth of the SEI throughout the cycling procedure can be considered as one major degradation process in Si/C-anodes. Therefore, future research should concentrate on new solutions to control the interface chemistry by either form a stable artificial SEI prior to the cycling process or by techniques to impede the continuous SEI growth. This thesis pointed out that a feasible electrolyte composition and an effective electrochemical pretreatment, could slow down the SEI growth resulting in a better cycling stability and higher specific capacity. Hence, the investigation of effective coatings prior to the cycling process by thin film techniques (e.g. CVD) could be a possible way to control the interface chemistry of Si/C-anodes and to improve the performance of future Li-Ion batteries.

Appendix

A References

- [1] E. Agency. Laying the foundations for greener transport. *TERM*, 7, 2011.
- [2] B. Scrosati and J. Garche. Lithium batteries: Status, prospects and future. *Journal of Power Sources*, 195: 2419–2430, 2010.
- [3] J. Ryu, J. Kim, Y. Sung and S. Oh. Failure Modes of Silicon Powder Negative Electrode in Lithium Secondary Batteries. *Electrochemical and Solid-State Letters*, 7: 306–309, 2004.
- [4] K. Aifantis, S. Hackney and R. Kumar. High Energy Density Lithium Batteries. *Wiley-VCH Verlag GmbH & Co. KGaA*, 2010.
- [5] G. Wedler. Lehrbuch der physikalischen Chemie. *VCH Verlagsgesellschaft GmbH*, 1987.
- [6] F. Linden and T. Reddy. Handbook of Batteries. *Mc Graw-Hill Companies Inc.*, 2002.
- [7] A. Kraytsberg and Y. Ein-Eli. Higher, Stronger, Better...A Review of 5 Volt Cathode Materials for Advanced Lithium-Ion Batteries. *Advanced Energy Materials*, 2: 922–939, 2012.
- [8] J. Dahn, A. Sleight, H. Shi, J. Reimers, Q. Zhong and B. Way. Dependence of the electrochemical intercalation of lithium in carbons on the crystal structure of the carbon. *Electrochimica Acta*, 38: 1179–1191, 1993.
- [9] K. Kinoshita and K. Zaghbi. Negative electrodes for Li-ion batteries. *Journal of Power Sources*, 6: 403–408, 1994.
- [10] J. Charlier, X. Gonze and J. Michenaud. Graphite interplanar bonding: electronic delocalization and van der Waals interaction. *Europhysics Letters*, 28: 403–408, 1994.
- [11] H. Shi, J. Barker, M. Saidi and R. Koksang. Structure and Lithium Intercalation Properties of Synthetic and Natural Graphite. *Journal of the Electrochemical Society*, 143: 3466–3472, 1996.
- [12] K.N. Tatsumi, H. Iwashita, H. Sakaebe, S. Shioyama, A. Higuchi, H. Mabuchi, H. Fujimoto. The Influence of the Graphitic Structure on the Electrochemical Characteristics for the Anode of Secondary Lithium Batteries. *Journal of The Electrochemical Society*, 142: 716–720, 1995.
- [13] B. Scrosati. Lithium Rocking Chair Batteries: An Old Concept? *Journal of The Electrochemical Society*, 139: 2776–2781, 1992.
- [14] M. Winter, J. Besenhard, M. Spahr and P. Novák. Insertion Electrode Materials for Rechargeable Lithium Batteries. *Advanced Materials*, 10: 725–763, 1998.

- [15] Y. Reynier, R. Yazami and B. Fultz. Thermodynamics of Lithium Intercalation into Graphites and Disordered Carbons. *Journal of The Electrochemical Society*, 151: 422–426, 2004.
- [16] T. Ohzuku, Y. Iwakoshi and K. Sawai. Formation of Lithium-Graphite Intercalation Compounds in Nonaqueous Electrolytes and Their Application as a Negative Electrode for a Lithium Ion (Shuttlecock) Cell. *Journal of The Electrochemical Society*, 140: 2490–2498, 1993.
- [17] R. Baddour-Hadjean and J. Pereira-Ramos. Raman Microspectrometry Applied to the Study of Electrode Materials for Lithium Batteries. *Chemical Reviews*, 110: 1278–1319, 2010.
- [18] G. Chung, H. Kim, S. Yu, S. Jun, J. Choi and M. Kim. Origin of Graphite Exfoliation An Investigation of the Important Role of Solvent Cointercalation. *Journal of The Electrochemical Society*, 147: 4391–4398, 2000.
- [19] J. Gnanaraj, R. Thompson, J. DiCarlo and K. Abraham. The Role of Carbonate Solvents on Lithium Intercalation into Graphite. *Journal of The Electrochemical Society*, 154: 185–191, 2007.
- [20] C. Wang, A. Appleby and F. Little. Irreversible capacities of graphite anode for lithium-ion batteries. *Journal of Electroanalytical Chemistry*, 519: 9–17, 2002.
- [21] V. Agubra and J. Fergus. Lithium Ion Battery Anode Aging Mechanisms. *Materials*, 7: 414–429, 2013.
- [22] W. Zhang. Lithium insertion/extraction mechanism in alloy anodes for lithium-ion batteries. *Journal of Power Sources*, 196: 877–885, 2011.
- [23] H. Wu and Y. Cui. Designing nanostructured Si anodes for high energy lithium ion batteries. *nanotoday*, 7: 414–429, 2012.
- [24] D. Larcher, S. Beattie, M. Morcrette, K. Edström, J. Jumas and J. Tarascon. Recent findings and prospects in the field of pure metals as negative electrodes for Li-ion batteries. *Journal of Materials Chemistry*, 17: 3759–3772, 2007.
- [25] J. Besenhard, M. Hess and P. Komenda. Dimensionally stable Li-alloy electrodes for secondary batteries. *Solid State Ionics*, 40-41: 525–529, 1990.
- [26] U. Kasavajjula, C. Wang and A. Appleby. Nano- and bulk-silicon-based insertion anodes for lithium-ion secondary cells. *Journal of Power Sources*, 163: 1003–1039, 2007.
- [27] M. McDowell, S. Lee, W. Nix and Y. Cui. 25th Anniversary Article: Understanding the lithiation of Silicon and Other Alloying Anodes for Lithium-Ion Batteries. *Advanced Materials*, 25: 4966–4985, 2013.
- [28] R. Sharma and R. Seefurth. Thermodynamic Properties of the Lithium-Silicon System. *Journal of The Electrochemical Society*, 123: 1763–1768, 1976.

- [29] C. Wen and R. Huggins. Chemical diffusion in intermediate phases in the lithium-silicon system. *Journal of Solid State Chemistry*, 37: 271–278, 1981.
- [30] B. Boukamp, G. Lesh and R. Huggins. All-Solid Lithium Electrodes with Mixed-Conductor Matrix. *Journal of The Electrochemical Society*, 128: 725–729, 1981.
- [31] M. Obrovac and L. Christensen. Structural Changes in Silicon Anodes during Lithium Insertion/Extraction. *Electrochemical and Solid-State Letters*, 7: 93–96, 2004.
- [32] S. Beattie, D. Larcher, M. Morcrette, B. Simon and J. Tarascon. Si Electrodes for Li-Ion Batteries-A New Way to Look at an Old Problem. *Journal of The Electrochemical Society*, 155: 158–163, 2008.
- [33] M. Chan, C. Wolverton und J. Greeley. First principles simulations of the electrochemical lithiation and delithiation of faceted crystalline silicon. *Journal of the American Society*, 134: 14362–14374, 2012.
- [34] R. Benedek and M. Thackeray. Lithium reactions with intermetallic-compound electrodes. *Journal of Power Sources*, 110: 406–411, 2002.
- [35] A. Anani and R. Huggins. Multinary alloy electrodes for solid state batteries I. A Phase diagram approach for the selection and storage properties determination of candidate electrode materials. *Journal of Power Sources*, 38: 351–362, 1992.
- [36] M. Wachtler, M. Winter and J. Besenhard. Anodic materials for rechargeable Li-batteries. *Journal of Power Sources*, 105: 151–160, 2002.
- [37] M. Chon, V. Sethuraman, A. McCormick, V. Srinivasan and P. Guduru. Real-Time Measurement of Stress and Damage Evolution during Initial Lithiation of Crystalline Silicon. *PHYSICAL REVIEW LETTERS*, 107: p.045503, 2011.
- [38] P. Limthongkul, Y. Jang, N. Dudney and Y. Chiang. Electrochemically-driven- solid-state amorphization in lithium-silicon alloys and implications for lithium storage. *Acta Materialia*, 51: 1103–1113, 2003.
- [39] H. Li, X. Huang, L. Chen, G. Zhou, Z. Zhang, D. Yu, Y. Mo and N. Pei. The crystal structural evolution of nano-Si anode caused by lithium insertion and extraction. *Solid State Ionics*, 135: 181–191, 2000.
- [40] B. Key, M. Morcrette, J. Tarascon and C. Grey. Pair Distribution Function Analysis and Solid State NMR Studies of Silicon Electrodes for Lithium Ion batteries: Understanding the (De)lithiation Mechanisms. *Journal of the American Chemical Society*, 133: 503–512, 2010.
- [41] B. Key, R. Bhattacharyya, M. Morcrette, V. Seznec, J. Tarascon and C. Grey. Real-Time NMR Investigations of Structural Changes in Silicon Electrodes for Lithium-Ion Batteries. *Journal of the American Chemical Society*, 126: 9239–9249, 2009.

- [42] W. Weydanz, M. Wolfahrt-Mehrens and R. Huggins. A room temperature study of the binary lithium-silicon and the ternary lithium-chromium-silicon system for use in rechargeable lithium batteries. *Journal of Power Sources*, 81-82: 237–242, 1999.
- [43] T. Hatchard and J. Dahn. In Situ XRD and Electrochemical Study of the Reaction of Lithium with Amorphous Silicon. *Journal of The Electrochemical Society*, 151: 838–842, 2004.
- [44] H. Li, X. Huang, L. Chen, z. Wu and Y. Liang. A High Capacity Nano Si Composite Anode Material for Lithium Rechargeable Batteries. *Electrochemical and Solid-State Letters*, 2: 547–549, 1999.
- [45] H. Kim, C. Chou, J. Ekerdt and G. Hwang. Structure and Properties of Li-Si Alloys: A First-Principles Study. *The Journal of Physical Chemistry C*, 115: 2514–2521, 2011.
- [46] V. Chevrier, J. Zwanziger and J. Dahn. First principles study of Li-Si crystalline phases: Charge transfer, electronic structure, and lattice vibrations. *Journal of Alloys and Compounds*, 496: 25–36, 2010.
- [47] A. Morris, R. Needs, E. Salager, C. Grey and C. Pickard. Lithiation of silicon via lithium Zintl-defect complexes from first principles. *Physical Review B*, 87: p174108, 2013.
- [48] W. Wan, Q. Zhang, Y. Cui and E. Wang. First principles study of lithium insertion in bulk silicon. *Journal of physics:Condensed Matter*, 22: p.415501, 2010.
- [49] J. Li and J. Dahn. An In Situ X-Ray Diffraction Study of the Reaction of Li with Crystalline Si. *Journal of The Electrochemical Society*, 154: 156–161, 2007.
- [50] J. Christensen and J. Newman. Stress generation and fracture in lithium insertion materials. *Journal of Solid State Electrochemistry*, 10: 293–319, 2006.
- [51] M. Obrovac and L. Krause. Reversible Cycling of Crystalline Silicon Powder. *Journal of The Electrochemical Society*, 154: 103–108, 2007.
- [52] C. Chan, H. Peng, G. Liu, K. McIlwrath, X. Zhang, R. Huggins and Y. Cui. High Performance Lithium Battery Anodes Using Silicon Nanowires. *Nature Nanotechnology*, 3: 31–35, 2008.
- [53] L. Beaulieu, K. Eberman, R. Turner, L. Krause and J. Dahn. Colossal Reversible Volume Changes in Lithium Alloys. *Electrochemical and Solid-State Letters*, 4: 137–140, 2001.
- [54] J. Graetz, C. Ahn, R. Yazami and B. Fultz. Highly Reversible Lithium Storage in Nanostructured Silicon. *Electrochemical and Solid-State Letters*, 6: 194–197, 2003.
- [55] S. Nadimpalli, V. Sethuraman, S. Dalavi, B. Lucht, M. Chon, V. Shenoy and P. Guduru. Quantifying capacity loss due to solid-electrolyte-interphase layer formation on silicon negative electrodes in lithium-ion batteries. *Journal of Power Sources*, 215: 145–151, 2012.

- [56] X. Liu, L. Zhong, S. Huang, S. Mao, T. Zhu and J. Huang. Size-Dependent Fracture of Silicon Nanoparticles During Lithiation. *ACS NANO*, 6: 1522–1531, 2012.
- [57] H. Kim, M. Seo, M. Park and J. Cho. A Critical Size of Silicon Nano-Anodes for Lithium Rechargeable Batteries. *Angewandte Chemie International Edition*, 49: 2146–2149, 2010.
- [58] H. Jung, M. Park, Y. Yoon, G. Kim and S. Joo. Amorphous silicon anode for lithium-ion rechargeable batteries. *Journal of Power Sources*, 115: 346–351, 2003.
- [59] K. Lee, J. Jung, S. Lee, H. Moon and J. Park. Electrochemical characteristics of a-Si thin film anode for Li-ion rechargeable batteries. *Journal of Power Sources*, 129: 270–274, 2004.
- [60] S. Ohara, J. Suzuki, K. Sekine and T. Takamura. A thin film silicon anode for Li-ion batteries having a very large specific capacity and long cycle life. *Journal of Power Sources*, 136: 303–306, 2004.
- [61] H. Kim, M. So and S. Lee. Improved Cycling Performance of Si Thin Film Anode for Lithium Rechargeable Batteries. *Bulletin of the Korean Chemical Society*, 29: 2441–2444, 2008.
- [62] L. Cui, R. Ruffo, C. Chan, H. Peng and Y. Cui. Crystalline-Amorphous Core-Shell Silicon Nanowires for High Capacity and High Current Battery Electrodes. *Nano Letters*, 9: 491–495, 2009.
- [63] M. Park, M. Kim, J. Joo, K. Kim, J. Kim, S. Ahn, Y. Cui and J. Cho. Silicon Nanotube Battery Anodes. *Nano Letters*, 9: 3844–3847, 2009.
- [64] H. Wu, G. Chan, J. Choi, I. Ryu, Y. Yao, M. McDowell, S. Lee, A. Jackson, Y. Yuang, L. Hu and Y. Cui. Stable cycling of double-walled silicon nanotube battery anodes through solid-electrolyte interphase control. *Nature Nanotechnology*, 7: 310–315, 2012.
- [65] Y. Yao, M. McDowell, I. Ryu, H. Wu, N. Liu, L. Hu, W. Nix and Y. Cui. Interconnected Silicon Hollow Nanospheres for Lithium-Ion Battery Anodes with Long Cycle Life. *Nano Letters*, 11: 2949–2954, 2011.
- [66] L. Ji, Z. Lin, M. Alcoutlabi and X. Zhang. Recent developments in nanostructured anode materials for rechargeable lithium-ion batteries. *Energy & Environmental Science*, 4: 2682–2699, 2011.
- [67] H. Lee and S. Lee. Graphite-FeSi alloy composites as anode materials for rechargeable lithium batteries. *Journal of Power Sources*, 112: 649–654, 2002.
- [68] J. Kim, H. Lee, K. Lee, S. Lim and S. Lee. Fe/Si multi-layer thin film anodes for lithium rechargeable thin film batteries. *Electrochemistry Communications*, 5: 544–548, 2003.
- [69] V. Sethuraman, K. Kowolik and V. Srinivasan. Increased cycling efficiency and rate capability of copper-coated silicon anodes in lithium-ion batteries. *Journal of Power Sources*, 196: 393–398, 2011.

- [70] M. Au, Y. He, Y. Zhao, H. Ghassemi, R. Yassar, B. Garcia-Diaz and T. Adams. Silicon and silicon-copper composite nanorods for anodes of Li-ion rechargeable batteries. *Journal of Power Sources*, 196: 9640–9647, 2011.
- [71] M. Park, S. Rajendran, Y. Kang, K. Han, Y. Han and J. Lee. Si-Ni alloy-graphite composite synthesized by arc-melting and high-energy mechanical milling for use as anode in lithium-ion batteries. *Journal of Power Sources*, 158: 650–653, 2006.
- [72] Z. Wang, W. Tian, X. Liu, Y. Li and X. Li. Nanosized Si-Ni alloys anode prepared by hydrogen plasma-metal reaction for secondary lithium batteries. *Materials Chemistry and Physics*, 100: 92–97, 2006.
- [73] E. Lotfabad, P. Kalisvaart, A. Kohandehghan, K. Cui, M. Kupsta, B. Farbod and D. Mitlin. Si nanotubes ALD coated with TiO₂, TiN or Al₂O₃ as high performance lithium ion battery anodes. *Journal of Material Chemistry A*, 2: 2504–2516, 2014.
- [74] Y. Kang, S. Lee, S. Kim, G. Jeong, M. Sung, W. Choi and S. Kim. Phase transitions explanatory of the electrochemical degradation mechanisms of Si based materials. *Electrochemistry Communications*, 9: 959–964, 2007.
- [75] Z. Zeng, J. Tu, Y. Yang, J. Xiang, X. Huang, F. Mao and M. Ma. Nanostructured Si/TiC composite anode for Li-ion batteries. *Electrochimica Acta*, 53: 2742–2728, 2008.
- [76] J. Yan, H. Huang, J. Zhang and Y. Yang. The study of Mg₂Si/carbon composited as anode materials for lithium ion batteries. *Journal of Power Sources*, 175: 547–552, 2008.
- [77] C. Park, J. Kim, H. Kim and H. Sohn. Li-alloy based anode materials for Li secondary batteries. *Chemical Society Reviews*, 39: 3115–3141, 2010.
- [78] L. Fransson, J. Vaugney, R. Benedek, K. Edström, J. Thomas and M. Thackeray. Phase transitions in lithiated Cu₂Sb anodes for lithium batteries: an in situ X-ray diffraction study. *Electrochemistry Communications*, 3: 317–323, 2001.
- [79] M. Stjerndahl, H. Bryngelsson, T. Gustafsson, J. Vaughey, M. Thackeray and K. Edström. Surface chemistry of intermetallic AlSb-anodes for Li-ion batteries. *Electrochimica Acta*, 52: 4947–4955, 2007.
- [80] I. Amadei, S. Panero, B. Scrosati, G. Cocco and L. Schiffini. The Ni₃Sn₄ intermetallic as a novel electrode in lithium cells. *Journal of Power Sources*, 143: 227–230, 2005.
- [81] K. Ehnion, S. Naille, R. Dedyvère, P. Lippens, J. Jumas and D. Gonbeau. Ni₃Sn₄ Electrodes for Li-Ion Batteries: Li-Sn Alloying Process and Electrode/Electrolyte Interface Phenomena. *Chemistry of Materials*, 20: 5388–5398, 2008.
- [82] W. Liu, Z. Guo, W. Young, D. Shieh, H. Wu, M. Yang and N. Wu. Effect of electrode structure on performance of Si anode in Li-ion batteries: Si particle size and conductive additive. *Journal of Power Sources*, 140: 139–144, 2005.

- [83] A. Wilson and J. Dahn. Lithium Insertion in Carbons Containing Nanodispersed Silicon. *Journal of The Electrochemical Society*, 142: 326–332, 1995.
- [84] N. Dimov, S. Kugino and M. Yoshio. Mixed silicon-graphite composites as anode material for lithium ion batteries: Influence of preparation conditions on the properties of the material. *Journal of Power Sources*, 136: 108–114, 2004.
- [85] Z. Luo, D. Fan, X. Liu, H. Mao, C. Yao and Z. Deng. High performance silicon carbon composite anode materials for lithium ion batteries. *Journal of Power Sources*, 189: 16–21, 2009.
- [86] S. Ng, J. Wang, D. Wexler, K. Konstantinov, Z. Guo and H. Liu. Highly Reversible Lithium Storage in Spheroidal Carbon-Coated Silicon Nanocomposites as Anodes for Lithium-Ion Batteries. *Angewandte Chemie International Edition*, 45: 6896–6899, 2006.
- [87] N. Liu, H. Wu, M. McDowell, Y. Yao, C. Wang and Y. Cui. A Yolk-Shell Design for Stabilized and Scalable Li-Ion Battery Alloy Anodes. *Nano Letters*, 12: 3315–3321, 2012.
- [88] S. Iwamura, H. Nishihara and T. Kyotani. Effect of Buffer Size around nanosilicon Anode Particles for Lithium-Ion Batteries. *The Journal of Physical Chemistry C*, 116: 6004–6011, 2012.
- [89] L. Ji and X. Zhang. Fabrication of porous Carbon/Si composite nanofibers as high-capacity battery electrodes. *Electrochemistry Communications*, 11: 1146–1149, 2009.
- [90] Y. Hu, R. Demir-Cakan, M. Titirici, J. Müller, R. Schlögl, M. Antonietti and J. Maier. Superior Storage Performance of Si@SiO_x/C Nanocomposite as Anode Material for Lithium-Ion Batteries. *Angewandte Chemie International Edition*, 47: 1645–1649, 2008.
- [91] J. Li, R. Lewis and J. Dahn. Sodium Carboxymethyl Cellulose. *Electrochemical and Solid-State Letters*, 10: 17–20, 2007.
- [92] K. Xu. Nonaqueous Liquid Electrolytes for Lithium-Based Rechargeable Batteries. *Chemical Reviews*, 104: 4303–4418, 2004.
- [93] J. Goodenough and Y. Kim. Challenges for Rechargeable Li Batteries. *Chemistry of Materials*, 22: 587–603, 2010.
- [94] C. Campion, W. Li and B. Lucht. Thermal Decomposition of LiPF₆-Based Electrolytes for Lithium-Ion Batteries. *Journal of The Electrochemical Society*, 152: 2327–2334, 2005.
- [95] U. Heider, R. Oesten and M. Jungnitz. Challenge in manufacturing electrolyte solutions for lithium and lithium ion batteries quality control and minimizing contamination level. *Journal of Power Sources*, 81-82: 119–122, 1999.
- [96] D. Aurbach, K. Gamolsky, B. Markovsky, G. Salitra, Y. Gofer, U. Heider, R. Oesten and M. Schmidt. The Study of Surface Phenomena Related to Electrochemical Lithium Inter-calation into Li_xMO_y Host materials (M = Ni, Mn). *Journal of The electrochemical Society*, 147: 1322–1331, 2000.

- [97] X. Zhang, R. Kostecki, T. Richardson, J. Pugh and P. R. Jr. Electrochemical and Infrared Studies of the Reduction of Organic Carbonates. *Journal of The Electrochemical Society*, 148: 1341–1345, 2001.
- [98] J. Goodenough and Y. Kim. Challenges for rechargeable batteries. *Journal of Power Sources*, 196: 6688–6694, 2011.
- [99] R. Fong, U. v. Sacken and J. Dahn. Studies of Lithium Intercalation into Carbons Using Nonaqueous Electrochemical Cells. *Journal of The Electrochemical Society*, 137: 2009–2013, 1990.
- [100] E. Peled. The Electrochemical Behavior of Alkali and Alkaline Earth Metals in Nonaqueous Battery Systems-The Solid Electrolyte Interphase Model. *Journal of The Electrochemical Society*, 126: 2047–2051, 1979.
- [101] E. Peled, D. Golodnitsky and G. Ardel. Advanced Model for Solid Electrolyte Interphase Electrodes in Liquid and Polymer Electrolytes. *Journal of The Electrochemical Society*, 144: 208–210, 1997.
- [102] D. Aurbach. Review of selected electrode-solution interactions which determine the performance of Li and Li ion batteries. *Journal of Power Sources*, 89: 206–218, 2000.
- [103] A. Zaban and D. Aurbach. Impedance spectroscopy of lithium and nickel electrodes in propylene carbonate solutions of different lithium salts A comparative study. *Journal of Power Sources*, 54: 289–295, 1995.
- [104] D. Aurbach, B. Markovsky, I. Weissman, E. Levi and Y. Ein-Eli. On the correlation between surface chemistry and performance of graphite negative electrodes for Li ion batteries. *Electrochimica Acta*, 45: 1–2, 1999.
- [105] R. Dedryère, L. Gireaud, S. Grugeon, S. Lacruelle, J. Tarascon and D. Gonbeau. Characterization of Lithium Alkyl Carbonates by X-ray Photoelectron Spectroscopy: Experimental and Theoretical Study. *The Journal of Physical Chemistry B*, 109: 15868–15875, 2005.
- [106] P. Verma, P. Maire and P. Novák. A review of the features and analyses of the solid electrolyte interphase in Li-ion batteries. *Electrochimica Acta*, 55: 6332–6341, 2010.
- [107] A. Andersson and K. Edström. Chemical Composition and Morphology of the Elevated Temperature SEI on Graphite. *Journal of The Electrochemical Society*, 148: 1100–1109, 2001.
- [108] S. Leroy, F. Blanchard, R. Dedryère, H. Martinez, B. Carré, D. Lemordant and D. Gonbeau. Surface film formation on a graphite electrode in Li-ion batteries: AFM and XPS study. *Surface and Interface Analysis*, 37: 773–781, 2005.

- [109] A. Andersson, A. Henningson, H. Siegbahn, U. Jansson and K. Edström. Electrochemically lithiated graphite characterised by photoelectron spectroscopy. *Journal of Power Sources*, 119-121: 522–527, 2003.
- [110] D. Aurbach, A. Zaban, Y. Gofer, Y. Ely, I. Weissman, O. Chusid and O. Abramson. Recent studies of the lithium-liquid electrolyte interface Electrochemical, morphological and spectral studies of a few important systems. *Journal of Power Sources*, 54: 76–84, 1995.
- [111] H. Yoshida, T. Fukunaga, T. Hazma, M. Terasaki, M. Mizutani and M. Yamachi. Degradation mechanism of alkyl carbonate solvents used in lithium-ion cells during initial charging. *Journal of Power Sources*, 68: 311–315, 1997.
- [112] S. Laruelle, S. Pilard, P. Guenot, S. Grugeon and J. Tarascon. Identification of Li-Based Electrolyte Degradation Products Through DEI and ESI High-Resolution Mass Spectrometry. *Journal of The Electrochemical Society*, 151: 1202–1209, 2004.
- [113] M. Nie, D. Abraham, Y. Chen, A. Bose and B. Lucht. Silicon Solid Electrolyte Interphase (SEI) of Lithium Ion Battery Characterized by Microscopy and Spectroscopy. *The Journal of Physical Chemistry C*, 117: 13403–13412, 2013.
- [114] C. Pereira-Nabais, J. Swiatowska, A. Chagnes, A. Gohier, S. Zanna, A. Seyeux, P. Tran-Van, C. Cojocar, M. Cassir and P. Marcus. Insight into the Solid Electrolyte Interphase on Si nanowires in Lithium-Ion Battery: Chemical and Morphological Modifications upon Cycling. *The Journal of Physical Chemistry C*, 118: 2919–2928, 2014.
- [115] V. Etacheri, O. Haik, Y. Goffer, G. Roberts, I. Stefan, R. Fasching and D. Aurbach. Effect of Fluoroethylene Carbonate (FEC) on the Performance and Surface Chemistry of Si-Nanowire Li-Ion Battery Anodes. *Langmuir*, 28: 965–976, 2012.
- [116] C. Chan, R. Ruffo, S. Hong and Y. Cui. Surface Chemistry and morphology of the solid electrolyte interphase on silicon nanowire lithium-ion battery anodes. *Journal of Power Sources*, 189: 1132–1140, 2009.
- [117] D. Arrega-Salas, A. Sra, K. Roodenko, Y. Chabal and C. Hinkle. Progression of Solid Electrolyte Interphase Formation on Hydrogenated Amorphous Silicon Anodes for Lithium-Ion Batteries. *The Journal of Physical Chemistry C*, 116: 9072–9077, 2012.
- [118] C. Pereira-Nabais, J. Swiatowska, A. Chagnes, F. Ozanam, A. Gohier, P. Tran-Van, C. Cojocar, M. Cassir and P. Marcus. Interphase chemistry of Si electrodes used as anodes in Li-ion batteries. *Applied Surface Science*, 266: 5–16, 2013.
- [119] W. Chang, C. Park, J. Kim, Y. Kim, G. Jeong and H. Sohn. Quartz (SiO₂): a new energy storage anode material for Li-ion batteries. *Energy & Environmental Science*, 5: 6895–6899, 2012.

- [120] B. Guo, J. Shu, Z. Wang, H. Yang, L. Shi, Y. Liu and L. Chen. Electrochemical reduction of nano-SiO₂ in hard carbon as anode material for lithium ion batteries. *Electrochemistry Communications*, 10: 1876–1878, 2008.
- [121] Q. Sun, B. Zhang and Z. Fu. Lithium electrochemistry of SiO₂ thin film electrode for lithium-ion batteries. *Applied Surface Science*, 254: 3774–3779, 2008.
- [122] M. Broussely, P. Biensan, F. Bonhomme, P. Blanchard, S. Herreyre, K. Nechev and R. Staniewicz. Main aging mechanisms in Li ion batteries. *Journal of Power Sources*, 146: 90–96, 2005.
- [123] S. Zhang. A review on electrolyte additives for lithium-ion batteries. *Journal of Power Sources*, 162: 1379–1394, 2006.
- [124] S. Dalavi, P. Guduru and B. Lucht. Performance Enhancing Electrolyte Additives for Lithium Ion Batteries with Silicon Anodes. *Journal of The Electrochemical Society*, 159: 642–646, 2012.
- [125] N. Choi, K. Yew, K. Lee, M. Sung, H. Kim and S. Kim. Effect of fluoroethylene carbonate additive on interfacial properties of silicon thin-film electrode. *Journal of Power Sources*, 161: 1254–1259, 2006.
- [126] L. Martin, H. Martinez, M. Uldemolins, B. Pecquenard and F. L. Cras. Evolution of the Si electrode/electrolyte interface in lithium batteries characterized by XPS and AFM techniques: The influence of vinylene carbonate additive. *Solid State Ionics*, 215: 36–44, 2012.
- [127] L. Chen, K. Wang, X. Xie and J. Xie. Effect of vinylene carbonate (VC) as electrolyte additive on electrochemical performance of Si film anode for lithium ion batteries. *Journal of Power Sources*, 174: 538–543, 2007.
- [128] H. Nakai, T. Kubota, A. Kita and A. Kawashima. Investigation of the Solid Electrolyte Interphase Formed by Fluoroethylene Carbonate on Si Electrodes. *Journal of The Electrochemical Society*, 158: 798–801, 2011.
- [129] K. Schroder, H. Celio, L. Webb and K. Stevenson. Examining Solid Electrolyte Interphase Formation on Crystalline Silicon Electrodes: Influence of Electrochemical Preparation and Ambient Exposure Conditions. *The Journal of Physical Chemistry C*, 116: 19737–19747, 2012.
- [130] M. Li, M. Qu, X. He and Z. Yu. Effects of electrolytes on the electrochemical performance of Si/graphite/disordered carbon composite anode for lithium-ion batteries. *Electrochimica Acta*, 54: 4506–4513, 2009.
- [131] N. Choi, K. Yew, H. Kim, S. Kim and W. Choi. Surface layer formed on silicon thin-film electrode in lithium bis(oxalato) borate-based electrolyte. *Journal of Power Sources*, 172: 404–409, 2007.

- [132] S. Komaba, K. Shimomura, N. Yabuuchi, T. Ozeki, H. Yui and K. Konno. Study on Polymer Binders for High-Capacity SiO Negative Electrode of Li-Ion Batteries. *Journal of Physical Chemistry C*, 115: 13487–13495, 2011.
- [133] J. Li, R. Lewis and J. Dahn. Sodium carboxymethyl cellulose: A potential binder for Si negative electrodes for Li-ion batteries. *Electrochemical and Solid-State Letters*, 10: 17–20, 2007.
- [134] W. Liu, M. Yang, H. Wu, S. Chiao and N. Wu. Enhanced Cycle Life of Si Anode for Li-Ion Batteries by Using Modified Elastomeric Binder. *Electrochemical and Solid-State Letters*, 8: 100–103, 2005.
- [135] N. Choi, K. Yew, W. Choi and S. Kim. Enhanced electrochemical properties of a Si-based anode using an electrochemically active polyamide imide binder. *Journal of Power Sources*, 177: 590–594, 2008.
- [136] N. Hochgatterer, M. Schweiger, S. Koller, P. Raimann, T. Wöhrle, C. Wurm and M. Winter. Silicon/Graphite composite electrodes for high-capacity anodes: Influence of binder chemistry on cycling stability. *Electrochemical and Solid-State Letters*, 11: 76–80, 2008.
- [137] J. Birdel, T. Azais, M. Morcrette, J. Tarascon and D. Larcher. In Situ Observation and Long-Term Reactivity of Si/C/CMC Composites Electrodes for Li-Ion Batteries. *Journal of The Electrochemical Society*, 158: 750–759, 2011.
- [138] J. Birdel, T. Azais, M. Morcrette, J. Tarascon and D. Larcher. Key Parameters Governing the Reversibility of Si/Carbon/CMC Electrodes for Li-Ion Batteries. *Chemistry of Materials*, 22: 1229–1241, 2010.
- [139] S. Komaba, N. Yabuuchi, T. Ozeki, Z. Han, K. Shimomura, H. Yui, Y. Katayama and T. Miura. Comparative Study of Sodium Polyacrylate and Poly-(vinylidene fluoride) as Binders for High Capacity Si-Graphite Composite Negative Electrodes in Li-Ion Batteries. *Journal of Physical Chemistry C*, 116: 1380–1389, 2012.
- [140] A. Magasinski, B. Zdyrko, I. Kovalenko, B. Hertzberg, R. Burtovyy, C. Huebner, T. Fuller, I. Luzinov and G. Yushin. Toward Efficient Binders for Li-Ion Battery Si-Based Anodes: Polyacrylic Acid. *Applied Materials & Interfaces*, 2: 3004–3010, 2010.
- [141] I. Kovalenko, B. Zdyrko, A. Magasinski, B. Hertzberg, Z. Milicevec, R. Burtovyy, I. Luzinov and G. Yushin. A Major Constituent of Brown Algae for Use in High-Capacity Li-Ion Batteries. *Science*, 334: 74–79, 2011.
- [142] G. Liu, S. Xun, N. Vukmirovic, X. Song, P. Velasco, H. Zheng, V. Battaglia, L. Wang and W. Yang. Polymers with Tailored Electronic Structure for High Capacity Lithium Battery Electrodes. *Advanced Materials*, 23: 4679–4683, 2011.

- [143] D. Larcher, S. Beattie, M. Morcette, K. Edström, J. Jumas und J. Tarascon. Recent findings and prospects in the field of pure metals as negative electrodes for Li-ion batteries. *Journal of Materials Chemistry*, 17: 3759–3772, 2007.
- [144] X. Liang, Z. Wen, Y. Liu, M. Wu, J. Jin, H. Zhang and X. Wu. Improved cycling performances of lithium sulfur batteries with LiNO₃-modified electrolyte. *Journal of Power Sources*, 196: 9839–9843, 2011.
- [145] J. Guo, A. Sun, X. Chen, C. Wang and A. Manivannan. Cyclability study of silicon-carbon composite anodes for lithium-ion batteries using electrochemical impedance spectroscopy. *Electrochimica Acta*, 56: 3981–3987, 2011.
- [146] J. Tarascon and M. Armand. Issues and challenges facing rechargeable lithium batteries. *Nature*, 414: 359–367, 2001.
- [147] R. Marom, S. Amalraj, N. Leifer, D. Jacob and D. Aurbach. A review of advanced and practical lithium battery materials. *Journal of Materials Chemistry*, 21: 9938–9954, 2011.
- [148] M. Wittingham. History, Evolution and Future Status of Energy Storage. *IEEE Proceedings*, pages 1518–1534, 2012.
- [149] T. Song, J. Xia, J. H. Lee, D. Lee, M. Kwon, J. Choi, J. Wu, S. Doo, H. Chang, W. Park, D. Zang, H. Kim, Y. Huang, K. Hwang, J. Rogers and U. Paik. Arrays of Sealed Silicon Nanotubes As Anodes for Lithium Ion Batteries. *Nano Letters*, 10: 1710–1716, 2010.
- [150] C. Nguyen and S. Song. Interfacial structural stabilization on amorphous silicon anode for improved cycling performance in lithium-ion batteries. *Electrochimica Acta*, 55: 3026–3033, 2010.
- [151] S. Song and S. Baek. Silane-derived SEI stabilization on thin-film electrodes of nanocrystalline Si for lithium batteries. *Electrochemical and Solid-State Letters*, 12: 23–27, 2009.
- [152] Y. Yen, S. Chao, H. Wu and N. Wu. Study on Solid-Electrolyte-Interphase of Si and C-Coated Si Electrodes in Lithium Cells. *Journal of The Electrochemical Society*, 153: 95–102, 2009.
- [153] L. Cui, L. Hu, H. Wu, J. Choi and Y. Cui. Inorganic Glue Enabling High Performance of Silicon Particles as Lithium Ion Battery Anode. *Journal of The Electrochemical Society*, 158: 592–596, 2011.
- [154] W. Xu, S. Vegunta and J. Flake. Surface-modified silicon nanowire anodes for lithium-ion batteries. *Journal of Power Sources*, 196: 8583–8589, 2011.
- [155] V. Chevrier and J. Dahn. First Principles Model of Amorphous Silicon Lithiation. *Journal of The Electrochemical Society*, 156: 454–458, 2009.
- [156] X. Zhou, Y. Yin, L. Wan and Y. Guo. Facile synthesis of silicon nanoparticles inserted into graphene sheets as improved anode materials for lithium-ion batteries. *Chemical Communications*, 48: 2198–2200, 2012.

- [157] C. Wang, H. Wu, Z. Chen, M. McDowell, Y. Cui and Z. Bao. Self-healing chemistry enables the stable operation of silicon microparticle anodes for high-energy lithium-ion batteries. *Nature Chemistry*, 5: 1042–1048, 2013.
- [158] G. Han, M. Ryou, K. Cho, Y. lee and J. Park. Effect of succinic anhydride as an electrolyte additive on electrochemical characteristics of silicon thin-film electrode. *Journal of Power Sources*, 195: 3709–3714, 2010.
- [159] K. Takkahashi, M. Saitoh, M. Sano, M. Fujita and K. Kifune. Electrochemical and Structural Properties of a 4.7 V-Class $\text{LiNi}_{0.5}\text{Mn}_{1.5}\text{O}_4$ Positive Electrode Material Prepared with a Self-Reaction Method. *Journal of The Electrochemical Society*, 151: 173–177, 2004.
- [160] K. Numata, C. Sakaki and S. Yamanaka. Synthesis of Solid Solutions in a System of LiCoO_2 - Li_2MnO_3 for Cathode Materials of Secondary Lithium Batteries. *Chemical Letters*, 8: 725–726, 1997.
- [161] S. Xun, X. Song, L. Wang, M. Grass, Z. Liu, V. Battaglia and G. Liu. The Effects of Native Oxide Surface Layer on the Electrochemical Performance of Si Nanoparticle-Based Electrodes. *Journal of The Electrochemical Society*, 158: 1260–1266, 2011.
- [162] K. Xu, S. Zhang, U. Lee, J. Allen and T. Jow. LiBOB: Is it an alternative salt for lithium ion chemistry? *Journal of Power Sources*, 146: 79–85, 2005.
- [163] D. Aurbach, Y. Ein-Eli, B. Markovsky, A. Zaban, S. Luski, Y. Carmeli and H. Yamin. The Study of Electrolyte Solutions Based on Ethylene and Diethyl Carbonates for Rechargeable Li Batteries II. Graphite Electrodes. *Journal of The Electrochemical Society*, 142: 2882–2890, 1995.

B List of Abbreviations

A	Surface area of electrode
a	Activity of ionic species
Ah g ⁻¹	Ampere hours per gram
c	Concentration
CVD	Chemical vapor deposition
D	Diffusion coefficient
DEC	Diethyl carbonate
DMC	Dimethyl carbonate
C-rate	Current rate implying the time a battery needs to fully charge or discharge
CE	Coulombic efficiency
CC-CV	Constant current constant voltage
CMC	Carboxyl methyl cellulose
CV	Cyclic voltammetry
e ⁻	Electron
E	Energy
EC	Ethylene carbonate
EDX	Energy Dispersive X-ray Diffraction
EIS	Electrochemical impedance spectroscopy
EMC	Ethylmethyl carboante
F	Faraday constant (96485 C mol ⁻¹)
FEC	Fluoroethylene carbonate
FTIR	Fourier transformation infrared spectroscopy
ΔG	Change of Gibbs free energy
ΔH	Change of enthalpy
HOMO	Highest occupied molecular orbital
i	Current
k	Rate constant
Li	Lithium
Li ⁺	Lithium ion
LiCoO ₂	Lithium-Cobalt-Oxide
LFP	Lithium-Iron-Phosphate
LiBOB	Lithium(bis)oxalato borate
LUMO	Lowest Unoccupied Molecular Orbital

M	Mass
M _r	Molecular mass
n	Number of transferred electrons
NCA	Lithium-Nickel-Cobalt-Aluminium-Oxide
Ni-Cd	Nickel Cadmium
Ni-MH	Nickel-Metal Hydride
NMC	Lithium-Nickel-Manganese-Cobalt-Oxide
NMR	Nuclear Magnetic Resonance Spectroscopy
OCV	Open Circuit Voltage
P	Power
PAA	Polyacrylicacid
PAN	Polyacrylnitril
PEO	Poly(ethyleneoxide)
PFFO	Poly-9,9-dioctylfluorene
PFFOMB	Poly-(9,9-dioctylfluorene-co-fluorene-co-methylbenzoic-acid)
PVDF	Polyvinylidene fluoride
Q	Charge
R	Resistance
R	Gas constant (8.314 J mol ⁻¹ K ⁻¹)
RF	Radio frequency
ΔS	Change of entropy
SBR	Styrene butadiene rubber
SEI	Solid Electrolyte Interphase
SEM	Secondary Electron Microscopy
Si/C	Silicon/Carbon
SIMS	Secondary Ion Mass Spectrometry
T	Temperature
T _b	Boiling temperature
TF	Flash temperature
T _m	Melting temperature
TOF-SIMS	Time of Flight Secondary Ion Mass Spectrometry
TEM	Transmission Electron Microscopy
U	Voltage
VC	Vinylene carbonate
Wh	Watt hour
XPS	X-ray Photoelectron Spectroscopy

XRD	X-ray Diffraction
z	Charge number of ionic species
α	Transfer coefficient
ε	Dielectricity
η	Overpotential
η (cP)	Viscosity
σ	Conductivity
ρ	Density
μ	Chemical potential

C List of Figures

Figure 1: Comparison between the hexagonal (ABA) and rhomboedric (ABC) modification of graphite with the respective stacking order of the graphene layers (adapted and modified from [9]).	12
Figure 2: Change of the ABA stacking order in hexagonal graphite to an AAA stacking order due to the intercalation of Li^+ [14].	13
Figure 3: Schematic representation of the different intercalation steps of Li^+ into graphite depending on the potential U vs. Li/Li^+ and the molar fraction x of Li in Li_xC_6 (adapted and modified from [14]).	14
Figure 4: Voltage profile vs. Li/Li^+ for the first electrochemical lithiation and delithiation of crystalline Si at room temperature and its influence on the formation of different Li_xSi compounds (solid line). For comparison reason the dashed line indicates the formation of the different Li_xSi compounds at 415°C (sharp steps indicating the phase transitions) [38].	18
Figure 5: The different phases and structures proposed during the lithiation of Si . The structures were concluded from ^7Li -NMR measurements and include Si -clusters, chains, rings, and dumbbells [41].	19
Figure 6: Schematic representation of the structural changes and existing and co-existing phases that occur during the lithiation of micrometric Si (adapted from [49]).	20
Figure 7: Relationship of the total specific capacity of a Li -Ion battery cell with a constant cathode specific capacity as a function of the specific anode capacity [26].	25
Figure 8: Energy and potential diagram of the electronic HOMO and LUMO states in the cathode, electrolyte, and anode of a schematic Li -Ion battery cell (adapted from [93]).	28
Figure 9: Schematic representation of the proposed SEI model in Si -based anodes, consisting of an inner part which is more inorganic and an outer part which is more organic [116, 118].	34
Figure 10: Proposed decomposition reaction of FEC in Li -Ion battery cells, during the SEI formation process [128].	37
Figure 11: Proposed decomposition process of LiBOB during the SEI formation process on the surface of the anode in Li -Ion batteries [92].	38
Figure 12: Charging capacities with different electrolytes to optimize the cycling stability of Si/C -anodes: a.) reference electrolyte LP 71 b.) 1 wt. %, 5 wt. %, 10 wt. %, and 20 wt. % FEC additive c.) 0.1 wt. %, 0.3 wt. %, and 0.5 wt. % LiNO_3 additive d.) new electrolyte formulation with 10 wt. % FEC and 0.5 wt. % LiNO_3 as well as LP 71 + 10 wt. % FEC + 0.1 wt. % LiNO_3 , and LP 71 + 10 wt. % FEC + 0.3 wt. % LiNO_3 .	48
Figure 13: a.) Charging capacities to compare the cycling stability of Si/C -anodes cycled in	

the different electrolyte solutions b.) Long term cycling stability of a Si/C-anode cycled in the new electrolyte formulation	49
Figure 14: a.) Cyclic voltammetry measurements of Si/C-based anode between 0.01 V and 1.25 V in the standard reference electrolyte (LP 71) using a scan rate of 0.1 mV s^{-1} b.) Cyclic voltammetry measurements using the new electrolyte formulation.....	50
Figure 15: a) Ratio of the constant voltage step (CV-step) capacity compared to the total capacity (CC-CV-step) b) Rate capability and specific capacities at C/10, C/2, 1C, 5C, and again C/10 for 10 cycles respectively.....	51
Figure 16: a) Overview SEM image of the fresh, uncycled anode surface b.) Higher magnification SEM image of the fresh and uncycled Si/C-anode indicating the different anode components: conductive C (spot a), Si (spot b), and graphite (spot c) c.) EDX-spectra's of the spots in Figure 16b.	52
Figure 17: TEM image of the pristine Si nanoparticles. The image displays the characteristic crystalline Si-core of the Si nanoparticles which is surrounded with a ~1-2 nm thin amorphous SiO_x -shell	53
Figure 18: a-c.) Overview SEM images of the anodes cycled in the standard electrolyte after 1 (a.), 15 (b.), and 100 cycles (c.) d-f) Higher magnification SEM images of the anode surfaces after 1 (d.), 15 (e.), and 100 cycles (f.).....	54
Figure 19: Magnified SEM image of the Si/C-anodes after 15 cycles cycled in the LP 71 reference electrolyte, showing the beginning formation of fiberlike and netlike structures due to enhanced SEI growth.....	54
Figure 20: a-c.) Overview SEM images of the anodes cycled in the new electrolyte after 1 (a.), 15 (b.), and 100 cycles (c.) d-f) higher magnification SEM images of the anode surfaces after 1 (d.), 15 (e.), and 100 cycles (f.).....	55
Figure 21: a.) In-detail SEM image of the new structure formed during cycling in the new electrolyte indicated as spot a (framed) in Figure 20d b.) EDX-spectra of the new formed structure shown in Figure 21a.....	56
Figure 22: a.) Overview EDX-spectra of the anodes cycled in the new electrolyte for 1, 15, and 100 cycles b.) Overview EDX-spectra of the anodes cycled in the standard electrolyte for 1, 15, and 100 cycles.....	57
Figure 23: EDX measurement of a Si/C-based anode after 100 cycles in LP 71 standard electrolyte and an increased accelerating voltage of 15 kV. The increased Si signal indicates that the Si is not dissolved during the cycling process but rather buried under a thick SEI layer.....	58
Figure 24: a.) Experimental setup for the pretreatment procedure b.) Potential vs. time plot during the pretreatment process of the Si/C-anodes in the pretreatment solution containing	

FEC, LiBOB, and LiNO ₃	65
Figure 25: Differential capacity (dQ) vs. potential behavior during the pretreatment process. The peaks indicate the reductive decomposition of the pretreatment solution components..	66
Figure 26: Comparison of the capacity vs. cycling performance between the pretreated and non-pretreated Si/C-anodes for 100 cycles.	67
Figure 27: Long term cycling behavior of the pretreated Si/C-anodes using the LP 71 electrolyte without any additives.....	68
Figure 28: Performance of the pretreated and non-pretreated Si/C-anodes at different C-rates.	69
Figure 29: a) Current vs. time plot for 100 cycles of the pretreated Si/C-anode; b) Magnified area for the current vs. time behavior, indicated by the red square in Figure 29a; c) Magnified area for the current vs. time behavior, indicated by the blue square in Figure 29a; d) Current vs. time plot for 100 cycles of the non-pretreated Si/C-anode; e) Magnified area for the current vs. time behavior, indicated by the red square in Figure 29c; f) Magnified area for the current vs. time behavior, indicated by the blue square in Figure 29c	70
Figure 30 a-f.): SEM images of the non-pretreated Si/C-anode before cycling (a+d), after 1 cycle (b+e), and after 100 cycles (c+f).	71
Figure 31 a-f): SEM images of the pretreated Si/C-anodes directly after the pretreatment (a+d), after 1 cycle (b+e) and after 100 cycles (c+f).	72
Figure 32: a.) EDX overview spectra's before cycling, after 1 cycle, and 100 cycles for the non-pretreated Si/C-anode b.) EDX overview spectra's directly after the pretreatment, after 1 cycle, and after 100 cycles for the pretreated Si/C-anode.	73
Figure 33: a.) SEM image of the forming fiberlike structures of the pretreated Si/C-anode after 100 cycles in the secondary electron mode to better visualize the morphology of the anode components b.) EDX spectra's of the area indicated with a white square in Figure 33a with 5 kV and 15 kV accelerating voltage.....	74
Figure 34: a). ATR-FTIR spectra's are of the pristine Si/C-anode (reference) and directly after the pretreatment process b.) Comparison of ATR-FTIR spectra's of pretreated and non-pretreated Si/C-anodes after 100 cycles in the LP 71 reference electrolyte.	75

D List of Tables

Table 1: Comparison of the different characteristics between different possible active materials in anodes for Li-Ion batteries (adapted from [22]).	15
Table 2: Structure and physical and chemical properties of typical solvents in liquid electrolytes for Li-Ion batteries [92].	26
Table 3: Physical and chemical properties of certain Li-salts for application in electrolytes for Li-Ion batteries [92].	27
Table 4: Possible reactions taking place for EC, DMC, and LiPF ₆ during the SEI formation process at the anode/electrolyte interface [105, 107, 110, 111].	31
Table 5: Possible reactions of H ₂ O and HF in Li-Ion battery cells which could contribute to the SEI formation on the anode surface [21, 104, 112].	32

E Curriculum Vitae

Personal Information

Day of birth: 17.01.1987
Place of birth: Peine / Germany
Nationality: German
Marital status: married, 1 child

Academic Education

10/2006-09/2009 Bachelor of Science in Advanced Materials at the Justus-Liebig-University Giessen
Title of the thesis: *Investigation of the SEI formation on graphite electrodes for Lithiumionbatteries*
Supervisor: Prof. Dr. Jürgen Janek

10/2009-10/2011 Master of Science in Advanced Materials at the Justus-Liebig-University Giessen
Title of the thesis: *Electrochemical and analytical investigations of electrodes on Li-conducting garnets*
Supervisor: Prof. Dr. Jürgen Janek

Since 11/2011 Internal PhD at the Research Department of Battery and Fuels at the Volkswagen AG in Isenbüttel / Germany

PhD thesis at the Fritz-Haber-Institute of the Max-Planck-Society in Berlin and the Technical University of Berlin; Department of Inorganic Chemistry
Title of the thesis: *Investigation of Si/C-based anodes for Li-ion batteries*
Supervisor: Prof. Dr. Robert Schlögl

Working experience

02/2009-04/2009	Internship at the Schunk Carbon Group in Heuchelheim / Germany – <i>Synthesis of new anode materials for Li-Ion batteries</i>
09/2009-10/2011	Scientific Assistant at the Physical Chemistry Department in the group of Prof. Dr. Jürgen Janek at the Justus-Liebig-University Giessen – <i>Synthesis and electrochemical investigation of new solid electrolytes for Li-Ion batteries</i>
07/2010-09/2010	Scientific Assistant at the Optoelectronics Center at the Korean Institute of Science and Technology (KIST) in the Group of Dr. Il-Doo Kim in Seoul / South Korea (Scholarship of the German Academic Exchange Service (DAAD) and the National Research Foundation of Korea (NRF)) – <i>Electrospinning of LiMn_2O_4 as cathode materials in Li-Ion batteries</i>
Since 11/2011	Employee at the Research Department of Battery and Fuels (Powertrain) at the Volkswagen AG in Isenbüttel / Germany – <i>Research and development concerning the Cell Chemistry and Cell Testing of new anode materials in Li-ion batteries</i>

Linguistic proficiency

German:	Mother tongue (native speaker)
English:	Fluent (negotiable)
French:	Basic knowledge
Korean:	Basic knowledge

F List of Publications

1. **A new LiNO_3 based electrolyte formulation for Si/C-anodes with enhanced performance in Li-Ion batteries**
Janis Doelle, Mirko Herrmann, Nicole Giliard, Gisela Weinberg, Julian Tornow, Robert Schloegl
to be submitted
2. **Solid Electrolyte Interphase in a beaker-New pretreatment method for improved Si/C-anodes in Li-Ion batteries**
Janis Doelle, Nicole Giliard, Gisela Weinberg, Julian Tornow, Robert Schloegl
to be submitted
3. H. Buschmann, J. Doelle, S. Berendts, A. Kuhn, P. Bottke, M. Wilkening, P. Heitjans, A. Senyshyn, H. Ehrenberg, A. Lotnyk, V. Duppel, L. Kienle, J. Janek. Structure and dynamics of the fast lithium ion conductor " $\text{Li}_7\text{La}_3\text{Zr}_2\text{O}_{12}$ ". *Physical Chemistry Chemical Physics*, 13:19378–19392, 2011.

G List of Patents

1. Patent application with official identification number **DE10 2013 210 631 A1**:
"Neue Elektrolytzusammensetzung für Hochenergieanoden"
2. Patent application with official identification number **DE10 2013 014 627 A1**:
"Pre-lithiierung von Siliziumpartikeln"
3. Patent application with official identification number **DE10 2014 207 881 A1**:
"Herstellverfahren von nanoskaligen Siliziumpartikeln mit einer reduzierten Siliziumdioxid-Beschichtung"
4. Patent application with official identification number **DE10 2014 207 882 A1**:
"Neue Beschichtung von Siliziumpartikeln für Lithium-Ionen-Batterien zur verbesserten Zyklenstabilität"
5. Patent application with official identification number **DE10 2014 201 499 A1**:
"Neue Vorbehandlungsmethode für Anoden in Lithiumionenbatterien"

H Eidesstattliche Versicherung

Hiermit versichere ich an Eides statt, dass ich die Dissertation

„Investigation of Si/C-based anodes for Li-Ion batteries“

selbstständig verfasst habe. Ich versichere weiterhin an Eides statt, dass alle benutzten Hilfsmittel und Quellen sowie evtl. zur Hilfeleistung herangezogene Institutionen vollständig angegeben wurden.

Die Dissertation wurde nicht schon als Diplom- oder ähnliche Prüfungsarbeit verwendet.

Braunschweig, den 09.09.2014

Janis Dölle